

11-2017

Modelling and Simulation of Hydrogen Production via Membrane Reactor

Aya Abdel-Hamid smail Mourad

Follow this and additional works at: https://scholarworks.uaeu.ac.ae/chem_petro_theses

 Part of the [Chemical Engineering Commons](#)



جامعة الإمارات العربية المتحدة
United Arab Emirates University

United Arab Emirates University

College of Engineering

Department of Chemical and Petroleum Engineering

MODELLING AND SIMULATION OF HYDROGEN PRODUCTION
VIA MEMBRANE REACTOR

Aya Abdel-Hamid Ismail Abdel-Hamid Mourad

This thesis is submitted in partial fulfilment of the requirements for the degree of
Master of Science in Chemical Engineering

Under the Supervision of Professor Nayef Ghasem

November 2017

Declaration of Original Work

I, Aya Abdel-Hamid Ismail Abdel-Hamid Mourad, the undersigned, a graduate student at the United Arab Emirates University (UAEU), and the author of this thesis entitled “*Modelling and Simulation of Hydrogen Production via Membrane Reactor*”, hereby, solemnly declare that this thesis is my own original research work that has been done and prepared by me under the supervision of Prof. Nayef Ghasem, in the College of Engineering at UAEU. This work has not previously been presented or published, or formed the basis for the award of any academic degree, diploma or a similar title at this or any other university. Any materials borrowed from other sources (whether published or unpublished) and relied upon or included in my thesis have been properly cited and acknowledged in accordance with appropriate academic conventions. I further declare that there is no potential conflict of interest with respect to the research, data collection, authorship, presentation, and/or publication of this thesis.

Student's Signature: Aya Mourad

Date: 17/12/2017

Approval of the Master Thesis

This Master Thesis is approved by the following Examining Committee Members:

- 1) Advisor (Committee Chair): Prof. Nayef Ghasem

Title: Professor

Department of Chemical and Petroleum Engineering

College of Engineering

Signature  _____

Date 4/12/2017

- 2) Member (Co-Advisor): Dr. Abdulrahman Alraeesi

Title: Assistant Professor

Department of Chemical and Petroleum Engineering

College of Engineering

Signature  _____

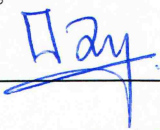
Date 4/12/2017

- 3) Member (Internal Examiner): Dr. Muhammad Zafar Iqbal

Title: Assistant Professor

Department of Chemical and Petroleum Engineering

College of Engineering

Signature  _____

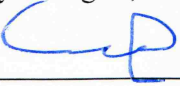
Date 4/12/17

- 4) Member (External Examiner): Prof. David deMontigny

Title: Professor

Department of Industrial Systems Engineering

Institution: University of Regina, Canada

Signature  _____

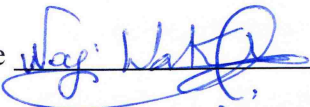
Date 4/12/2017

This Master Thesis is accepted by:

Dean of the College of Engineering: Professor Sabah Alkass

Signature  Date 17/12/2017

Dean of the College of Graduate Studies: Professor Nagi T. Wakim

Signature  Date 18/12/2017

Copy 9 of 10

Copyright © 2017 Aya Abdel-Hamid Ismail Abdel-Hamid Mourad
All Rights Reserved

Advisory Committee

1) Advisor: Prof. Nayef Ghasem

Title: Professor

Department of Chemical and Petroleum Engineering

College of Engineering

2) Co-advisor: Dr. Abdulrahman Alraeesi

Title: Assistant Professor

Department of Chemical and Petroleum Engineering

College of Engineering

Abstract

A membrane reactor is a promising device to produce pure hydrogen and enrich CO₂ from syngas. A simulation study of a double tubular catalytic membrane reactor for the water–gas shift reaction (WGS) under steady-state operation is presented in this work. The membrane consists of a dense Pd layer (selective to H₂) deposited on a porous glass cylinder support. The reaction side was filled with a commercial iron-chromium oxide catalyst, designed as Girdler G-3. The mass of the catalyst was 12.1 g and the height of the catalyst bed was 8 cm. The WGS model was carried out with and without the membrane at a temperature of 673 K, pressure of 2 atm, argon flow rate of 400 cm³ min⁻¹, and steam-to-carbon (S/C) ratio of 1. The membrane reactor could achieve a CO conversion efficiency of up to 93.7%, whereas a maximum value of only 77.5% was attained without using a membrane under the same operating conditions. The WGS membrane model was tested under different operating conditions. In order to find the optimum operating conditions, the response surface method was used at a temperature of 673 K and sweep gas (argon) flow rate of 3200 cm³/min in the Minitab software package. It was found that a nearly complete CO conversion could be achieved under the following conditions: S/C ratio = 4, total retentate pressure = 12 atm, and membrane thickness = 5 μm. Under these conditions, the S/C ratio obtained is satisfactory and a nearly complete conversion of CO was achieved. The developed model results were verified with available experimental results in the literature. It was found that the model results are in good agreement with the experimental results.

Key words: Membrane reactor, palladium (Pd) composite membrane, water–gas shift reaction (WGSR), H₂ production, carbon monoxide (CO) conversion, mathematical model, simulation, response surface method (RSM).

Title and Abstract (in Arabic)

النمذجة والمحاكاة لإنتاج الهيدروجين عن طريق المفاعل الغشائي

الملخص

المفاعل الغشائي هو جهاز واعد لإنتاج الهيدروجين النقي و ثاني أكسيد الكربون الغني من الغاز الطبيعي (syngas). الهدف من هذا العمل هو دراسة المحاكاة (Simulation) لمفاعل غشائي انبوبي مزدوج لتحويل تفاعل الغاز مع الماء (WGS) تحت حالة غير متغيره (steady state). تمت تعبئة جانب التفاعل بمحفز أكسيد الحديد الكروم التجاري، والذي صمم ك (Girdler G-3). وزن الحافز 12.1 غرام وارتفاعه 8 سم. تم تنفيذ النموذج (WGS) مع وبدون الغشاء تحت درجة حرارة 673K، ضغط 2 atm، معدل تدفق الأرجون 400 سم³/دقيقة ونسبة البخار إلى الكربون (S/C) = 1. كان مفاعل الغشائي قادرا على تحويل 93.7% من اول أكسيد الكربون (CO) ، في حين أن أقصى قيمة 77.5% فقط تم تحقيقها دون استخدام الغشاء في ظل ظروف التشغيل نفسها. تم اختبار المفاعل الغشائي (WGS) تحت ظروف تشغيل مختلفة. من أجل العثور على ظروف التشغيل المثلى، تم استخدام طريقة سطح الاستجابة (RSM) عند درجة حرارة 673K و معدل تدفق 3200 سم³/دقيقة من غاز الارجون في برنامج (Minitab). وقد وجد أن تحويل شبه الكامل لاول اكسيد الكربون (CO) يمكن أن يتحقق في ظل الظروف التالية: نسبة البخار إلى الكربون (S/C) = 4، مجموع الضغط في جانب التفاعل = 12 atm وسمك الغشاء = 5µm. وفي ظل هذه الظروف، فإن نسبة البخار إلى الكربون (S/C) التي تم الحصول عليها مرضية وقد تحقق تحويل كامل تقريبا من اول أكسيد الكربون (CO). تم مقارنة النتائج التي تم الحصول عليها من المحاكاة مع النتائج المتاحة من تجارب عملية سابقة. وقد وجد أن النتائج متفقة تماما مع نتائج التجارب العملية السابقة.

مفاهيم البحث الرئيسية: مفاعل غشائي، غشاء البلاتينيوم (Pd) المركب، تفاعل (WGS)، إنتاج الهيدروجين، تحويل أول أكسيد الكربون (CO)، النموذج الرياضي، المحاكاة، طريقة سطح الاستجابة (RSM).

Acknowledgements

I would like to express my sincere gratitude to my supervisors, Prof. Nayef Ghasem and Dr. Abdulrahman Alraeesi, for their continuous support, inestimable guidance, and the valuable knowledge during the research program.

I would like also to thank all faculty members of the Chemical and Petroleum Engineering Department at United Arab Emirates University for assisting me throughout my studies and research. I would also like to acknowledge and thank Dr. Chafik Bouhaddiou of the Business Department at UAE University, for his valuable help and assistance in performing the statistical analysis of this study.

Finally, I must express my very profound gratitude to my great father, Prof. Abdel-Hamid Mourad, and my lovely mother, who contributed, aided, and encouraged me throughout my years of study and through the process of researching and writing this thesis. This accomplishment would not have been possible without both of them.

I would also like to thank, in particular, my beloved husband, Eng. Ahmed Morad, who provided me with all the support and strength to complete this work. Special thanks also go to my brother, Eng. Bahaa Mourad, and sister, Ameera Mourad, who helped me along the way.

Dedication

To my beloved parents and family

Table of Contents

Title	i
Declaration of Original Work	ii
Copyright	iii
Advisory Committee	iv
Approval of the Master Thesis	v
Abstract	vii
Title and Abstract (in Arabic)	ix
Acknowledgements	x
Dedication	xi
Table of Contents	xii
List of Tables.....	xiv
List of Figures	xv
List of Abbreviations.....	xvii
Chapter 1: Introduction	1
1.1 Overview	1
1.2 Scope and Objectives	5
1.3 Outline and Structure of the Thesis.....	6
Chapter 2: Literature Review	8
2.1 Hydrogen Production Processes.....	9
2.1.1 Conventional Technologies	10
2.1.1.1 Hydrocarbon Reforming Methods.....	10
2.1.1.1.1 Steam Reforming Method.....	11
2.1.1.1.2 Partial Oxidation Method.....	14
2.1.1.1.3 Autothermal Reforming Method (ATR).....	16
2.1.1.2 Hydrocarbon Pyrolysis	17
2.1.2 Renewable Technologies	18
2.1.2.1 Biomass Methods	18
2.1.2.1.1 Thermochemical Methods.....	18
2.1.2.1.2 Biological Methods	20
2.1.2.2 Water Splitting.....	22
2.1.2.2.1 Electrolysis.....	22
2.1.2.2.2 Thermolysis.....	23
2.1.2.2.3 Photolysis	24
2.1.2.3 Wind Power	24
2.2 Comparison of Hydrogen Production Technologies.....	25

2.3 Steam Methane Reforming in Conventional Reactor	28
2.3.1 Operating Condition of Conventional Reactors	28
2.3.2 Disadvantages of Conventional Reactor.....	29
2.4 Steam Methane Reforming in Membrane Reactor.....	29
2.4.1 Palladium-Based MRs	33
2.4.2 Water–Gas Shift Membrane Reactors	36
Chapter 3: Model Development	43
3.1 Reactor Configuration	43
3.2 Model Development.....	44
3.3 Model Assumptions	45
3.4 Boundary Conditions	45
3.5 Governing Equations.....	46
3.5.1 Governing Equation Used in Shell (retentate) Side.....	46
3.5.2 Governing Equation Used in Tube (permeate) Side.....	50
Chapter 4: Results and Discussion.....	52
4.1 Effect of Using Membrane on CO Conversion.....	52
4.2 Effect of Steam to Carbon Ratio (S/C)	55
4.2.1 Change of CO Conversion at Different S/C Ratios.....	63
4.2.2 Change of Molar Flow Rate at Different S/C Ratios	64
4.2.3 Model Validation.....	66
4.3 Effect of Membrane Thickness and Sweep Gas Flowrate	67
4.4 Effect of Hydrogen Partial Pressure at Retentate Side.....	69
4.5 Effect of Hydrogen Partial Pressure at Permeate Side.....	70
4.5.1 Effect of Hydrogen Permeate Partial Pressure on CO Conversion.....	77
4.6 Effect of Residence Time.....	79
4.6.1 Effect of Residence Time on CO Conversion	84
4.7 Statistical Model	86
4.7.1 Residual Analysis	89
4.7.2 Optimum Operating Conditions	92
Chapter 5: Conclusion and Recommendation.....	97
References	101

List of Tables

Table 2.1: Comparison of different hydrogen production processes	25
Table 2.2: Some of the major advantages and disadvantages of membrane reactors.....	32
Table 4.1: Retentate pressure and its corresponding residence time	80
Table 4.2: Identification of affecting parameters (factors) used in the response surface design	86
Table 4.3: Full design of 64 runs with different combinations of factors and their corresponding responses.....	87

List of Figures

Figure 1.1: Feedstock used in the current global production of hydrogen.....	2
Figure 2.1: Hydrogen production processes	10
Figure 2.2: Diagram of methane steam reforming process	13
Figure 2.3: Flow diagram of the partial oxidation (or coal gasification) process	15
Figure 2.4: Flow diagram of the autothermal reforming of methane process	17
Figure 2.5: Schematic representation of membrane reactor.....	32
Figure 2.6: Schematic illustration of T-HFCMR [1. Ni-based catalyst layer; 2. porous ceramic support layer; 3. palladium-silver alloy membrane layer].....	35
Figure 2.7: Detailed view of the four-tube Pd-based membrane reactor	38
Figure 2.8: Scheme diagram for the tubular palladium membrane reactor.....	39
Figure 2.9: Schematic diagram of catalytic membrane reactor used	41
Figure 3.1: Schematic representation of gas flow model through reaction and permeation sides in palladium membrane reactor	44
Figure 4.1: Species molar flow rates as a function of distance for the water–gas shift reaction without the palladium membrane.....	53
Figure 4.2: Surface plot for the hydrogen concentration (mol/m^3) in the present of palladium membrane	54
Figure 4.3: Change in CO conversion with and without the membrane along the reactor length	55
Figure 4.4: Effect of S/C ratio = 1 on the CO, CO ₂ , H ₂ O, and H ₂ concentrations.....	57
Figure 4.5: Effect of S/C ratio = 2 on the CO, CO ₂ , H ₂ O, and H ₂ concentrations.....	58
Figure 4.6: Effect of S/C ratio = 3 on the CO, CO ₂ , H ₂ O and H ₂ concentrations.....	59
Figure 4.7: Effect of S/C ratio = 4 on the CO, CO ₂ , H ₂ O, and H ₂ concentrations.....	61
Figure 4.8: Effect of S/C ratio = 5 on the CO, CO ₂ , H ₂ O, and H ₂ concentrations.....	62
Figure 4.9: Effect of S/C ratio = 6 on the CO, CO ₂ , H ₂ O, and H ₂ concentrations.....	63
Figure 4.10: Change in CO conversion at different S/C ratios	64
Figure 4.11: Change in hydrogen molar flow rate along reactor length at different S/C ratios	65
Figure 4.12: Effect of S/C molar ratio on CO conversion. Experimental conditions: temperature, 673 K; retentate pressure, 2 atm; flow rate of sweep argon, $400 \text{ cm}^3 \text{ min}^{-1}$	67

Figure 4.13: Effect of thickness on CO conversion for constant CO feed rate of 25 cm ³ /min and argon flow rates of 3200, 400, and 100 cm ³ /min	68
Figure 4.14: Effect of partial pressure of hydrogen at reaction side on CO conversion. Experimental conditions: temperature, 673 K; and flow rate of sweep argon, 400 cm ³ min ⁻¹	69
Figure 4.15: Effect of hydrogen partial pressure of 1 atm at permeate side on concentrations of CO, CO ₂ , H ₂ O, and H ₂	71
Figure 4.16: Effect of hydrogen partial pressure of 0.8 atm on the permeate side on the concentrations of CO, CO ₂ , H ₂ O, and H ₂	72
Figure 4.17: Effect of hydrogen partial pressure of 0.6 atm on the permeate side on the concentrations of CO, CO ₂ , H ₂ O, and H ₂	73
Figure 4.18: Effect of hydrogen partial pressure of 0.4 atm on the permeate side on the concentrations of CO, CO ₂ , H ₂ O, and H ₂	74
Figure 4.19: Effect of hydrogen partial pressure of 0.2 atm on the permeate side on the concentrations of CO, CO ₂ , H ₂ O, and H ₂	76
Figure 4.20: Effect of hydrogen partial pressure of 0.0 atm on the permeate side on the concentrations of CO, CO ₂ , H ₂ O, and H ₂	77
Figure 4.21: CO conversion versus reactor length at fixed values of hydrogen partial pressure on the permeate side	78
Figure 4.22: Effect of hydrogen permeate partial pressure on CO conversion	79
Figure 4.23: Effect of residence time of 0.13 s on the concentrations of CO, CO ₂ , H ₂ O, and H ₂	81
Figure 4.24: Effect of residence time of 0.47 s on the concentrations of CO, CO ₂ , H ₂ O, and H ₂	82
Figure 4.25: Effect of residence time of 0.63 s on the concentrations of CO, CO ₂ , H ₂ O, and H ₂	83
Figure 4.26: Effect of residence time of 0.96 s on the concentrations of CO, CO ₂ , H ₂ O, and H ₂	84
Figure 4.27: CO conversion versus reactor length at fixed values of residence time	85
Figure 4.28: Effect of residence time on CO conversion.....	85
Figure 4.29: Residual plots for response (CO conversion)	90
Figure 4.30: Analysis of variance from Minitab software	92
Figure 4.31: Optimum conditions for response	92
Figure 4.32: Interaction effect between S/C ratio and thickness on CO conversion	94
Figure 4.33: Interaction effect between S/C ratio and total retentate pressure on CO conversion	95
Figure 4.34: Interaction effect between thickness and total retentate pressure on CO conversion.....	96

List of Abbreviations

ATR	Autothermal reforming
$C_{H_2,ret}$	Concentration of hydrogen in the retentate side, (mol/cm ³)
$C_{H_2,perm}$	Concentration of hydrogen in the permeate side, (mol/cm ³)
c_i	Species i concentration, (mol/cm ³)
CFD	Computational fluid dynamics
CMR	Catalytic membrane reactor
CO	Carbon monoxide
D_i	Inter-diffusion coefficient of species i
F_i	Molar flow rate of species i, (mol/min)
ΔH_r	Reaction heat of enthalpy, kJ/mol
HTS	High-temperature shift
\dot{j}_d	Rate of hydrogen permeation per unit area of the membrane
J_d	Rate of hydrogen permeation per unit length of catalyst bed, (cm ³ /cm·min)
k	Rate constant of WGS reaction, (cm ⁶)/(mol · min · cm)
K_p	Equilibrium constant of WGS reaction
LTS	Low-temperature shift
$P_{H_2,ret}$	Partial pressure of hydrogen in the retentate side, atm
$P_{H_2,perm}$	Partial pressure of hydrogen in the permeate side, atm
P_i	Partial pressure of component i, atm
PBR	Packed bed reactor
Pd	Palladium
POX	Partial oxidation

PSA	Pressure swing adsorption
q	Hydrogen permeation coefficient per unit length of catalyst bed, ($\text{cm}^3 \cdot \mu\text{m}$) / ($\text{cm} \cdot \text{min} \cdot \text{atm}^{0.76}$)
Q	Hydrogen permeation coefficient per unit area of the membrane
R	Ideal gas constant, 0.08206 (L·atm)/(mol·K)
\mathcal{R}	Reaction rate expression, (mol/cm·min)
RSM	Response surface method
S/C ratio	Steam-to-carbon ratio
SMR	Steam methane reforming
SR	Steam reforming
STP	Standard temperature and pressure
T-HFCMR	Triple-layer hollow fibre catalytic membrane reactor
t	Membrane thickness, μm
WGSR	Water–gas shift reaction
τ	Residence time, min

Chapter 1: Introduction

1.1 Overview

Hydrogen is one of the oldest known molecules, and it is used extensively in many industries (e.g., chemical and petrochemical industries) for a variety of applications [1]. The increasing demand for energy, diminishing worldwide petroleum reserves, high petroleum prices, and high environmental standards for clean fuels have incentivised consistent efforts for developing new and alternative energy sources [2]. The production of hydrogen has become an important topic in recent decades; however, it is currently of greater interest because of fuel-cell technological developments [3]. Fuel cells that use H₂ as an energy source are environmentally friendly as compared to the traditional forms of combustion using fuels such as gasoline and diesel, in the sense that the only by-product from H₂ fuel cells is water (carbon-free emission), and therefore, it eliminates the emission of greenhouse gases [4]. Moreover, in the automobile industry, cars are already being developed using hydrogen as energy source required for propulsion [5]. In addition, hydrogen is used in the production of certain chemical products, particularly methanol, and for ammoniac synthesis [6]. Furthermore, hydrogen is used in a range of other industries, including metal refining, food processing, and electronics manufacturing.

The annual production of hydrogen is approximately 55 million tonnes, and the usage increases by about 6% every year [5]. Hydrogen can be produced from many sources, including conventional and renewable resources [4].

The production of hydrogen using nuclear power or renewable resources (e.g., wind, solar, biomass, and geothermal) without consuming fossil fuels or releasing CO₂

is currently being researched. These methods are still not economically and technically feasible. Therefore, hydrogen generation has so far been dominated by fossil fuels [7].

There are four main sources for the commercial production of hydrogen: natural gas, oil, coal, and electrolysis; which account for 48%, 30%, 18%, and 4% of the world's hydrogen production, respectively [8]. Global hydrogen production relies on processes that extract hydrogen from fossil fuel feedstock, as shown in Figure 1.1. It can be seen from the figure that 96% of global hydrogen production comes from fossil fuels (e.g., oil, natural gas, and coal). Among them, natural gas is the main raw material (>75% of production) and steam reforming (SR) of natural gas is the most frequently used method [9]. Specifically, 95% of the total H₂ produced in the United States utilises SR of natural gas as the main process/source [10].

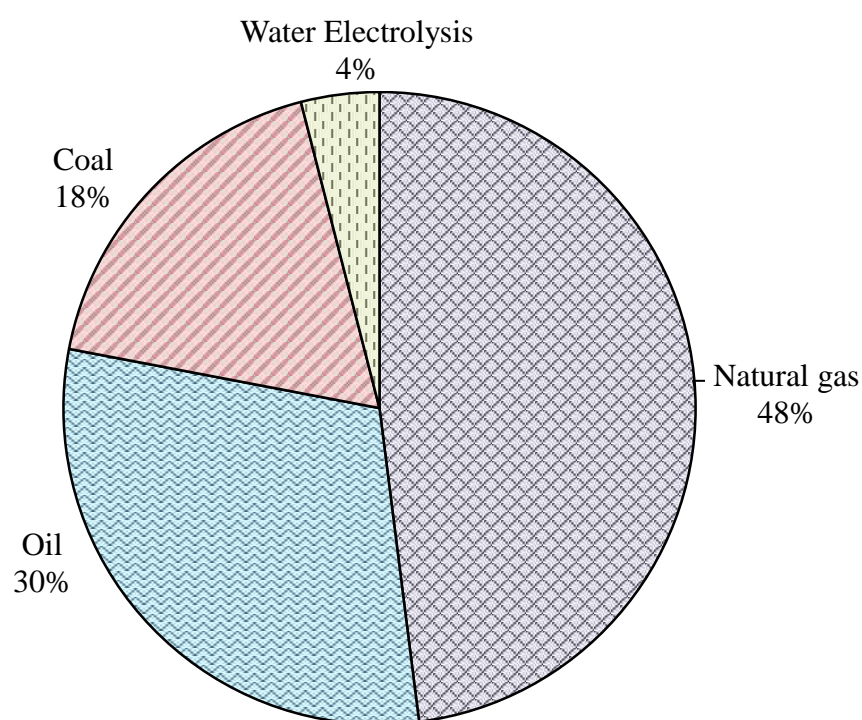


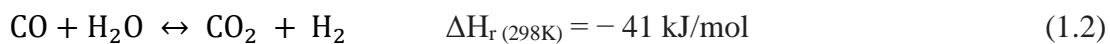
Figure 1.1: Feedstock used in the current global production of hydrogen [11]

The advantages of SR arises from the high efficiency of its operation and the low operational and production costs. The heat efficiency of hydrogen production by the SR process of methane on an industrial scale is approximately 70–85%. Natural gas and lighter hydrocarbons are the most frequently used raw materials [12].

The entire process is comprised of two main stages. In the first stage, methane is mixed with steam and fed into a tubular catalytic reactor. During this process, syngas (H_2/CO gas mixture) is produced, as shown in Equation 1.1 [6].



In the second stage, CO is converted to H_2 and CO_2 according to the water–gas shift (WGS) provided by Equation 1.2 [6].



Before feeding the natural gas to the reformer, it has to be desulphurised in order to avoid deactivation of the catalyst used. The desulphuriser can be removed if the natural gas feed is pure methane [13]. It is clear from Equation 1.1 that SR is a highly endothermic process. In order to achieve near-equilibrium conversion, SR in conventional technology is conducted on a supported nickel catalyst in a multitubular reactor operated at a temperature of 850°C, a pressure ranging from 1.6 to 4.1 MPa, and a steam-to-methane ratio between 2 and 4 [14]. Because the kinetics are rarely the limiting factor with conventional SR reactors, less expensive nickel catalysts are used on an industrial scale [12].

However, the purpose of the water–gas shift (WGS) is to reduce the carbon monoxide production and to optimise the production of hydrogen. The formula for the reaction, which is reversible and exothermic, is given by Equation 1.2. Typically, when high-purity H_2 is required, the WGSR is carried out in two stages. A high-temperature reaction stage operated at approximately 593–723 K and a low-temperature reaction stage operated at approximately 473–523 K [7]. Iron- and copper-based catalysts are commonly used in industry for the high- and low-temperature stages, respectively [15].

The product mixture from the WSGR (CO , H_2 , H_2O , and CO_2) is then passed either through a CO_2 -removal and methanation, or through a pressure swing adsorption (PSA), leaving H_2 with a high purity of near 100% [16]. PSA is the most widely used technology for hydrogen purification [17].

Membrane reactor (MR) technology plays an important role as an alternative solution to conventional systems in terms of the combination in a single stage of the reforming reaction for generating hydrogen and its purification, without needing any further processing/treatment [18].

In a conventional system, CO from the syngas is converted into CO_2 via two separate WGS reactors as mentioned above; most of the CO in the syngas is shifted to a high-temperature WGS reactor and the small remaining amount of CO is shifted to a low-temperature WGS reactor, in which the operating conditions favour higher-equilibrium CO conversion. Both the WGS reaction processes and the CO_2/H_2 separation process can be combined in a single catalytic membrane reactor (CMR) using a high-temperature WGS catalyst to achieve CO conversion levels higher than that of the two-step WGS reactor configuration. This is explained by the continuous removal of one of the reaction products through the selective membrane, which drives

the equilibrium of the WGS reaction (Equation 1.2) to the right [19]. If the membrane is H₂-selective, the product streams would consist of a low-pressure, high-purity H₂ stream and a high-pressure CO₂-steam stream [7].

Palladium-based membranes have been used as a component of catalytic membrane reactor technology. Different Pd and Pd-alloy membranes have been used in industrial settings, demonstrating outstanding performance suitable for their application in large-scale settings. The use of Pd-membranes permits the continuous elimination of hydrogen from the reaction district, varying the composition inside the system and thus permitting greater conversions. This process is called process intensification, and it has been shown for processes such as the WGSR and methane SR [20].

1.2 Scope and Objectives

The efforts of this research work will lead to the development of a CMR system for the synthesis of hydrogen from the WGSR. The specific objectives are as follows:

1. Construction of mathematical model: Building a two-dimensional (2D) mathematical model that describes the production of hydrogen using the WGSR.
2. Sensitivity analysis: Solving the model equations by using MATLAB and COMSOL software packages. Studying the effect of various operating parameters on the rate of hydrogen production.
3. Response surface method analysis: Statistical analysis of the investigated operating parameters to find the optimum operating conditions. Response surface methodology (RSM) in the Minitab software package can be used for this purpose.

The work consists principally of modelling and simulation; accordingly, most of the work will relate to the use of software packages. These software packages are available in the research laboratories of the Department of Chemical and Petroleum Engineering. The major software packages are

- 1) MATLAB
- 2) COMSOL
- 3) Minitab

1.3 Outline and Structure of the Thesis

Chapter 1 is dedicated to the introduction of the thesis, in which the overview, scope, and objectives of the thesis are presented.

A literature review of the main hydrogen production processes (conventional and renewable) and a comparison between them are summarised and presented in Chapter 2. An extensive literature involving the disadvantages of using conventional reactors for SR of methane (SRM) and the advantages of using a CMR is also presented. In addition, Chapter 2 reviews the available studies on the use of the WGS in a Pd-based MR.

Chapter 3 presents a detailed description of the 2D mathematical model developed to analyse and predict the conversion of CO and production of hydrogen using a WGS catalytic Pd-membrane reactor.

The performance of a WGS reactor with and without a membrane is presented in Chapter 4. The results of the tested 2D-axisymmetric CMR model under different operating conditions (S/C ratio, membrane thickness, hydrogen partial pressure at permeate and retentate sides, and residence time) are also analysed and discussed.

Most of the results were supported by the experimental data obtained from the available literature on experimental work conducted under the same operating conditions. The optimum operating conditions are also investigated.

Finally, Chapter 5 presents a summary of the results obtained and provides suggestions for further research involving Pd MRs.

Chapter 2: Literature Review

Hydrogen is the simplest and most abundant element on earth. It consists of two hydrogen atoms and has the chemical symbol H_2 . At standard temperature and pressure, hydrogen is a colourless and odourless gas. The name Hydrogen is Greek for 'water-former', and it was chosen because water is created when hydrogen is burned [12].

Hydrogen combines readily with other chemical elements, and it is always found as part of other substances such as natural gas, coal, oil, or water. It is also found in natural biomass, which includes plants and animals. For this reason, hydrogen is considered as an energy carrier [21]. It is not a primary energy source, but can be used to transport and provide energy. The costs and technical challenges associated with the production, storage, and distribution of H_2 are daunting [12].

Hydrogen is primarily used to create water. In addition, it is a major industrial product used in the production of many chemicals, mainly ammonia and methanol. Ammonia is the backbone of the fertiliser industry and is produced by a reaction between nitrogen and hydrogen. Ammonia consumes approximately 50% of all the hydrogen produced in the world [1].

Moreover, pure hydrogen can be used as a power generator. For example, hydrogen fuel cells produce electricity by combining hydrogen and oxygen atoms. This combination results in an electrical current. A fuel cell is two to three times more efficient than an internal combustion engine running on gasoline. During the combustion of H_2 in an engine or fuel cell, only water vapor is emitted. By contrast, the combustion of fossil fuels releases CO_2 , thereby increasing the atmospheric

concentration of this greenhouse gas. Therefore, hydrogen will play a key role in the necessary transition from fossil fuels to a sustainable energy system, and it is expected to become a significant fuel that will largely contribute to the quality of atmospheric air [7].

Other uses of hydrogen are in the food and chemical industries. The food industries use the element to make hydrogenated vegetable oils, such as margarine and butter. In this process, vegetable oils are combined with hydrogen, and by using nickel as a catalyst, solid fat substances are produced. Additionally, hydrogen is required in the petrochemical industry for crude oil refinement [1].

2.1 Hydrogen Production Processes

There is an enormous variety of processes available for H₂ production, which depend on the raw materials used. The process can be divided into two main categories, namely, conventional and renewable technologies. Figure 2.1 shows the various methods for hydrogen production [22].

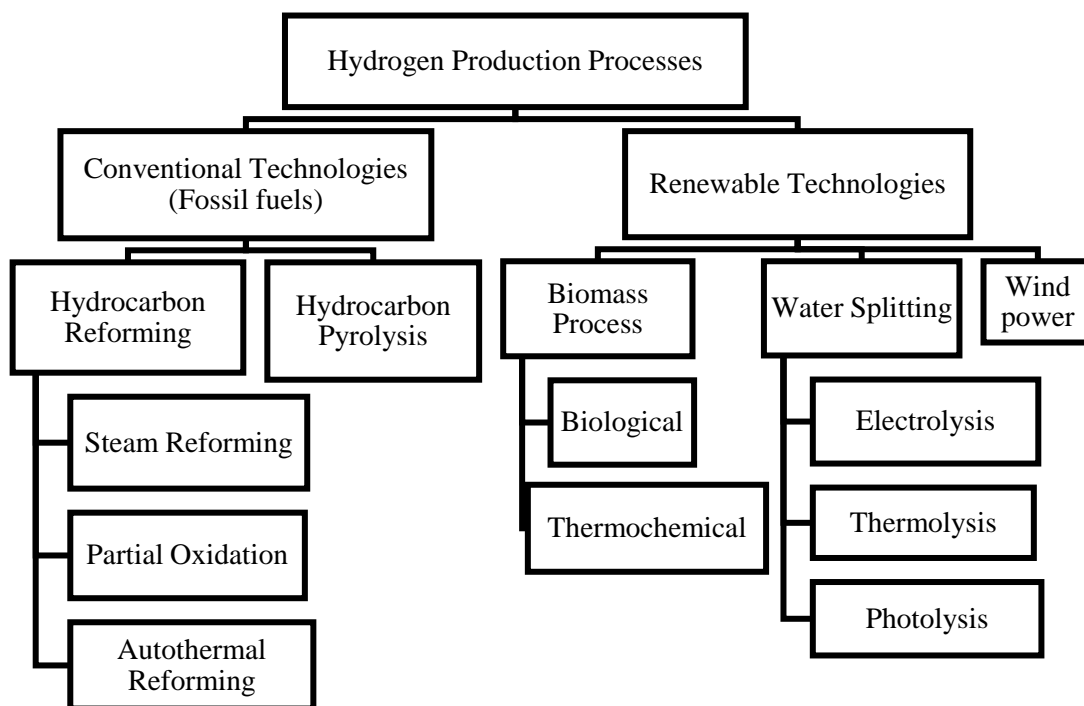


Figure 2.1: Hydrogen production processes [22]

2.1.1 Conventional Technologies

As shown in Figure 2.1, fossil fuels are the first category of processes, which includes the methods of hydrocarbon reforming and pyrolysis.

2.1.1.1 Hydrocarbon Reforming Methods

Hydrogen gas can be produced from hydrocarbon fuels through three basic technologies [22]:

- Steam reforming (SR).
- Partial oxidation (POX).
- Autothermal reforming (ATR).

These technologies produce a great deal of carbon monoxide (CO). Thus, in a subsequent step, one or more chemical reactors are used to largely convert CO into

carbon dioxide (CO₂) via the WGS, and this is followed by preferential oxidation (PrOx) or methanation reactions. In addition, most fossil fuels contain a certain amount of sulphur, the removal of which is a significant task in the planning of the hydrogen-based economy. As a result, the desulphurization process will take place as well [12].

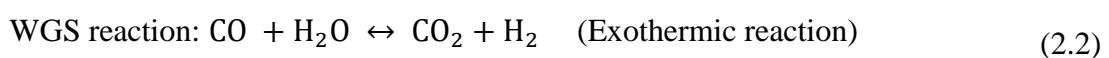
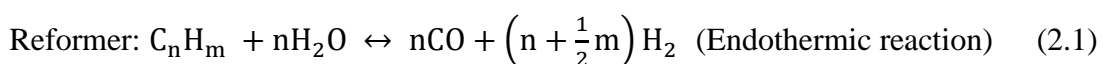
2.1.1.1.1 Steam Reforming Method

Most of the world's hydrogen is generated by SR of natural gas in parallel fixed bed reactors, followed by PSA for hydrogen purification. The SR of methane (SRM) is currently the most cost-effective and highly developed method for the production of hydrogen, with a relatively low cost and high hydrogen-to-carbon ratios that are desired for hydrogen production.

The SR of natural gas consists of three main steps [22]:

- Reforming or synthesis gas generation.
- WGSR.
- Methanation or gas purification (PSA).

The first two steps can take place in a series–parallel configuration, not in a separate reactor, i.e., the processes all occur in the same reactor if the conditions/catalyst are satisfied. Or the processes can each be dominant in one reactor, if the reaction conditions can be controlled for each reaction at once. The chemical reactions that take place in the reformer are shown in Equations (2.1)–(2.3) [23].



To protect the catalyst, which is usually based on nickel owing to its activity, ready availability, and low cost [23], natural gas has to be desulphurised before being fed to the reformer. Most fuels contain some amount of sulphur, with the exception of methanol. For this reason, desulphurisation is considered as a very important step in fuel processing technologies [12].

As shown in Equation 2.1, which is the reforming reaction, the natural gas is mixed with steam and fed into a tubular catalytic reactor to produce syngas (H_2/CO gas mixture); this can subsequently be converted to several valuable products such as methanol and ammonia. This reaction is strongly endothermic, and energy is supplied by the combustion of natural gas. Steam methane reforming (SMR) is the most common and developed method used for large-scale hydrogen production [22].

After this, the product gas is passed through a heat recovery step and fed into a WGS reactor (Equation 2.2) to decrease the CO content, while at the same time increasing the hydrogen content. The WGSR is moderately exothermic [22].

The WGSR is limited by the thermodynamic equilibrium at low temperatures; however, high temperatures are required to ensure the necessary reaction rates. In order to take advantage of both the thermodynamics and kinetics of the reaction, the industrial-scale WGSR is conducted in multiple adiabatic stages consisting of a high-temperature shift (HTS) followed by a low-temperature shift (LTS) with intersystem cooling, as shown in Figure 2.2. Typically, high temperature is desired in order to favour fast kinetics; however, it is thermodynamically limited, which results in the incomplete conversion of CO. This step is carried out in the 310–450 °C range with the use of an $\text{Fe}_3\text{O}_4/\text{Cr}_2\text{O}_3$ catalyst, resulting in a CO composition of approximately 2–4%. The high-temperature iron oxide-based catalyst is promoted with chromium oxide,

which increases the catalyst life by suppressing sintering. Iron oxide catalysts can tolerate low sulphur concentrations [12]. To shift the equilibrium towards hydrogen production, a subsequent LTS reactor (180–250 °C range) is employed to produce a CO exit composition of less than 1% using Cu/ZnO/Al₂O₃ catalysts [24].

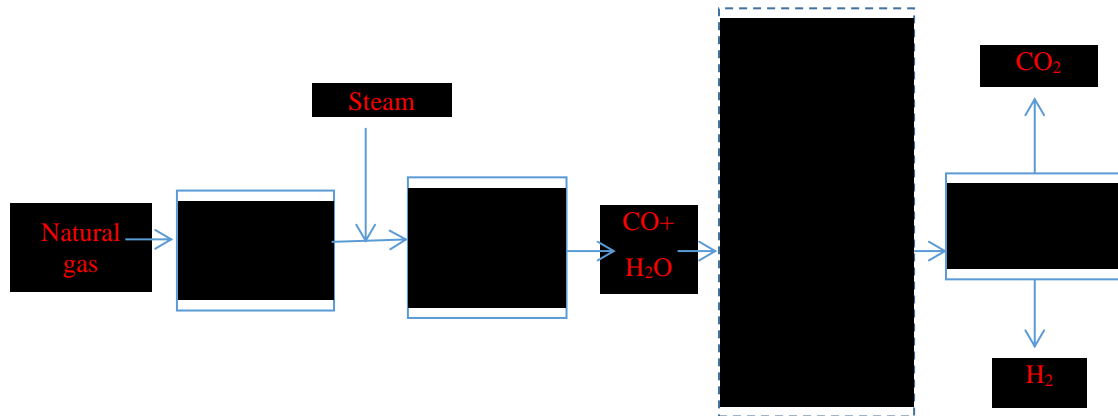


Figure 2.2: Diagram of methane steam reforming process [22]

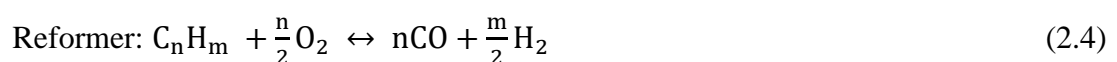
As shown in Figure 2.2, the overall product of the reaction passes either through a CO₂ removal and methanation, or through a PSA. PSA works by passing a gas mixture through a high-surface-area adsorber that has the ability to adsorb impurity gases whilst allowing hydrogen to permeate through the material. Impurity gas species are adsorbed onto an adsorbent material at high gas partial pressures and conversely desorbed at lower partial pressures. A common adsorbent material used is zeolite. The tail gas (low pressure) from PSA is usually utilised as a fuel at low pressures, which presents an economic benefit; however, high costs are incurred in compressing the tail gas, which is comparable to the cost of the PSA unit. Another drawback is the scale of the operation and infrastructure. PSA can be adapted for the medium-to-large industrial scale, but is impractical to use on smaller portable scales [25].

2.1.1.1.2 Partial Oxidation Method

Partial oxidation (POX) occurs when a sub-stoichiometric fuel–air mixture is partially combusted in a high-temperature reformer, creating a hydrogen-rich syngas, which is an exothermic process. Thus, it is considered more economical than the processes of SR or dry reforming, because it requires less thermal energy. The ideal reaction for the POX process is given in Equation 2.4 considering only hydrogen and CO as the main products. It is noticeable that other species may appear during the POX of the fuel; however, their final compositions are presumably small [2].

A difference is made between catalytic POX and non-catalytic (thermal) POX. The catalytic process, which takes place at approximately 950 °C, operates with feed stock ranging from methane to naphtha, whereas the non-catalytic process, which occurs at 1150–1315 °C, can operate with hydrocarbons including methane, heavy oil, and coal [16]. The choice of reforming technique depends on the sulphur content of the fuel being used. The catalytic process can be employed if the sulphur content is below 50 ppm. Higher sulphur contents up to 400 ppm can poison the catalyst, and thus, the non-catalytic procedure is used for such fuels [22].

After the desulphurisation process, pure O₂ is used to partially oxidise the hydrocarbon feed stock and the syngas produced is treated in the WGS reactor, which is referred to in Equation 2.2. The overall product from the WGSR is treated in the same way as for SR, where the produced is passed either through a CO₂ removal and methanation process (Equation 2.3), or through PSA.



Water is added to the process to obtain both the extreme temperatures as well as extra control of the formation of soot.

POX is the most appropriate technology to produce H_2 from heavier feed stock, such as heavy oil residues and coal [11]. Figure 2.3 illustrates the flow sheet for the POX method, where coal is used as the feed stock. The process is named coal gasification. The production of hydrogen from coal can generate large volume of this gas, because coal is the cheapest and most abundant natural resource. The difference between the POX of heavy oils and coal is that coal requires additional handling of the relatively unreacted fuel as a solid. In addition, removing large quantities of ash have a severe impact on the costs [22].

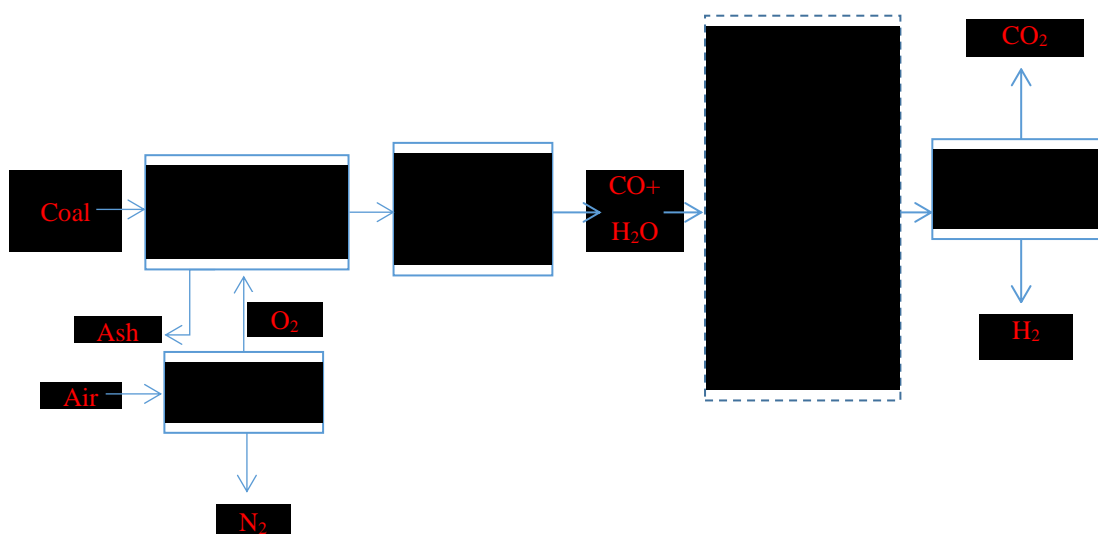


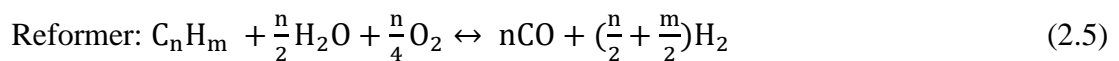
Figure 2.3: Flow diagram of the partial oxidation (or coal gasification) process [22]

The cost of the oxygen plant and the additional costs of desulphurization steps make such a plant extremely capital-intensive [26]. Nevertheless, the POX reforming of hydrocarbons produces a smaller concentration of hydrogen than that obtained from the SR. This is due to the fact that in the SR, the steam, as well as the hydrocarbons,

are split apart, whereas in the POX reforming, the amount of hydrogen that is split from the steam is much smaller [2].

2.1.1.1.3 Autothermal Reforming Method (ATR)

Autothermal reforming (ATR) combines POX and SR in a single process. The method uses the exothermic POX to provide the heat and endothermic SR to increase the hydrogen production. First, the steam and oxygen are injected into the reformer, causing the reforming and oxidation reactions to occur simultaneously, as shown in Equation 2.5 [27].



The process explained by Equation 2.5 is presented in Figure 2.4 as a simplified flow diagram for methane. The syngas produced is further treated in the same way as the product gas of the SR process. The advantage, though, is that it would have a thermally neutral system component, be more responsive than a SR reformer, and exhibit moderate cost, size, and weight requirements. However, a more extensive control system is needed for ATRs to ensure powerful operation of the fuel processing system. Moreover, ATR reactors consist of a thermal zone where POX occurs, which generates heat to drive the SR reactions in a downstream catalytic zone. The temperature profile has a sharp rise to the peak in the POX zone and then a decrease due to the endothermic reactions to a relatively low level in the SR zone. The non-uniform axial temperature distribution could cause the problem of so-called ‘hot-spots’. This problem is the cause of the technology’s risk and can reduce the catalytic effect [28].

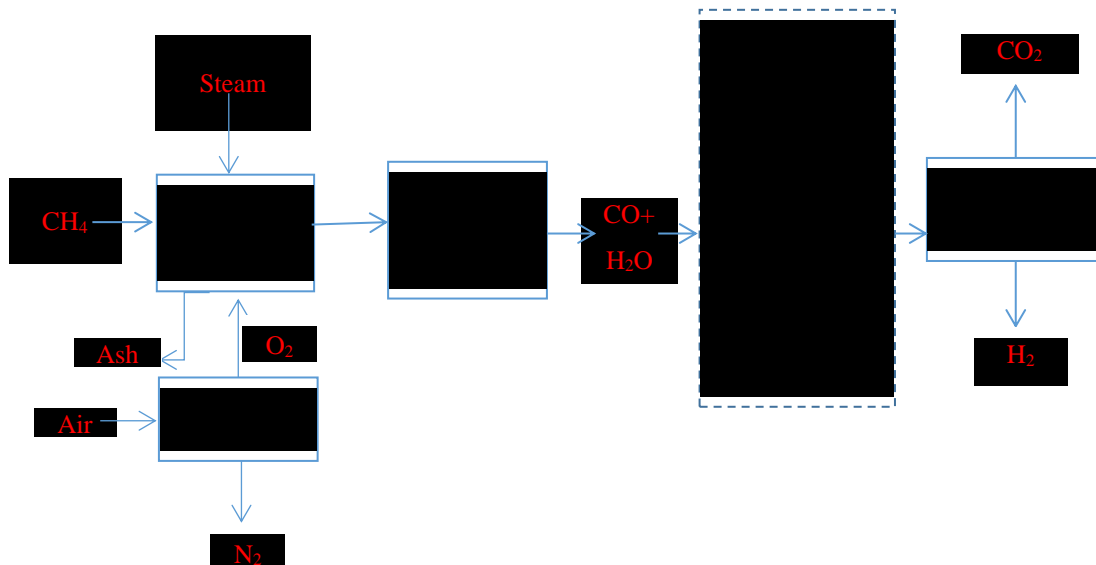


Figure 2.4: Flow diagram of the autothermal reforming of methane process [22]

2.1.1.2 Hydrocarbon Pyrolysis

Hydrocarbon (CHs) pyrolysis is a well-known process that involves the thermal decomposition of methane and other hydrocarbons in an air- and water-free environment with the production of hydrogen and elemental carbon. Equation 2.6 shows the general pyrolysis reaction [22]:



The energy requirement per mole of hydrogen produced by using hydrocarbon pyrolysis process is less than that for the SMR methods. This does not include WGS and PSA stages, or other CO₂ capture and storage steps. Hence, the capital investments for large plants are lower than for the processes of steam conversion or POX, resulting in 25–30% lower hydrogen production cost compared to that of the SMR process. If hydrogen is produced in the future using this process at a commercial scale, large amounts of carbon will be produced, and the price of hydrogen will be further reduced.

From an environmental point of view, it would be more advantageous to produce both hydrogen and carbon by the catalytic dissociation of natural gas, as opposed to the production of hydrogen by SMR coupled with CO₂ sequestration [29].

2.1.2 Renewable Technologies

Hydrogen generated from renewable sources is likely to play an important role as an energy carrier in future energy supply. As fossil fuels are declining and the greenhouse effect is attracting greater attention, renewable technologies will increase in the near future, and in the long term, they are expected to dominate over conventional technologies. There are many processes for H₂ production from renewable resources, and brief descriptions of some biomass-based technologies, along with approaches related to water splitting and wind power, are presented in this section [11].

2.1.2.1 Biomass Methods

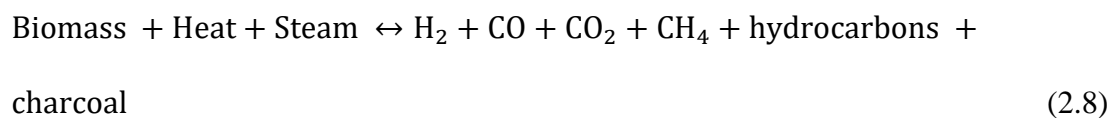
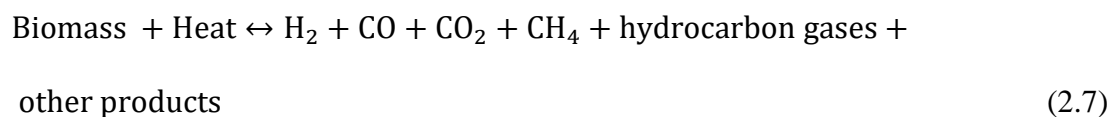
Biomass is a renewable source of primary energy derived from plant and animal materials. The most important biomass energy sources are wood and wood wastes, agricultural crops and their waste by-products, municipal solid waste, animal wastes, waste from food processing, and aquatic plants and algae [30]. Biological and thermochemical methods are the two modes for hydrogen production from biomass [22].

2.1.2.1.1 Thermochemical Methods

Thermochemical processes constitute the techniques through which biomass can be transformed into hydrogen and hydrogen-rich gases. Thermochemical

technology mainly involves pyrolysis and gasification. Biomass pyrolysis is the thermochemical process of generating liquid oils, solid charcoal, and gaseous compounds by heating the biomass at a temperature of 650–800 K under pressures of 0.1–0.5 MPa, as shown in Equation 2.7 [31]. It takes place in the total absence of oxygen, except in cases where partial combustion is allowed to provide the thermal energy needed for the process.

Biomass gasification (Equation 2.8) is the thermochemical conversion of biomass into a gaseous fuel (syngas) in a gasification medium such as air, oxygen, and/or steam. It takes place at high temperatures (above 1000 K) and operating pressures from atmospheric to 33 bar, depending on the plant scale and the final application of the produced syngas. Methane and other hydrocarbon vapours produced can be steam reformed (Equation 2.1) for further hydrogen production and in to this end, the WGSR (Equation 2.2) can be applied as well [31].



One of the major issues in biomass gasification is to deal with the tar formation that occurs during the process. In addition, the formation of ash may cause deposition, sintering, slagging, fouling, and agglomeration [32,33].

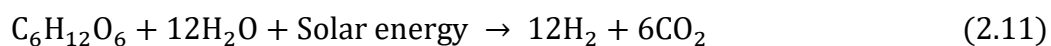
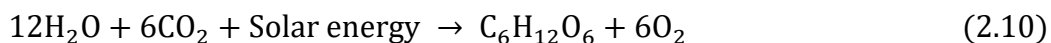
2.1.2.1.2 Biological Methods

Biological processes utilise renewable energy resources that are long-winded as well as various waste materials as feedstock [34]. The major biological processes utilised for hydrogen gas production are

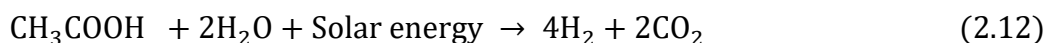
- 1- Direct bio-photolysis: a biological process that can produce hydrogen directly from water using a microalgae (green algae) photosynthesis system to convert solar energy into chemical energy in the form of hydrogen [35].



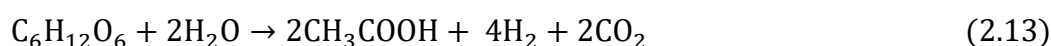
- 2- Indirect bio-photolysis: a biological process that can produce hydrogen from water using microalgae and cyanobacteria photosynthesis to convert solar energy into chemical energy in the form of hydrogen through several steps [31]:



- 3- Photo-fermentation: owing to the presence of nitrogenase, certain photosynthetic bacteria are capable of converting the organic acids into hydrogen and carbon dioxide using solar energy according to reaction 2.12. In recent years, some attempts have been made for hydrogen production from industrial and agricultural wastes to effect waste management [36].



4- Dark-fermentation: fermentation by anaerobic bacteria as well as some microalgae, such as green algae on carbohydrate-rich substrates, can produce hydrogen at 30–80 °C, especially in dark conditions. The products are mostly H₂ and CO₂ combined with other gases, depending on the reaction process and the substrate used. Equation 2.13 shows the reaction with glucose as the model substrate [22].



It is important to note that the direct and indirect bio-photolysis are still under active research and development, and have been applied only at the laboratory scale. Several factors are still crucial for further technological improvement. Hydrogen production by fermentation has higher stability and efficiency compared to hydrogen production by bio-photolysis. The fermentation process is more suitable at an industrial scale, because the operational cost is less as it uses a simple control system. It can utilise a variety of organic waste as substrates, and thus, hydrogen production can play a dual role: waste reduction and energy production [31].

To sum up, biological processes are more environmentally friendly and less energy-intensive, as they operate under mild conditions. On the contrary, they provide low rates and yields (mol H₂/mol feedstock) of hydrogen, depending on the raw materials used [22]. However, thermochemical processes are much faster and provide higher stoichiometric yields of hydrogen, with gasification being a promising option based on economic and environmental considerations [37].

2.1.2.2 Water Splitting

Water is one of the most abundant and unfailing raw materials on earth and can be used for hydrogen production through water-splitting processes. Water splitting is the general term for a chemical reaction in which water is separated into oxygen and hydrogen. Efficient and economical water splitting would be a key technological component of a hydrogen economy [22]. If the required energy input is provided from renewable energy sources, the hydrogen produced will be the cleanest energy carrier that could be used by humanity. Various techniques for water splitting have been reported, such as electrolysis, thermolysis, and photo-electrolysis [38].

2.1.2.2.1 Electrolysis

Electrolysis of water is the decomposition of water (H₂O) into oxygen (O₂) and hydrogen gas (H₂) by passing an electric current through water. The reaction is very endothermic and thus requires energy input in the form of electricity. A typical electrolysis unit consists of a cathode and an anode immersed in an electrolyte. Generally, when an electrical current is applied, water splits and hydrogen is produced at the cathode while oxygen is generated at the anode by the following reaction [39].



Although extremely pure hydrogen could be simply produced from water by electrolysis, the high consumption of electricity prevents the production cost from competing with other large-scale technologies (e.g., coal or natural gas) [40].

2.1.2.2.2 Thermolysis

Thermal decomposition or thermolysis is a chemical reaction by which water is heated to high temperature, generally above 2500 °C, until it decomposes into its atomic compounds hydrogen and oxygen.



Several thermochemical water-splitting cycles have been developed to lower the temperature and improve the overall efficiency. Thermochemical cycles consist of a series of chemical reactions at different temperatures and constitute one of the most promising process through which heat is converted into chemical energy in the form of hydrogen. Currently, the most promising low-temperature thermochemical cycles require temperatures at least 550 °C [22]. The high temperatures still required can be achieved by concentrating solar power through the use of solar collectors. By increasing the solar light intensity, energy efficiencies and rates of hydrogen produced increase as well [41].

It should be noted that, apart from the capital investment for the necessary equipment, criteria such as toxicity of the elements involved, availability and cost of chemicals, materials separation, and corrosion problems, are reflected in the H₂ production cost. For industrial or commercial applications, the material constraints have limited the success of applications for hydrogen production from direct thermal water splitting, with few exceptions [22].

2.1.2.2.3 Photolysis

Photo-electrolysis, or photolysis, integrates solar energy collection and water electrolysis into a single photo-electrode. Sunlight is absorbed through some semiconducting materials and the process of water splitting is similar to electrolysis. The semiconductor device acts as an electrode which absorbs solar energy and generates the necessary voltage to split water molecules. Photo-electrolysis is still in the experimental stage. Research is ongoing to make this process more efficient and to prevent semiconductors from corroding too quickly so that they can have a useful service life [12].

2.1.2.3 Wind Power

Wind power is currently utilised as a renewable power technology for generating electricity. It is one of the most cost-competitive renewable energy technologies available today, and in some places, it is beginning to compete with new fossil fuel electricity generation. By combining this electricity with water electrolysis, wind can provide hydrogen with few emissions and with very low consumption of petroleum. It is essentially emission-free, producing no CO₂ or criteria pollutants, such as oxides of nitrogen (NO_x) and sulphur dioxide (SO₂). However, wind energy is not free of problems. There are environmental and technical issues that must be dealt with. One of these drawbacks is that the wind power generation is not possible at all times, because it is strongly dependent on the weather. There are also some places where sufficient wind speed is not available [11].

2.2 Comparison of Hydrogen Production Technologies

In this section, a comparison of the major hydrogen production processes is presented. The advantages and disadvantages for each process are summarised in Table 2.1.

Table 2.1: Comparison of different hydrogen production processes

Processes	Advantages	Disadvantages
Conventional Technologies		
Steam Reforming (SR)	<ul style="list-style-type: none"> • Most developed and cost-effective technology. • High hydrogen-to-carbon ratios. 	<ul style="list-style-type: none"> • Dependence on fossil fuels. • Requires high temperature (endothermic process). • CO₂ is a by-product. • Requires hydrogen purification steps.
Partial Oxidation (POX)	<ul style="list-style-type: none"> • Exothermic system (no external heat is required). 	<ul style="list-style-type: none"> • Dependence on fossil fuels. • Heat generated needs to be removed or utilised in the system. • Oxygen plant and desulphurization steps make it extremely capital-intensive. • Produces lower concentration of hydrogen than SR. • CO₂ is a by-product. • Requires hydrogen purification steps.

Table 2.1: Comparison of different hydrogen production processes (Cont.)

Processes	Advantages	Disadvantages
Conventional Technologies		
Autothermal Reforming (ATR)	<ul style="list-style-type: none"> Thermally neutral system component (not requiring external heat). Moderate in cost, size, and weight requirements. 	<ul style="list-style-type: none"> Dependence on fossil fuels. More extensive control system is needed. Needs thermal zone where POX occurs. 'Hot-spots' can cause technological risk and reduce the catalytic effect. Lower hydrogen yield than SR. CO₂ is a by-product. Requires hydrogen purification steps.
Hydrocarbon Pyrolysis	<ul style="list-style-type: none"> Air- and water-free environment. Energy requirement is lower than SR method. No CO₂ emission. Does not include WGS and PSA stages. 	<ul style="list-style-type: none"> Dependence on fossil fuels. Carbon is a by-product.
Renewable Technologies		
Biomass Processes: Thermochemical process	<ul style="list-style-type: none"> Abundant and cheap feedstock. 	<ul style="list-style-type: none"> Built on a large scale [12]. Tar formation Varying H₂ content owing to seasonal availability and feedstock impurities.
Biomass Processes: Biological process	<ul style="list-style-type: none"> More environmentally friendly. Less energy-intensive. Operates under mild conditions. Photo-fermentation utilises variety of organic waste, and thus it reduces waste. Dark-fermentation can produce H₂ without light. 	<ul style="list-style-type: none"> Provides lower yields of hydrogen than thermochemical processes. Bio-photolysis still under active research and development. Requires large reactor volume.

Table 1.2: Comparison of different hydrogen production processes (Cont.)

Processes	Advantages	Disadvantages
Renewable Technologies		
Water Splitting	<ul style="list-style-type: none"> • Abundant feedstock. • No pollution with renewable sources. • O₂ is the only by-product. 	<ul style="list-style-type: none"> • High capital costs. • Low conversion efficiency. • Corrosive problems. • Still under development.
Wind Power	<ul style="list-style-type: none"> • Emission-free. • Most cost-competitive renewable energy. 	<ul style="list-style-type: none"> • Environmental and technical issues. • In some places, sufficient wind speed is not available.

From the above summary, it can be noted that most renewable resources are still under development and currently being researched. Although these methods are employed to produce H₂ without consuming fossil fuels or releasing CO₂, such techniques are not yet economically and technically feasible. Therefore, in the near term, fossil fuels are expected to be the dominant feedstock for H₂ generation [7].

Overall, regardless the type of process, hydrogen production via SR of natural gas is the preferred method on an industrial scale, owing to its low operational and production costs [5]. SR of methane (natural gas) is an important chemical operation in the worldwide energy matrix, as it accounts for approximately half the global hydrogen production [12]. Research and development programs are currently concerned with the development of small-scale technologies for SR of methane to enable distribution of hydrogen and improve delivery infrastructure.

2.3 Steam Methane Reforming in Conventional Reactor

As mentioned in Section 2.1.1.1.1, SR of methane (natural gas) consists of three steps:

- 1) Synthesis gas generation.
- 2) WGSR.
- 3) Methanation or gas purification (PSA).

By replacing n and m in Equation 2.1 by 1 and 4, respectively, we obtain



Syngas generation is followed by the WGSR and methanation or gas purification, which are given by Equations 2.2 and 2.3, respectively.



Syngas generation is a strongly endothermic reaction, whereas WGSR is moderately exothermic.

2.3.1 Operating Condition of Conventional Reactors

Product distribution is governed by various factors such as the type and temperature of the reactor, and the operating pressure and composition of the feed gas [23]. Owing to its endothermic character, reforming is favoured by high temperatures (up to 900 °C). In addition, because volume expansion occurs, low pressure is favoured (1–4 MPa). Moreover, the molar S/C ratios employed are in the range 3:1–5:1 [42]. In

contrast, the exothermic shift reaction is favoured by low temperature, whereas it is unaffected by changes in pressure [12].

2.3.2 Disadvantages of Conventional Reactor

In general, the conventional SR process has disadvantages such as high temperature gradient and low efficiency of the catalyst and catalyst coking. It is not possible to obtain satisfactory conversions of methane at moderate temperatures, because the reforming process is endothermic, and the thermodynamic equilibrium is limited by high temperature and low pressure [18]. Moreover, nickel has been the most suitable metal for SR of hydrocarbons, owing to its low cost and activity. The current SR catalysts are mainly nickel supported on refractory alumina and ceramic magnesium aluminate. These supports provide high crush strength and stability. However, coke formations and sulphur poisoning are two major problems associated with nickel catalysts [43]. Nevertheless, the aforementioned stages of hydrogen purification negatively affect the overall process in terms of costs and efficiency [44]. Therefore, efficient and economical methods of high-purity hydrogen production are needed. The development of membrane-based separation process could make it possible to increase the conversion efficiency of the process [45].

2.4 Steam Methane Reforming in Membrane Reactor.

Much attention has been paid to the development of alternative technologies to generate high-purity hydrogen. Among them, MR technology plays an important role as an alternative solution to conventional reactors. By combining MRs with H₂ generation from fossil fuels, further improvements occur in terms of efficiency, maximum operating temperature, and consequently, capital investments. Table 2.2

shows the major advantages and disadvantages of MRs [28]. When hydrogen is removed selectively from the reactor, the chemical balance goes to the product side and causes more methane to be converted to hydrogen and carbon monoxide [46]. The selective removal of hydrogen prevents the system from reaching the equilibrium conditions, and resulting in higher conversion rates at low temperatures. The main advantage of using membranes is a sharp drop in the reaction temperature from 900 °C to 500 °C [47].

Alamdari [45] compared the performance of the SMR in a packed bed reactor (PBR) and CMR with metal foam catalyst support. The effects of different variables such as pressure, reaction temperature, ratio of methane to steam in the feed stock, thickness of membrane, and sweep gas on the total methane conversion and hydrogen production were investigated qualitatively. The comparison was carried out over a temperature range of 350–750 °C and pressure range of 2–30 bar. Isothermal modelling has been performed and showed a higher performance of the MR than the PBR. The methane conversion can reach 100% for lower temperatures than used in industrial PBRs, and better performances are obtained with an increase in the operating pressure. Moreover, the maximum conversion of methane for the CMR is quickly reached, whereas the conversion evolution observed for the PBR is smoother. The optimum conditions for the CMR were obtained within the operating conditions ranges of temperature 565–600 °C, pressure ≥ 20 bar, thickness < 10 μm , steam-to-methane ratio $2 < m < 3$ and sweep factor $s \geq 10$.

Chibane and Brahim [6] investigated the optimal conditions leading to the improvement in the hydrogen production from methane SR reaction in a packed bed membrane reactor. The reaction was carried out in a Pd-membrane reactor at moderate temperatures and pressures and supported by a nickel catalyst (12%)/ γ Al_2O_3 with a mass of 11 g, as shown in Figure 2.5. An isothermal steady-state model was developed to simulate the operating parameters. The results obtained show that the conversion of methane was significantly enhanced by the removal of hydrogen from the reaction side under the following conditions: temperature ranging from 580–600 °C, pressure in the range 300–600 kPa, steam-to-methane ratio = 3, and sweeping ratio = 3. Under those conditions, the obtained H_2/CO ratio is satisfactory. Moreover, a nearly complete conversion of methane and a high hydrogen recovery were obtained.

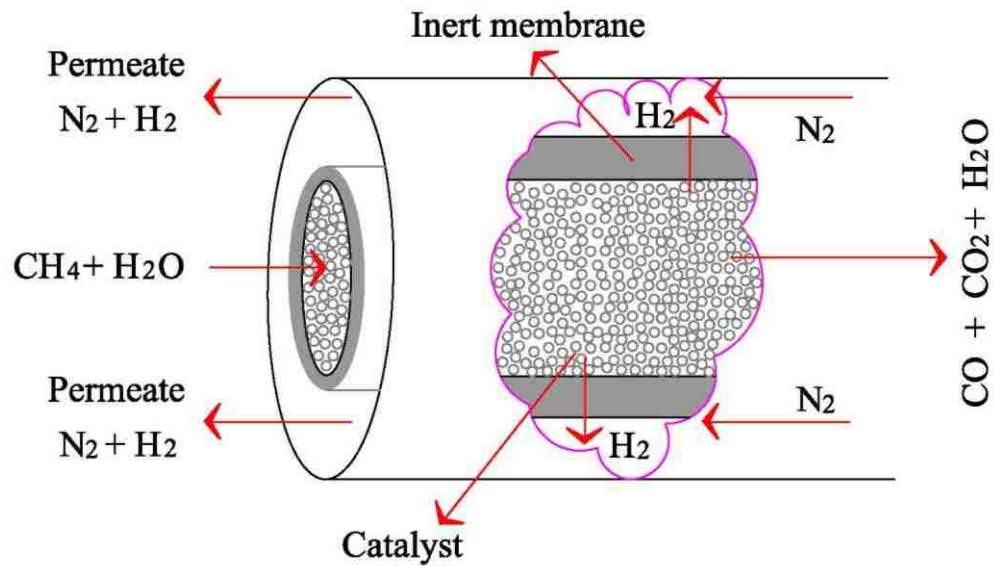


Figure 2.5: Schematic representation of membrane reactor [6]

Table 2.2: Some of the major advantages and disadvantages of membrane reactors

[18]

Advantages of MRs	Disadvantages of MRs
Compact unit in combining both reaction and hydrogen purification in a single stage without needing any further processing/treatment.	High costs and low mechanical resistance in case of dense palladium membrane reactors.
Higher conversions than conventional reactors (operated under the same MR conditions) or the same conversion of conventional reactors reached under moderate operating conditions.	In case of composite Pd-based MRs, the hydrogen production is not high.
In the case of a dense Pd-based MR, direct production of high-purity hydrogen in a single unit.	Contamination of H_2S , coke, CO , and so on, in the case of Pd-MRs.

2.4.1 Palladium-Based MRs

The membranes used in catalytic reactors are generally characterised by a high permeability, good selectivity of separation, and stability against the reaction temperature, particularly in the presence of gas [25]. Membranes can be divided into two classes: porous and dense. Dense metal membranes (e.g. Pd-based membranes) display extremely high levels of selectivity; however, the flux is low, whereas porous membranes have high rates of flux but very low selectivity. Therefore, the dense film is usually made extremely thin and is deposited onto asymmetric membranes [25]. Moreover, the transport mechanism for porous membranes is based on particle size. In order to achieve high selectivity, pores on the membrane need to be relatively small compared to the particles in the mixture [25]. However, the driving force of a dense membrane is based on the difference in hydrogen partial pressure between the feed and permeate sides of the membrane [7]. Another disadvantage of using a porous membrane is the phenomenon of membrane fouling, which causes a decline in flux over time. Chemical and thermal stability are also significant factors to consider when selecting porous materials, because temperature and concentration affects the selectivity and flux of the membrane [25].

Among hydrogen selective membranes, Pd membranes remain the most favourable. These were the subject of most of the studies, because they have high hydrogen-selectivity, and good mechanical and chemical stability. Moreover, they can be operated for long periods at high temperatures. On the contrary, a disadvantage of dense Pd membranes is their high cost. In an attempt to lower the membrane cost, Pd is typically alloyed with various elements, including Ag, Cu, and Au. In addition, alloying Pd not only reduces the material cost but also enhances the membrane

performance by increasing the H₂ flux, in addition to enhancing the mechanical strength and sulphur resistance, under certain conditions [7]. Further improvements can be made by reducing the Pd-membrane thickness to enhance the hydrogen flux. Reducing the membrane thickness can also decrease mechanical strength; therefore, the use of a support is required. Selecting and developing a suitable support for Pd alloy thin film membranes has become a growing area of interest, with the most famous options being porous stainless steel, alumina, and Vycor glass [25].

Oklany et al. [48] simulated the SR of methane by using two types of catalytic membranes: a dense Pd/Ag composite membrane and a series of microporous membranes. It was found that the Pd/Ag membranes showed better performance for all parameters investigated, including temperature, pressure, sweep ratio, and membrane thickness. The study showed that membrane thickness is strongly dependent on the permeability values of the Pd/Ag membranes.

Maneerung et al. [4] successfully developed and used a triple-layer hollow fibre catalytic membrane reactor (T-HFCMR) for H₂ production via the catalytic decomposition of methane reaction. T-HFCMR consists of (i) an ultrathin Pd-based membrane (inner) layer; (ii) a porous ceramic hollow fibre membrane support (middle) layer; and (iii) a Ni-based catalyst (outer) layer, as shown in Figure 2.6. As compared to a fixed-bed reactor, T-HFCMR showed better reaction conversions under the same operating conditions. For example, 49.5% CH₄ conversion was obtained from the T-HFCMR performed at the reaction temperature of 600 °C and reaction pressure of 1 bar, whereas only 39% CH₄ conversion was obtained with the fixed-bed reactor performed under the same reaction conditions.

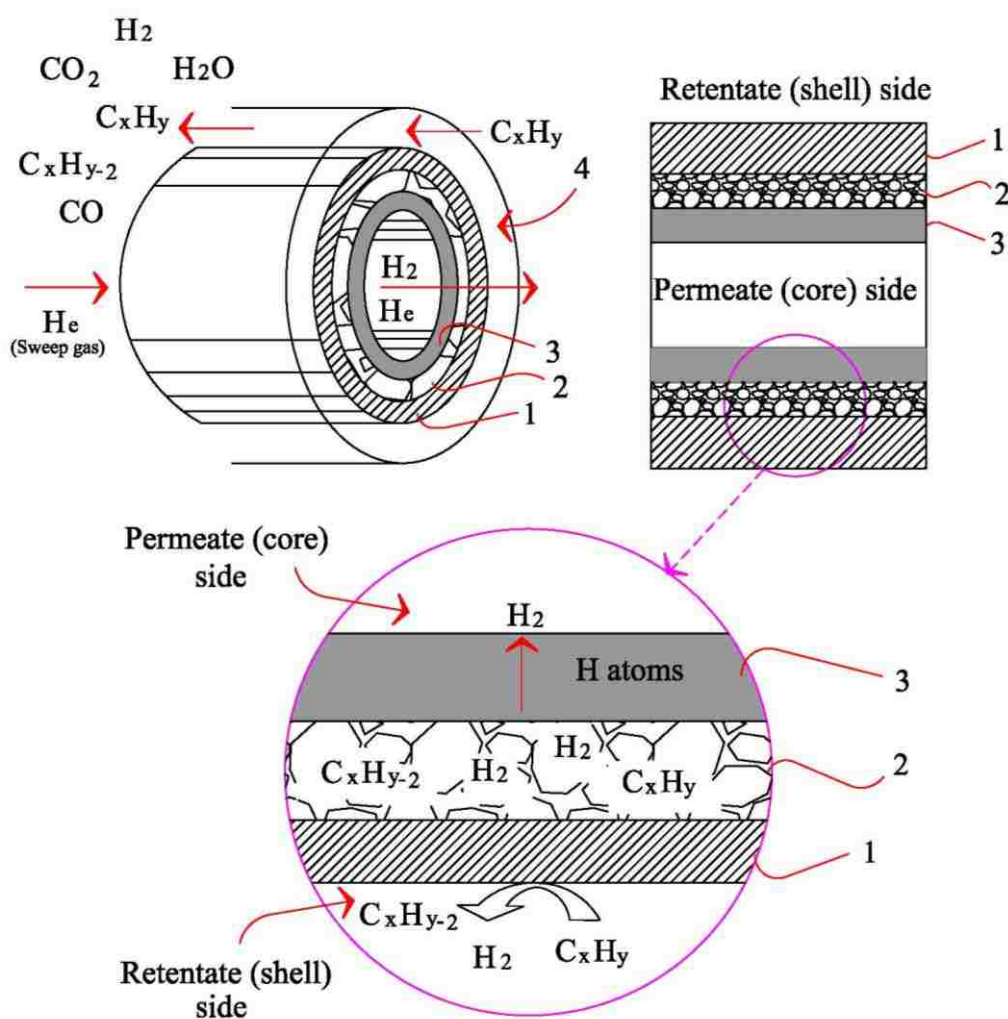


Figure 2.6: Schematic illustration of T-HFCMR [1. Ni-based catalyst layer; 2. porous ceramic support layer; 3. palladium-silver alloy membrane layer] [4]

The results showed that the amount of H₂ produced and recovered from the core side of the T-HFCMR is directly affected by temperature and pressure across the T-HFCMR. Moreover, owing to the high H₂ permeability of the ultrathin Pd-based membrane (1.2 μm), up to 84% of the total H₂ produced can be extracted from the reaction side at 600 °C and 2 bar. In addition, the reaction conversion is remarkably increased because of the constant permeation of H₂ from the reaction side. More particularly, an H₂ flux ranging from 0.06 to 0.15 mol m⁻² s⁻¹ with 80–90% of H₂

recovery and 95–99% of H₂ selectivity can be obtained from the T-HFCMR developed under different reaction temperatures ranging from 400 to 600 °C and reaction pressures ranging from 1 to 2 bar. Moreover, mechanical damage (e.g. scratching) of the Pd–Ag membrane can also be prevented as the Pd–Ag alloy membrane is not exposed directly to the external surface [4].

2.4.2 Water–Gas Shift Membrane Reactors

As mentioned before, SMR produces an effluent stream that is rich in CO and H₂. The produced CO is then combined with steam in a WGS reactor that converts the CO and steam to additional H₂ and CO₂.

WGS membrane reactor (WGSMR) combines the WGSR and the CO₂–H₂ separation processes into a single-unit operation. The use of a MR eliminates the need for traditional H₂ purification processes, such as PSA, because dense metal (Pd membrane) could result in H₂ recovery and purity levels as high as 99% and 99.9999%, respectively [49]. The high-pressure CO₂ in the retentate would then be injected into coal seams or oil or gas reservoirs, or deep-sea disposal. [50].

By changing the reaction conditions, such as pressure and temperature, the equilibrium of the reversible reactions can be shifted towards more product formation. The WSGR is an exothermic reaction, and thus, by increasing temperature, the equilibrium CO conversion decreases. The CO conversion can be enhanced at high reaction temperature by using a MR. This is achieved by extracting either CO₂ or H₂ from the reaction mixture, shifting the chemical equilibrium to more CO₂ and H₂ formation. When the Pd membrane is used, the high-purity H₂ extraction is accomplished at a lower pressure than the reaction pressure, because the rate of H₂

diffusion is proportional to H_2 partial pressure difference between the reaction and permeate sides [7].

The advantages of using WGS membrane reactors are summarised as follows:

- 1) Avoiding the need to cool the high-temperature methane-derived syngas stream to lower temperatures in an attempt to attain higher CO conversion in the WGS reactor.
- 2) The S/C ratio needed for the WGS in conventional reactor is significantly reduced by using a MR.
- 3) MR combines the chemical reaction and product separation into a single unit, eliminating the need for additional PSA purification equipment.
- 4) MR shifts the CO conversion above the equilibrium value, resulting in higher H_2 production.
- 5) The CO_2 produced is retained at high operating pressure owing to the complete selectivity of the membrane, which significantly reduces the power needed to recompress the CO_2 .

Iyoha. [7] studied the efficiency of 100wt% Pd and 80wt%Pd-20wt%Cu (Pd80wt%Cu) MRs placed immediately downstream of a coal gasifier to produce high-purity H_2 from coal-derived syngas by using the WGS. The work was conducted at 1173 K in a multitubular, 125- μ m thick Pd MR. The 3.175 mm OD, 125- μ m thick Pd tubes used each had an active membrane length of approximately 13 cm and internal radius of 0.146 cm, as shown in Figure 2.7. In order to maintain an isothermal reaction environment of 1173 K, a three-zone ceramic fibre heater with independent temperature control was used. The trans-membrane pressure differential was maintained at 241 kPa (35 psig) in the absence of heterogeneous catalyst particles.

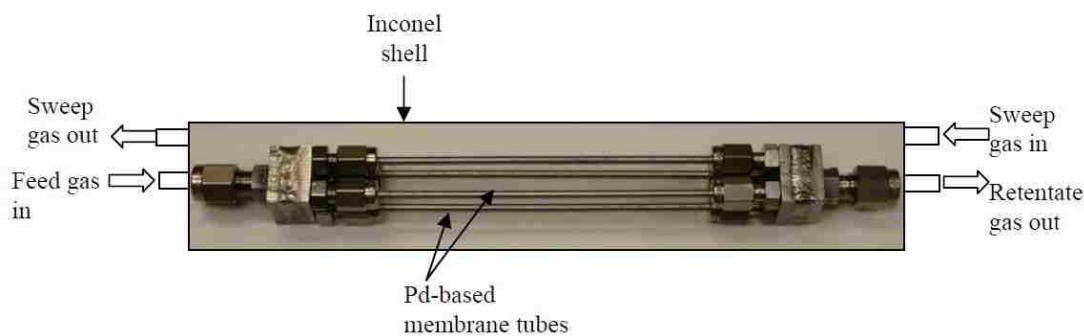


Figure 2.7: Detailed view of the four-tube Pd-based membrane reactor [7]

The rapid rate of H_2 extraction, and the long residence times (1–5 s), resulted in a dramatic shift in CO conversions of 93% at 1173 K and a steam-to-CO ratio of 1.5:1, which is well above the equilibrium value of approximately 54% associated with a conventional (non-membrane) reactor. When the Pd was replaced with Pd80wt%Cu, the CO conversion decreased from 93% to 66% and the hydrogen recovery decreased from 90% to 85% at a residence time of 5 s, owing to the lower permeance of the Pd80wt%Cu alloy. Moreover, the CO conversions increased with increasing steam-to-CO ratio in the 100% Pd MR system. A similar result was observed for the Pd80wt%Cu MR system; however, the CO conversions remained below the equilibrium conversion value because of the lower rate of H_2 extraction compared with the 100% Pd MR. Moreover, this performance would be enhanced if the membrane wall thickness were reduced.

Adrover et al. [3] analysed the influence of the WGSR operating pressure on the MR performance. The membrane consists of a dense Pd layer (selective to H_2) deposited on a porous ceramic support. The results indicated that an increase in the process gas pressure leads to a significant improvement in the CO conversion. In addition, the results obtained were compared with those corresponding to a reactor with no hydrogen permeation, which indicated that the conversion in the MR was

higher than that in conventional fixed-bed reactor owing to the shift in the equilibrium caused by hydrogen permeation.

Pinacci et al. [51] carried out a WGSR of a syngas mixture in a tubular Pd MR at a temperature of 410–414 °C. A composite Pd–porous-stainless-steel membrane of thickness 29 μm , obtained by electroless plating, was first extensively tested with pure gases (H_2 , He, and CO_2) and syngas mixtures in the 310–455 °C temperature range and in the 100–800 kPa feed pressure range. The MR, packed with a Fe/Cr commercial catalyst, was operated at a reaction pressure of 100–600 kPa in the counter-current mode, with a nitrogen sweep-gas, as shown in Figure 2.8.

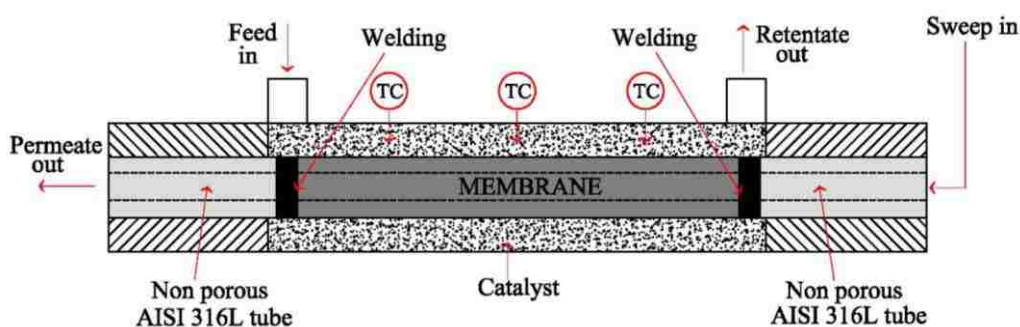


Figure 2.8: Scheme diagram for the tubular palladium membrane reactor [51]

The reactor was fed with a shift gas mixture with a 7.6% CO concentration and $\text{H}_2\text{O}/\text{CO}$ ratio in the range 2.7–3.6. The MR was able to achieve a CO conversion up to 85.0%, compared with a maximum conversion of only 37% obtained with a traditional reactor under the same operating conditions. Moreover, up to 82% of the hydrogen was recovered with a purity exceeding 97%.

Gosiewski et al. [52] simulated the WGSR in a MR applied for coal-derived gas processing and obtained high CO conversion in the reactor at S/C ratios of 2.0–

2.5. The simulations revealed that any present commercial catalysts are not directly appropriate for a one-stage membrane WGS reactor, owing to their overly narrow range of operating temperatures. The catalyst should withstand operation from approximately 200 to 550 °C. One disadvantage of this option is that the hydrogen is recovered on the low-pressure side, and thus, it should be compressed again for transport or possibly as supply for the majority of chemical syntheses.

Sanz et al. [53] used a laboratory reactor equipped with a Pd-composite (Pd thickness of 10.2 μm) for performing the WGS. The reaction experiments were carried out with and without the membrane under different operating conditions: $\text{H}_2\text{O}/\text{CO}$ ratio (1–3), temperature (350–400 °C) and gas hourly space velocity (GHSV) (4000–5500 h^{-1}). In all cases, the CO conversion was found to be higher when using the membrane to separate hydrogen comparing with the non-membrane reactor. In addition, the results concluded that this type of MR is capable of achieving high CO conversion (>99%) and hydrogen recovery (>99.5%), when operating with a GHSV of 1550 h^{-1} .

Morpeth and Michael [19] developed a 2D, axisymmetric computational fluid dynamics (CFD) model of a high-temperature WGS catalytic MR (HTWGS-CMR) using a commercial software package, FLUENT. The targeted operating reactor temperatures were from 350 °C to 450 °C. The optimum catalyst loading was found to be 11.6 $\text{kg}/(\text{CO}_{\text{mol}}/\text{s})$ for an inlet syngas temperature of 350 °C with a reactor having a 1' shell diameter. The CMR model was validated experimentally with a simulated coal-derived syngas (64.5% of CO, 33.0% of H_2 , and 2.5% of CO_2 with a 3:1 S:C ratio) at a total syngas flow of 4 $\text{L}_\text{N}/\text{min}$ and a feed pressure of 15 barg. These tests were performed using a prototype reactor incorporated with a tubular (0.1 mm thick, 150

cm², 3/8" OD) Pd/Ag23 wt% membrane. The catalytic MR schematic diagram used in this study is shown in Figure 2.9. The system consists of a tubular membrane inside a tubular shell with diameter D and length L . A commercial WGS high-temperature catalyst was packed in the annular space between the inner wall of the shell and the outer wall of the membrane [19].

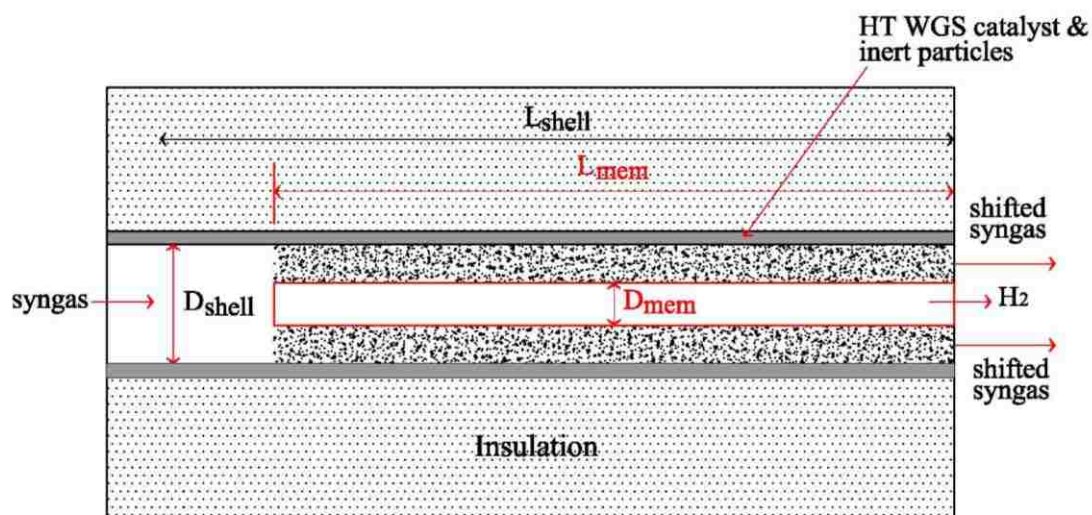


Figure 2.9: Schematic diagram of catalytic membrane reactor used [19]

There was a close agreement between the model and the experimental results. In general, higher CO conversion levels and H₂ yields can be achieved by increasing the inlet temperatures, loading more catalyst, increasing the H₂ permeation rate, reducing the pressure on the permeate side of the reactor, and reducing the S:C ratio. At the lower S:C ratio for a given total system pressure, the partial pressure of steam was reduced, and hence, the partial pressures of syngas gases species, including H₂, increased. As a result, the H₂ permeation rates were enhanced and higher hydrogen yields were obtained. Although the reduction of S:C ratio can improve the performance of the CMR, low S:C ratios up to a certain level can lead to carbon formation. Therefore, both the experimental tests and model simulations were undertaken with a

constant S:C ratio of 3:1 to avoid any possible carbon formation. Moreover, decreasing the pressure at the permeation side of the CMR is one of the effective ways to increase the CO conversion levels close to 100% [19].

Chen et al. [54] successfully developed a CFD model accounting for the WGSR in a Pd-based MR. The feed gas temperature and steam-to-CO molar ratio (S/C ratio) were in the ranges of 400–700 °C and 1–3, respectively. Under these investigated ranges of temperature and S/C ratio, the results showed that the CO conversion at high temperatures can be improved to 83% when the membrane is in the reactor compared to that without the membrane, achieving the breakthrough of the thermodynamic limit. As a result, the higher the feed gas temperature, the better the improvement in the CO conversion by the MR compared to that without the membrane. Moreover, in the MR, an increase in the S/C ratio facilitates pure H₂ production from the feed gas, and the optimal temperature is between 600 and 650 °C. However, more energy is consumed when the S/C ratio increases.

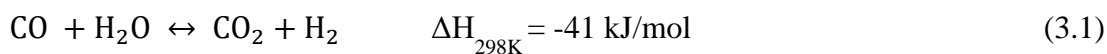
The literature review presented above shows that triggering the WGSR in a MR is able to separate H₂ and result in higher CO conversion. However, there is no extensive work taking into consideration the effects of different parameters on the rate of hydrogen production. Additionally, the studies on optimizing the parameters are very lacking. Keeping the above in mind, the current study has been conducted with the main objectives of development of a 2D, axisymmetric CMR to achieve a better understanding and optimization of the CMR performance under different operating conditions.

Chapter 3: Model Development

In this work, a 2D-axisymmetric MR model was developed to achieve a better understanding and optimization of the MR performance under different operating conditions. One of the main objectives of this reactor-optimization task is to run the MR within a targeted range of operating conditions to achieve the highest possible CO conversion.

3.1 Reactor Configuration

As mentioned before, the WGSR is a slightly exothermic reaction with equilibrium conversion decreasing with increasing temperature.



The model was developed to predict the experimental data for experiments conducted at 673 K in a double-tubular-type reactor with an iron-chromium oxide catalyst, which has been described elsewhere [55]. Briefly, the inner tube was fabricated from a palladium membrane with an outer diameter of 10 mm and the outer tube was made from a quartz tube with an inner diameter of 18 mm. The palladium membrane was of a composite structure consisting of a thin palladium film with a thickness of 20 μm supported on the outer surface of a porous-glass cylinder (mean pore size of 300 nm). The use of supported precious metal is preferred because of the high hydrogen flux requirement, which cannot be attained with most currently available dense metal membranes owing to their thickness. The active surface area of the palladium membrane for hydrogen separation was 25.1 cm^2 . The annular space

surrounding the membrane (reaction side) was filled with a commercial iron-chromium oxide catalyst, designed as Girdler G-3. The mass of the catalyst was 12.1 g and the height of the catalyst bed was 8 cm.

3.2 Model Development

The reactor geometry was constructed for a 2D-axisymmetric model using two software packages COMSOL and MATLAB to understand the function of the palladium MR. The model of the flow in the palladium MR is presented in Figure 3.1. The reactants flow in from the bottom of the reactor and after the catalytic reaction the products flow out of the top. The membrane is selectively permeable to H_2 , allowing H_2 to diffuse out of the reaction zone through the membrane walls, while being impermeable to the other components. A sweep gas, argon, was concurrently supplied to the permeation side to sweep the permeated hydrogen.

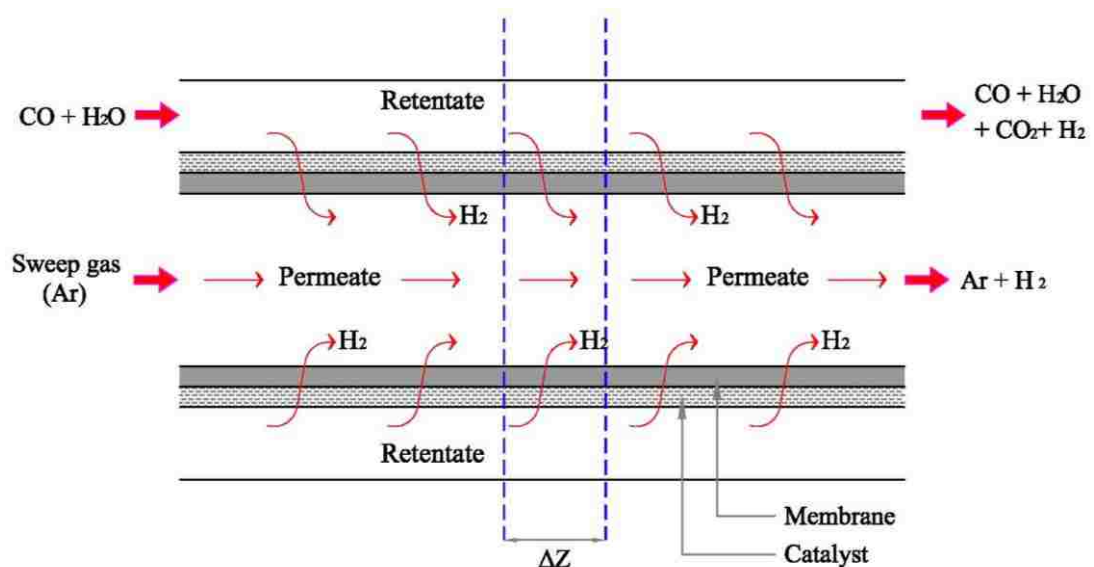


Figure 3.1: Schematic representation of gas flow model through reaction and permeation sides in palladium membrane reactor

3.3 Model Assumptions

The following assumptions were used in the modelling of the 2D catalyst MR:

1. The MR was assumed to operate in a steady state.
2. An isothermal environment was assumed.
3. The pressure drop was assumed to be negligible along the length of the membrane unit.
4. The flow was assumed to be a plug flow.
5. Co-current flow between the feed and permeate streams was assumed.
6. H₂ permeation across the membrane was based on the trans-membrane H₂ partial pressure difference.
7. The gases were assumed to obey the ideal gas law.
8. Complete selectivity of the Pd membrane reactor to H₂ was assumed.
9. The rate of hydrogen permeation was assumed to be unaffected by any of the coexisting gases and the reaction occurred only on the iron-chromium oxide catalyst, not on the palladium membrane.

3.4 Boundary Conditions

1. An axial symmetry boundary condition was used, where the flux at the centre (radius = 0) is equal to zero.
2. The inlet concentration for the reactants was equal to its initial concentration.

3.5 Governing Equations

3.5.1 Governing Equation Used in Shell (retentate) Side

The mass balances describing the transport and reactions in the shell side are given by diffusion–convection equation at steady state:

$$\nabla \cdot (-D_i \nabla c_i) + v \cdot \nabla c_i = \mathcal{R} \quad (3.2)$$

For cylindrical coordinates, Equation 3.2 can be written as

$$-D_i \left[\frac{\partial^2 c_i}{\partial r^2} + \frac{1}{r} \frac{\partial c_i}{\partial r} + \frac{1}{r^2} \frac{\partial^2 c_i}{\partial \theta^2} + \frac{\partial^2 c_i}{\partial z^2} \right] + \left[v_r \frac{\partial c_i}{\partial r} + \frac{v_\theta}{r} \frac{\partial c_i}{\partial \theta} + v_z \frac{\partial c_i}{\partial z} \right] = \mathcal{R} \quad (3.3)$$

where D_i is the inter-diffusion coefficient of species i , c_i is the species concentration, and V is the superficial velocity. The term \mathcal{R} corresponds to the reaction rate expression.

Under the plug flow assumption, the molecular diffusion term is cancelled from Equation 3.3:

$$\left[v_r \frac{\partial c_i}{\partial r} + \frac{v_\theta}{r} \frac{\partial c_i}{\partial \theta} + v_z \frac{\partial c_i}{\partial z} \right] = \mathcal{R} \quad (3.4)$$

$$\text{Molar flow rate } (F_i) = V c_i \quad (3.5)$$

$$\text{Thus, } \left[\frac{\partial F_i}{\partial r} + \frac{1}{r} \frac{\partial F_i}{\partial \theta} + \frac{\partial F_i}{\partial z} \right] = \mathcal{R} \quad (3.6)$$

- Mass balance for the CO component:

For CO, the convection flow is the dominant transport mechanism across the outflow boundary, that is,

$$\left[\frac{\partial F_{CO}}{\partial r} + \frac{1}{r} \frac{\partial F_{CO}}{\partial \theta} + \frac{\partial F_{CO}}{\partial z} \right] = -\mathcal{R} \quad (3.7)$$

The negative sign is added for the reaction because CO is one of the reactants

- Mass balance for the H₂O component:

The mass balance for the H₂O component is the same for the CO component, as shown below.

$$\left[\frac{\partial F_{H_2O}}{\partial r} + \frac{1}{r} \frac{\partial F_{H_2O}}{\partial \theta} + \frac{\partial F_{H_2O}}{\partial z} \right] = -\mathcal{R} \quad (3.8)$$

- Mass balance for the CO₂ component:

The mass balance for the CO₂ is given by

$$\left[\frac{\partial F_{CO_2}}{\partial r} + \frac{1}{r} \frac{\partial F_{CO_2}}{\partial \theta} + \frac{\partial F_{CO_2}}{\partial z} \right] = \mathcal{R} \quad (3.9)$$

The sign of the reaction is positive, because CO₂ is one of the products.

- Mass balance for the H₂ component:

For H₂, the flux term is considered in the equation, because part of the hydrogen is diffused across the membrane and the rest flows out from the retentate side.

$$\left[\frac{\partial F_{H_2}}{\partial r} + \frac{1}{r} \frac{\partial F_{H_2}}{\partial \theta} + \frac{\partial F_{H_2}}{\partial z} \right] = \mathcal{R} - J \quad (3.10)$$

The mechanism of H_2 permeation through Pd-based membranes has been investigated by many researchers. It has been found that H_2 permeates through the membrane via a solution–diffusion mechanism. The rate of H_2 permeation per unit area of the membrane is written in terms of Fick's first law as follows [55]:

$$j_{H_2} = \frac{Q}{t} \left[p_{H_2,ret}^n - p_{H_2,perm}^n \right] \quad (3.11)$$

where t is the membrane thickness, Q is the hydrogen permeation coefficient per unit area, $P_{H_2,ret}$ and $P_{H_2,perm}$ are the partial pressures of hydrogen in the retentate and permeate sides, respectively, and n is a constant indicating the pressure dependency.

The solution–diffusion model can be used to describe the transport mechanism of hydrogen through a dense metal membrane (Pd membrane). The model is involving the following sequential steps. These are, in order from the high-partial-pressure side to the low-partial-pressure side [56,57]:

1. Molecular transport from the bulk gas to the gas layer adjacent to the surface.
2. Dissociative adsorption onto the surface.
3. Transition of atomic H from the surface into the bulk metal.
4. Atomic diffusion through the bulk metal.
5. Transition from the bulk metal to the surface on the permeate side.
6. Associative desorption leading to H_2 molecules.
7. Diffusion from the surface into the bulk gas.

When the pressure exponent, n , is equal to 0.5, the rate-limiting step of the entire process of hydrogen permeation from the high-pressure side of the membrane to the low-pressure side is the diffusion of hydrogen through the bulk of the Pd, which is known as Sieverts Law [17].

For thinner membranes, the surface reaction is the rate limiting step and the n value will increase towards 1 [56].

It was observed by Uemiya et al. [55] that the rate of hydrogen permeation per unit length of catalyst bed through the membrane J_{H_2} ($\text{cm}^3/\text{cm}\cdot\text{min}$) is correlated to a hydrogen pressure order of 0.76. This means that the rate-limiting step is a combination of steps.

$$J_{H_2} = \frac{q}{t} \left[p_{H_2,ret}^{0.76} - p_{H_2,perm}^{0.76} \right] \quad (3.12)$$

where q is the hydrogen permeation coefficient per unit length of catalyst bed and it is determined to be 5.9×10^2 ($\text{cm}^3 \cdot \mu\text{m}) / (\text{cm}\cdot\text{min}\cdot\text{atm}^{0.76})$ [55].

Equation 3.12 is converted in terms of the concentration J_{H_2} ($\text{mol}/\text{cm}\cdot\text{min}$) by using ideal gas law:

The volume of one mole of ideal gas at STP is 22.4 L [59].

$$J_{H_2} = \frac{q}{t} \left[c_{H_2,ret}^{0.76} - c_{H_2,perm}^{0.76} \right] \quad (3.13)$$

where $q = 1.1 \times 10^2$ ($\text{mol}^{0.24} \cdot \mu\text{m} \cdot \text{cm}^{2.28}) / (\text{min}\cdot\text{cm reactor length})$.

The general WGSR occurring on an iron-based catalyst is given by Kodama et al. [58]. The rate equation \mathcal{R} (cm³/cm·min) at 673 K is determined by Uemiya et al. [55] as follows:

$$\mathcal{R} = k \frac{P_{\text{CO}} P_{\text{H}_2\text{O}} - K_p^{-1} P_{\text{CO}_2} P_{\text{H}_2}}{1 + 4.4 P_{\text{H}_2\text{O}} + 13 P_{\text{CO}_2}} \quad (3.14)$$

where P_i is the partial pressure of component i , K_p is the equilibrium constant, which is equal to 11.92, and the rate constant k is determined to be 5.4×10^3 (cm³) / (cm·min·atm) per unit length of catalyst bed at 673 K [55].

Equation 3.14 is converted in terms of the concentration \mathcal{R} (mol/cm·min) by the ideal gas law [59]:

$$\text{Molar volume (1 mol / 22.4 L) and } c_i = \frac{P_i}{RT}$$

where $R = 0.08206$ (L·atm) / (mol·K).

$$\mathcal{R} = k \frac{c_{\text{CO}} c_{\text{H}_2\text{O}} - K_p^{-1} c_{\text{CO}_2} c_{\text{H}_2}}{1 + 2.4 \cdot 10^5 c_{\text{H}_2\text{O}} + 7.2 \cdot 10^5 c_{\text{CO}_2}} \quad (3.15)$$

where $K_p = 11.92$ (dimensionless) and $k = 7.4 \times 10^8$ in units of (cm⁶)/(mol · min · cm reactor length) at 673 K.

3.5.2 Governing Equation Used in Tube (permeate) Side

On the permeate side, the material balance is performed only for two components, which are hydrogen and the sweep gas (argon).

- Mass balance for H₂ component:

From Equation 3.10, the reaction side is cancelled as there is no reaction on the permeate side and only the diffusion is considered:

$$\left[\frac{\partial F_{H_2}}{\partial r} + \frac{1}{r} \frac{\partial F_{H_2}}{\partial \theta} + \frac{\partial F_{H_2}}{\partial z} \right] = J \quad (3.16)$$

A positive sign for the flux is given because hydrogen was diffusing from the retentate side towards the permeate side.

- Mass balance for argon component:

As there was no reaction on the permeate side, and thus this term is cancelled from Equation 3.6, as shown below:

$$\left[\frac{\partial F_{Ar}}{\partial r} + \frac{1}{r} \frac{\partial F_{Ar}}{\partial \theta} + \frac{\partial F_{Ar}}{\partial z} \right] = 0 \quad (3.17)$$

Chapter 4: Results and Discussion

In this chapter, the results of the developed model for simulating the performance of the Pd MR for the WGSR and the analysis of the outcomes are presented. The results are presented in terms of the concentrations and molar flow rates for all reaction species (CO, CO₂, H₂O, and H₂), in addition to the CO conversion along the reactor length.

4.1 Effect of Using Membrane on CO Conversion

A MR is a device in which a chemical reaction and hydrogen separation are carried out simultaneously to simplify the hydrogen production process. The driving force for hydrogen transportation through a membrane is the hydrogen partial pressure difference between the two surfaces of the palladium membrane. If the membrane used is highly selective to hydrogen, the hydrogen can be directly recovered during the reaction, eliminating the need for additional product purification steps, thus resulting in a more compact design and a greater conversion efficiency [17].

Figure 4.1 provides an overview of the molar flow rates of CO, H₂O, H₂, and CO₂ along the reactor length without using a membrane at a temperature of 673 K, pressure of 2 atm, argon flow rate of 400 cm³ min⁻¹, and S/C ratio of 1. The results show that the flow rates of CO and H₂O decrease rapidly to a value of approximately 2.47×10^{-4} mol/min, at which the flow rate remains constant. This corresponds to a CO conversion of 77.5%. On the contrary, the flow rates of CO₂ and H₂ increase to a value of 8.53×10^{-4} mol/min, at which the flow rates remain stable.

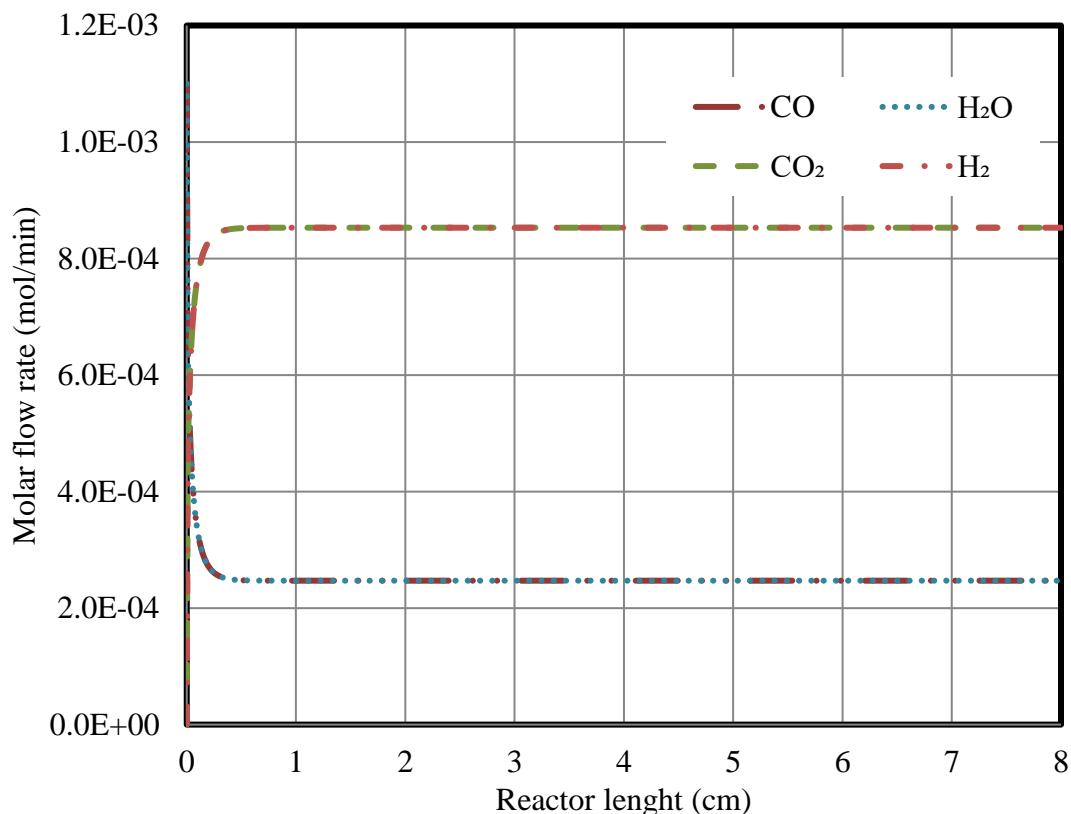


Figure 4.1: Species molar flow rates as a function of distance for the water–gas shift reaction without the palladium membrane

The hydrogen surface plot concentration generated by COMSOL Multiphysics software package is depicted in Figure 4.2. The figure illustrates the impact of using the membrane on the WGS species, at temperature of 673 K, retentate pressure of 2 atm, argon flow rate of $400 \text{ cm}^3 \text{ min}^{-1}$ and steam to ratio of 1. The hydrogen concentration increases along the membrane reactor due to increase in reaction rate and the continuous production rate of hydrogen. After certain length in the reactor, the concentration of the hydrogen is reduced in the reaction side because the high diffusivity of hydrogen through the permeable membrane. The hydrogen gas permeated through the palladium membrane to the shell side is continuously swept by argon gas to maintain its concentration to minimum and to maintain the highest possible concentration gradient and hence continues permeation of hydrogen and

hereafter the increase in CO conversion. The arrows display the hydrogen permeation pathway, from the reactor tube side through the membrane to shell side.

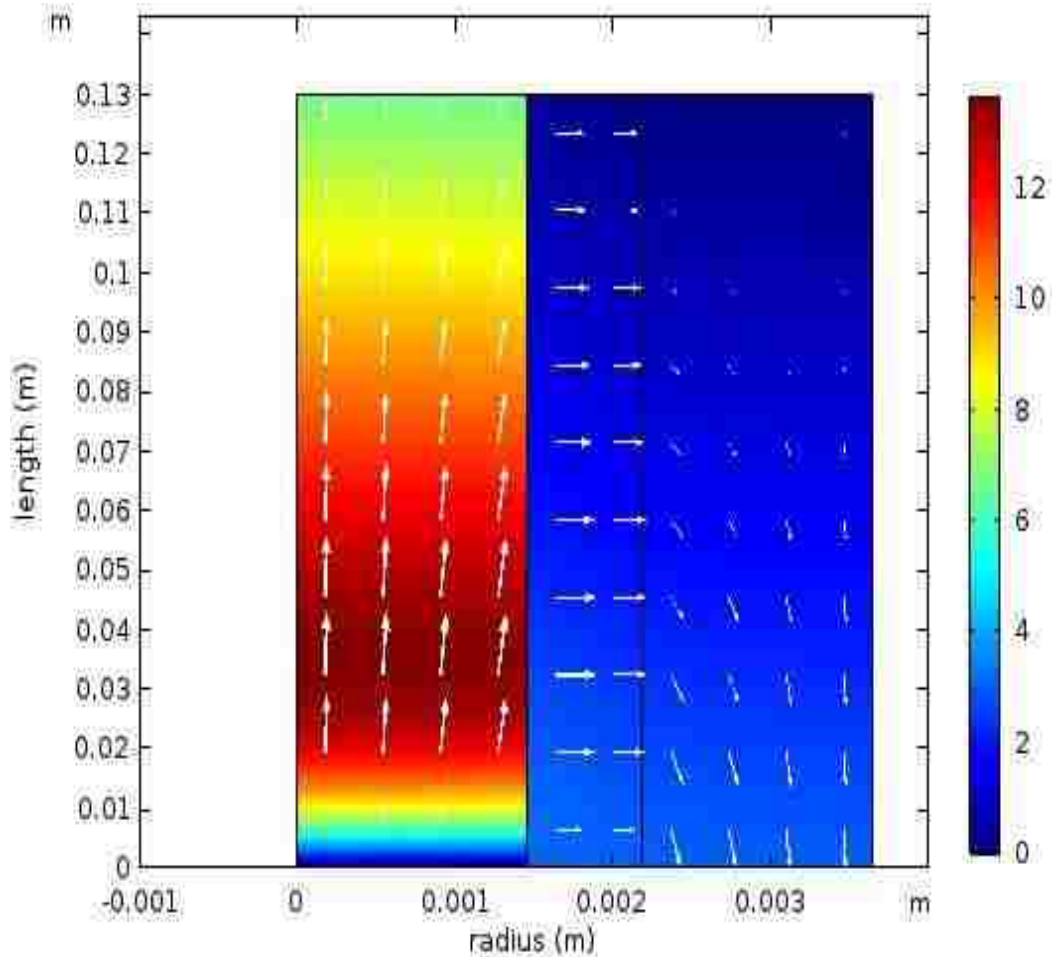


Figure 4.2: Surface plot for the hydrogen concentration (mol/m^3) in the presence of palladium membrane

Figure 4.3 compares the conversion of CO with and without the membrane. As might be expected, it is very clear from the data that the CO conversion of the MR is higher than that of the non-membrane reactor. As shown from the figure, the highest conversion reached by using the membrane is 93.7% compared with only 77.5% for the non-membrane reactor. The enhancement in the CO conversion and the reduction in the hydrogen flow rate on the retentate side after using the membrane (as shown in Figure 4.2) is due to the improvement in hydrogen selectivity through the membrane.

The membrane continuously removed the produced H_2 from the reaction zone and therefore increased the driving force across the membrane, shifting the chemical equilibrium towards the products side.

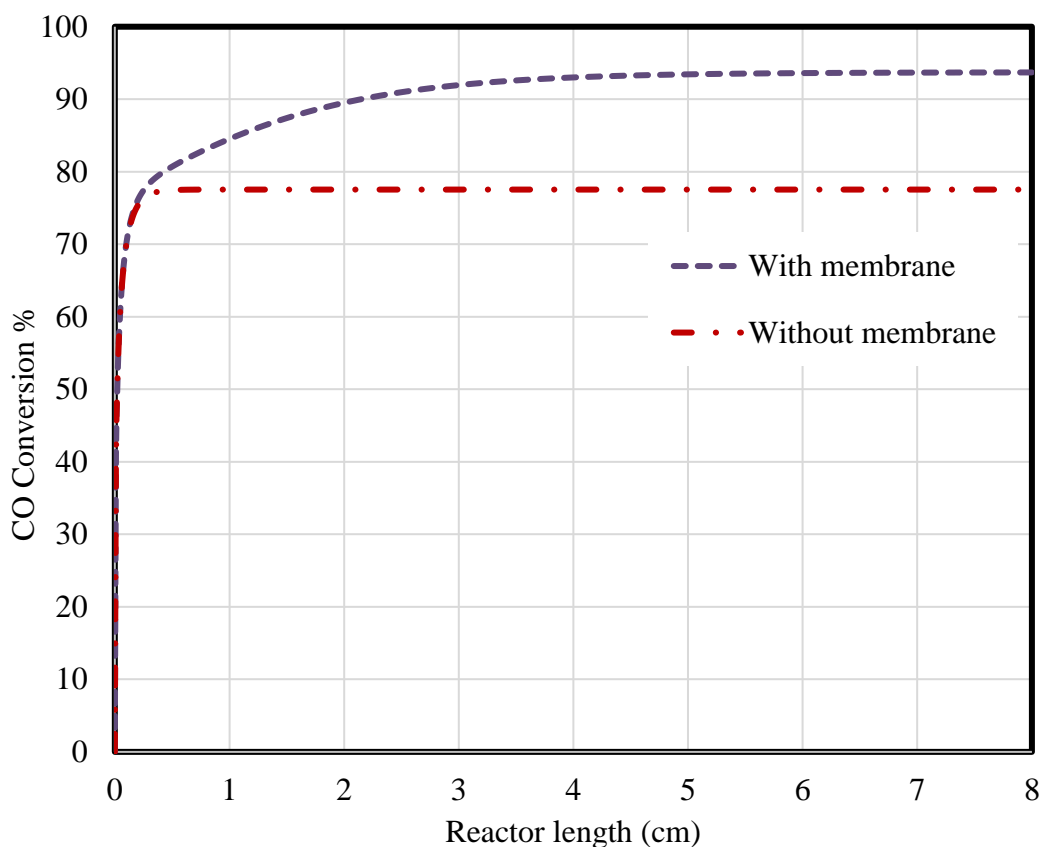


Figure 4.3: Change in CO conversion with and without the membrane along the reactor length

4.2 Effect of Steam to Carbon Ratio (S/C)

Figures 4.4–4.9 illustrate the axial concentration profiles of the WGSR components obtained along the centre of the reactor for S/C ratios of 1, 2, 3, 4, 5, and 6 respectively. The effect of the molar S/C ratio was examined under a temperature of 673 K, retentate pressure of 2 atm, and sweep argon flow rate of $400 \text{ cm}^3 \text{ min}^{-1}$.

Figure 4.4 demonstrates the effect of a S/C ratio of 1 on the concentrations of CO, CO₂, H₂O, and H₂. As an overall trend, the concentrations of CO and H₂O decrease along the reactor length until a value of approximately 1.18×10^{-6} mol/cm³, at which the concentration remains almost constant. However, the opposite trend of variation is observed for CO₂. The concentration increases until a value of 1.68×10^{-5} mol/cm³, at which the slope becomes almost zero. In addition, it is important to point out that the concentration of H₂ increases along reactor length until it reaches a maximum concentration of 1.16×10^{-5} mol/cm³, and this followed by a gradual decline until the concentration remains constant at a value of almost 9.08×10^{-7} mol/cm³. The increasing of H₂ concentration followed by a decrease in its concentration results from increasing H₂ permeation through the membrane due to an increase in H₂ production, leading to a higher H₂ concentration in the retentate, which results in a higher H₂ driving force.

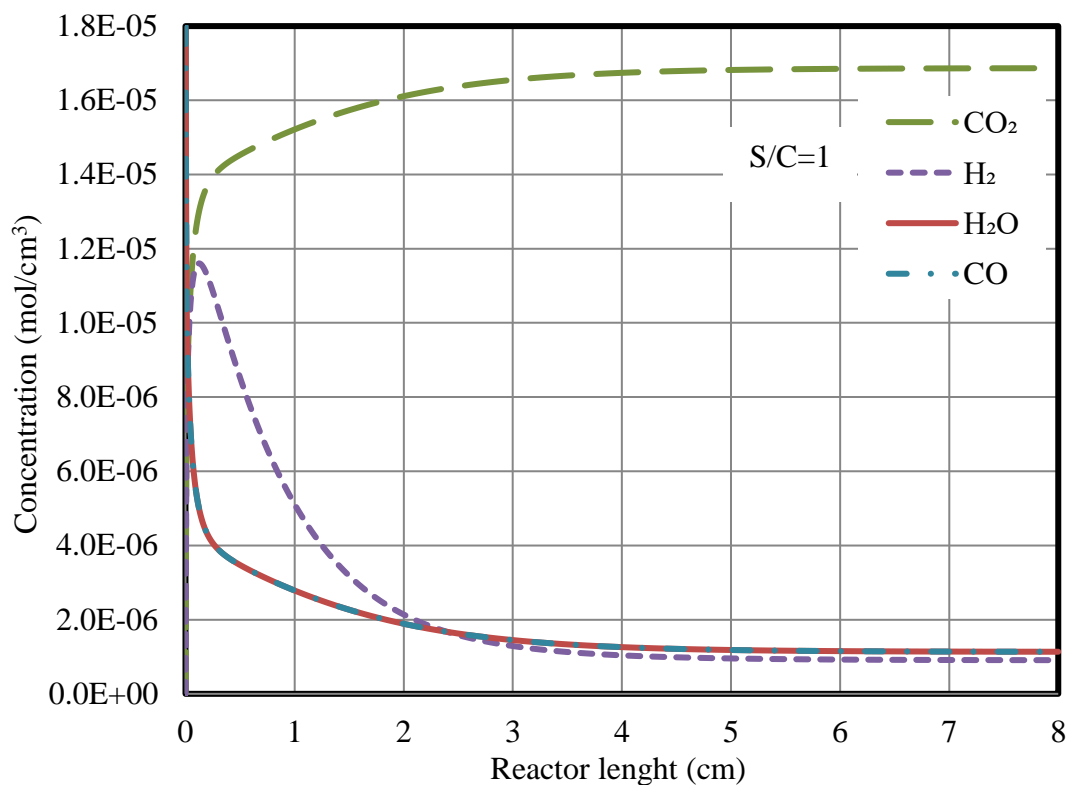


Figure 4.4: Effect of S/C ratio = 1 on the CO, CO₂, H₂O, and H₂ concentrations

The effect of a S/C ratio of 2 is illustrated in Figure 4.5. It can be seen that by increasing the S/C ratio from 1 to 2, the rate of CO conversion increases as well. Thus, CO concentration declines from a value of approximately 1.18×10^{-6} mol/cm³ (S/C = 1) to a value of almost 9.30×10^{-8} mol/cm³ (S/C = 2). Similarly, the CO₂ concentration decreases from a value of 1.68×10^{-5} mol/cm³ (S/C = 1) to 1.19×10^{-5} mol/cm³ (S/C = 2). The decrease in the CO₂ concentration is due to excess steam, which is expected to dilute the CO₂ concentration in the reaction zone. However, the H₂ concentration rapidly increases until it reaches a peak at a value of 9.48×10^{-6} mol/cm³, followed by a steady decrease until the concentration remains stable at a value of approximately 9.12×10^{-7} mol/cm³. The excess steam caused a reduction in the H₂ concentration on the reaction side. This can be seen by comparing the values obtained for S/C ratios of 1 and 2. The peak value of hydrogen decreased from a value of 1.16×10^{-5} mol/cm³

(S/C ratio of 1) to $9.48 \times 10^{-6} \text{ mol/cm}^3$ (S/C ratio of 2). Additionally, the concentration of hydrogen after entering the period of stability is $9.12 \times 10^{-7} \text{ mol/cm}^3$, which is slightly higher than that obtained for a S/C of 1 ($9.08 \times 10^{-7} \text{ mol/cm}^3$). This is due to the reduction in the driving force coming from the excess steam, which diluted the hydrogen on the reaction side.

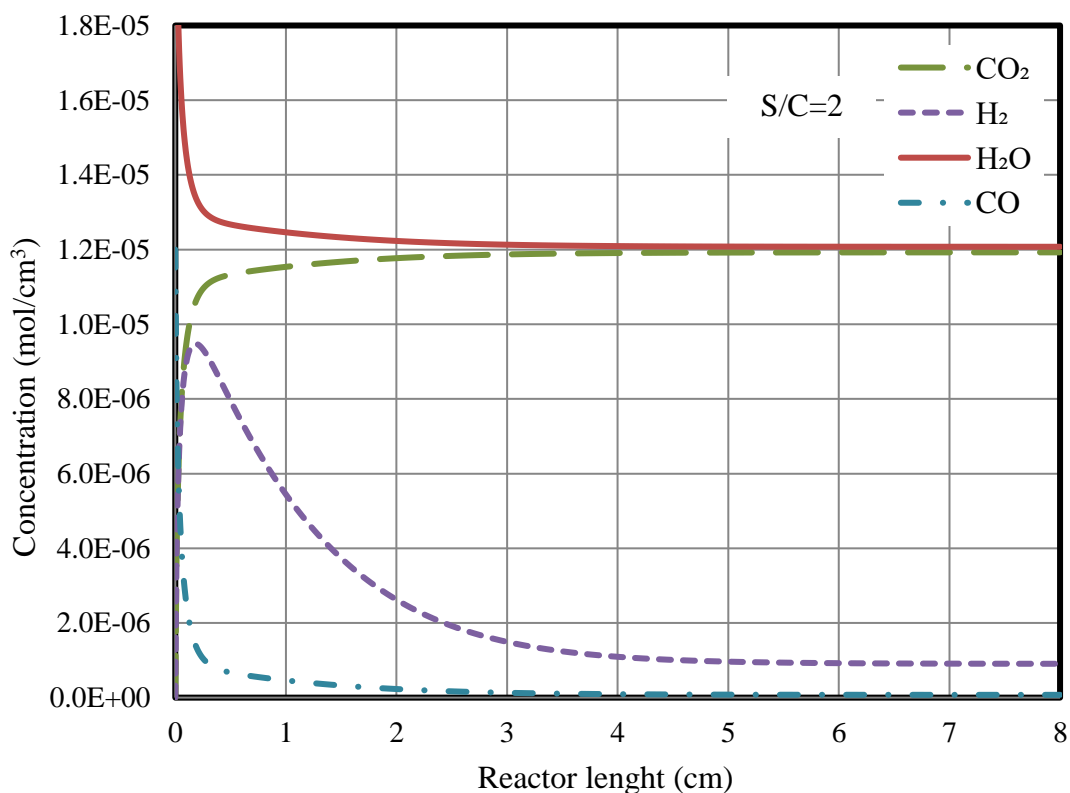


Figure 4.5: Effect of S/C ratio = 2 on the CO, CO₂, H₂O, and H₂ concentrations

As the S/C ratio further increases the rate of CO conversion also increases more, and as mentioned before, the extra steam causes a dilution in the concentration of both CO₂ and H₂ on the retentate side, which leads to a reduction in the concentrations. This difference can be determined by comparing Figure 4.6 with Figures 4.5 and 4.4. The results reveal that the concentration of CO decreases rapidly to a value of approximately $5.34 \times 10^{-8} \text{ mol/cm}^3$, at which the concentration enters a

period of stability. As expected, the value of the CO concentration obtained for a S/C ratio of 3 is lower than the values obtained for S/C ratios of 1 and 2. Additionally, the CO₂ concentration increases until the concentration stabilised at a value of 9.05×10^{-6} mol/cm³, which is lower than the values obtained for S/C ratios of 1 and 2. In addition, the concentration of the hydrogen rises rapidly until reaching a peak value of almost 7.58×10^{-6} mol/cm³ and this is followed by a declining trend until it remains stable at 9.14×10^{-7} mol/cm³. As predicted, the hydrogen concentration at the peak point decreased more for a S/C ratio of 3 than for 1 and 2. The reduction in hydrogen concentration caused the driving force to decrease and thus the concentration of hydrogen after entering the period of stability gradually increases from a value of 9.12×10^{-7} mol/cm³ (S/C = 2) to 9.14×10^{-7} mol/cm³ (S/C = 3).

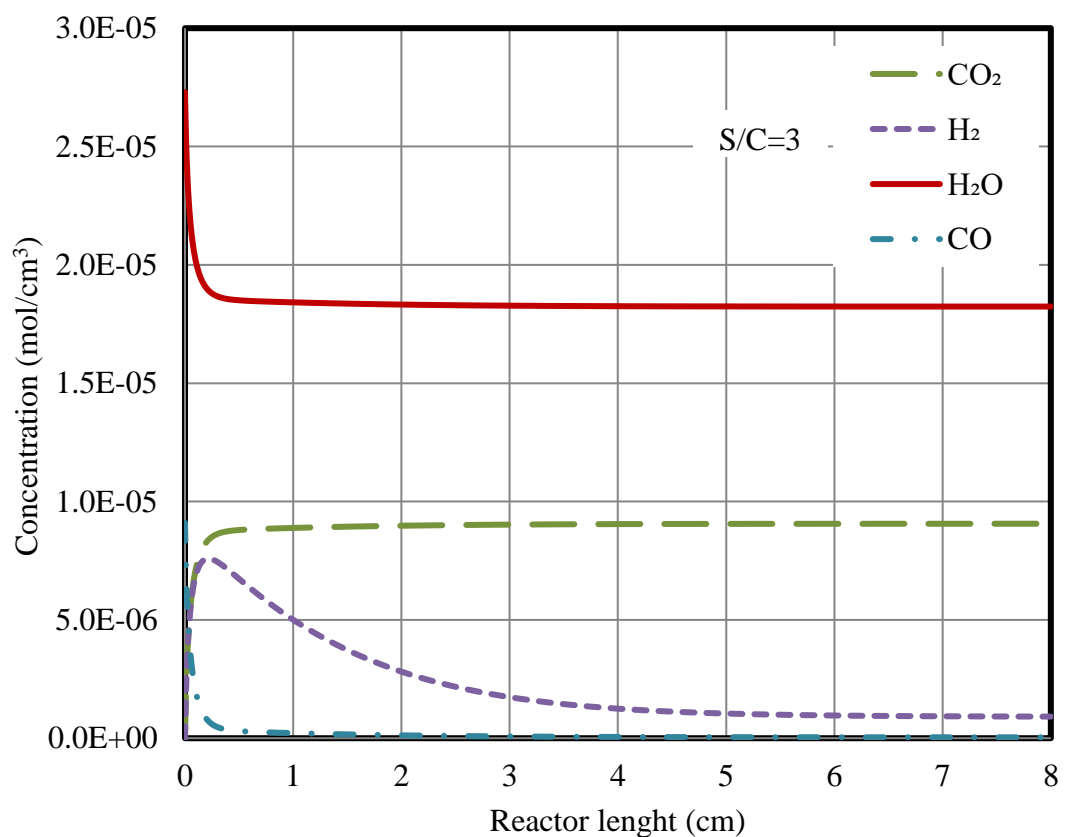


Figure 4.6: Effect of S/C ratio = 3 on the CO, CO₂, H₂O and H₂ concentrations

The effect of the S/C ratio of 4 is shown in Figure 4.7. The results illustrate that the concentration of CO declines rapidly until a value of almost 3.98×10^{-8} mol/cm³, at which the concentration enters a period of stability. However, a different variation trend is observed for CO₂. The concentration rises until a value of 7.15×10^{-6} mol/cm³, at which the slope becomes almost zero. On the contrary, the concentration of the hydrogen increases until reaching a maximum value of 6.15×10^{-6} mol/cm³ and this is followed by a declining trend until it enters a period of stability at 9.33×10^{-7} mol/cm³. It is clear from the results that the average CO conversion increased more for a S/C ratio of 4 than for S/C ratios of 1, 2, and 3, owing to Le Chatelier's principle and therefore, the value of the CO concentration is less than those obtained for S/C ratios of 1, 2, and 3. The excessive steam on the reaction side reduced the concentration of CO₂ and the hydrogen concentration at the peak point; this can be observed by comparing the values determined at a S/C ratio of 4 with those at the S/C ratios of 1, 2, and 3. In addition, decreasing the hydrogen concentration on the reaction side had a negative effect in the driving force across the membrane, which increased the hydrogen concentration (after reaching a period of stability), this can be observed by comparing the hydrogen concentration after reaching a constant value at the S/C of 4 (9.33×10^{-7} mol/cm³) with that at the S/C ratios of 1, 2, and 3.

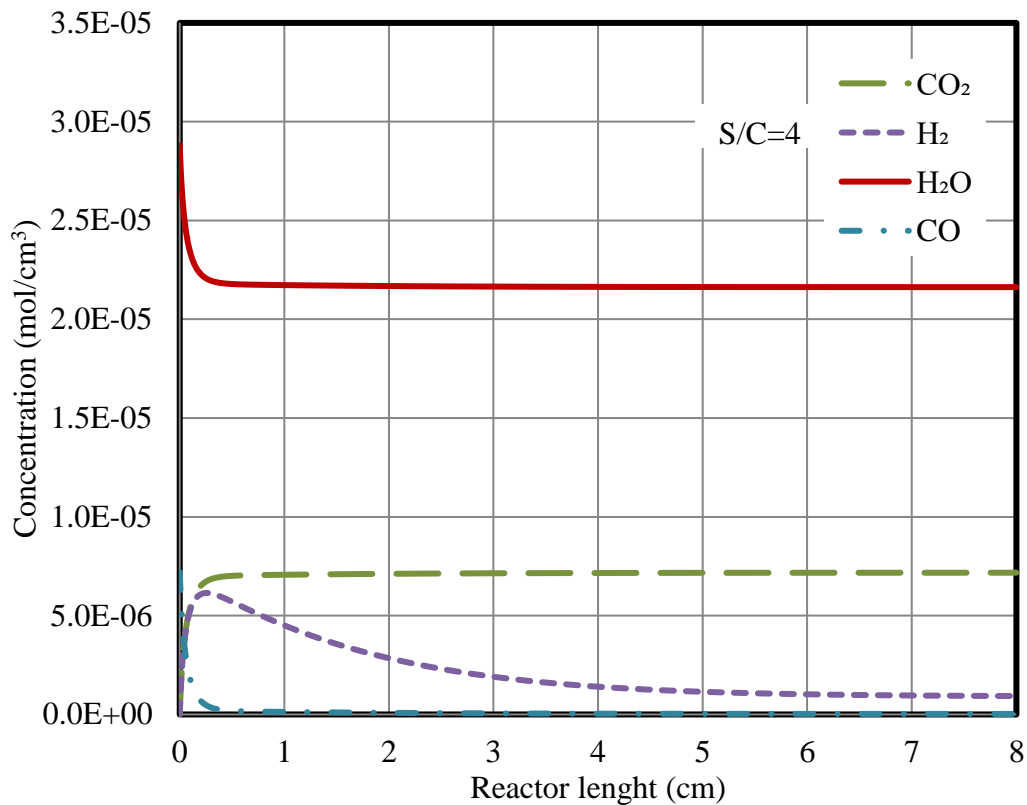


Figure 4.7: Effect of S/C ratio = 4 on the CO, CO₂, H₂O, and H₂ concentrations

As the S/C ratio increases further, the level of conversion of CO rises, as shown in Figure 4.8. The concentration of CO sharply decreases to a value of 2.64×10^{-8} mol/cm³, at which the concentration remains almost constant. In addition, the concentration of CO₂ increases until a value of 5.94×10^{-6} mol/cm³, at which the concentration does not change. Additionally, the concentration of H₂ increases along the reactor length until it reaches a maximum concentration of 5.20×10^{-6} mol/cm³, and this followed by a gradual drop until the concentration remains constant at a value of almost 9.60×10^{-7} mol/cm³. By comparing these values with the results obtained at the S/C ratio of 4, it can be seen that the CO concentration declined slightly. Meanwhile, the CO₂ and hydrogen concentrations at the peak value decreases further, and therefore the rate of permeability decreased, which caused the concentration of

hydrogen after stabilizing to be higher than the results obtained for the lower S/C ratios.

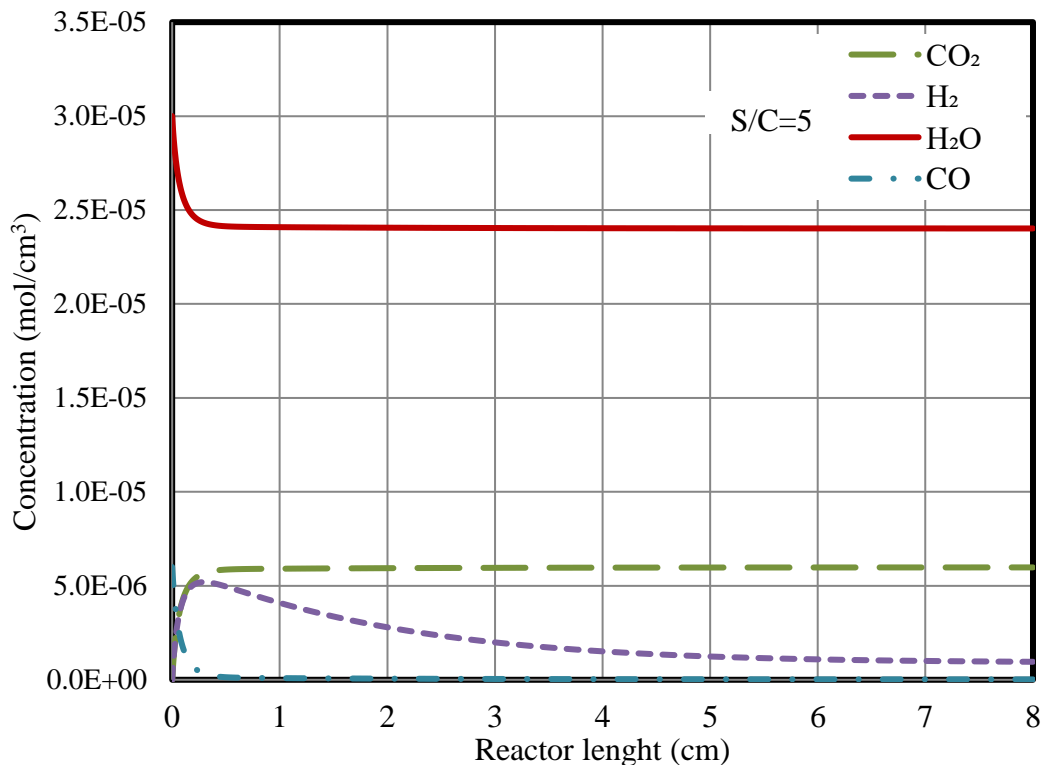


Figure 4.8: Effect of S/C ratio = 5 on the CO, CO₂, H₂O, and H₂ concentrations

By comparing the effect of the S/C ratio of 6, as shown in Figure 4.9, with that of the S/C of 5, it can be noted that the level of CO conversion climbs slightly. The concentration of CO started to decrease to a value $2.44 \times 10^{-8} \text{ mol/cm}^3$, at which the concentration starts to remain constant. However, the CO₂ concentration increases until it reaches a value of $4.42 \times 10^{-6} \text{ mol/cm}^3$, at which the concentration enters a period of stability. On the contrary, the hydrogen concentration increases until it reaches a peak value of $4.55 \times 10^{-6} \text{ mol/cm}^3$, after which the trend starts to decline to a value of $9.99 \times 10^{-7} \text{ mol/cm}^3$, where the slope becomes almost zero.

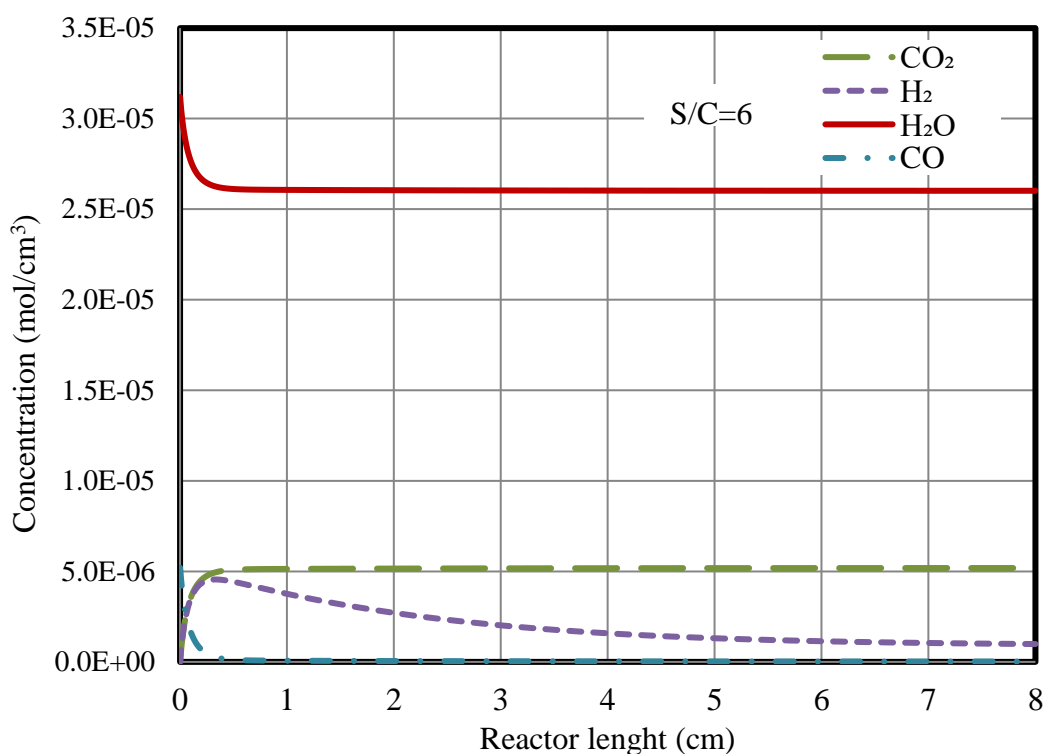


Figure 4.9: Effect of S/C ratio = 6 on the CO, CO₂, H₂O, and H₂ concentrations

In summary, results from the above S/C ratio analysis showed that as the S/C ratio increased, the CO conversion increased because the reaction was shifted towards the product side owing to Le Chatelier's principle. In contrast, the H₂ and CO₂ production decreased because the excess of steam diluted their concentrations on the reaction side. Thus, the rate of H₂ permeation through the membrane decreased as well.

4.2.1 Change of CO Conversion at Different S/C Ratios

Figure 4.10 demonstrates the change in CO conversion at different S/C ratios along the length of the reactor. As an overall trend, CO conversion increases by increasing the S/C ratio. In addition, it can be observed that the CO conversion is almost the same for the S/C ratios of 4, 5, and 6. This means that increasing the S/C ratio beyond 4 did not significantly affect the change in CO conversion.

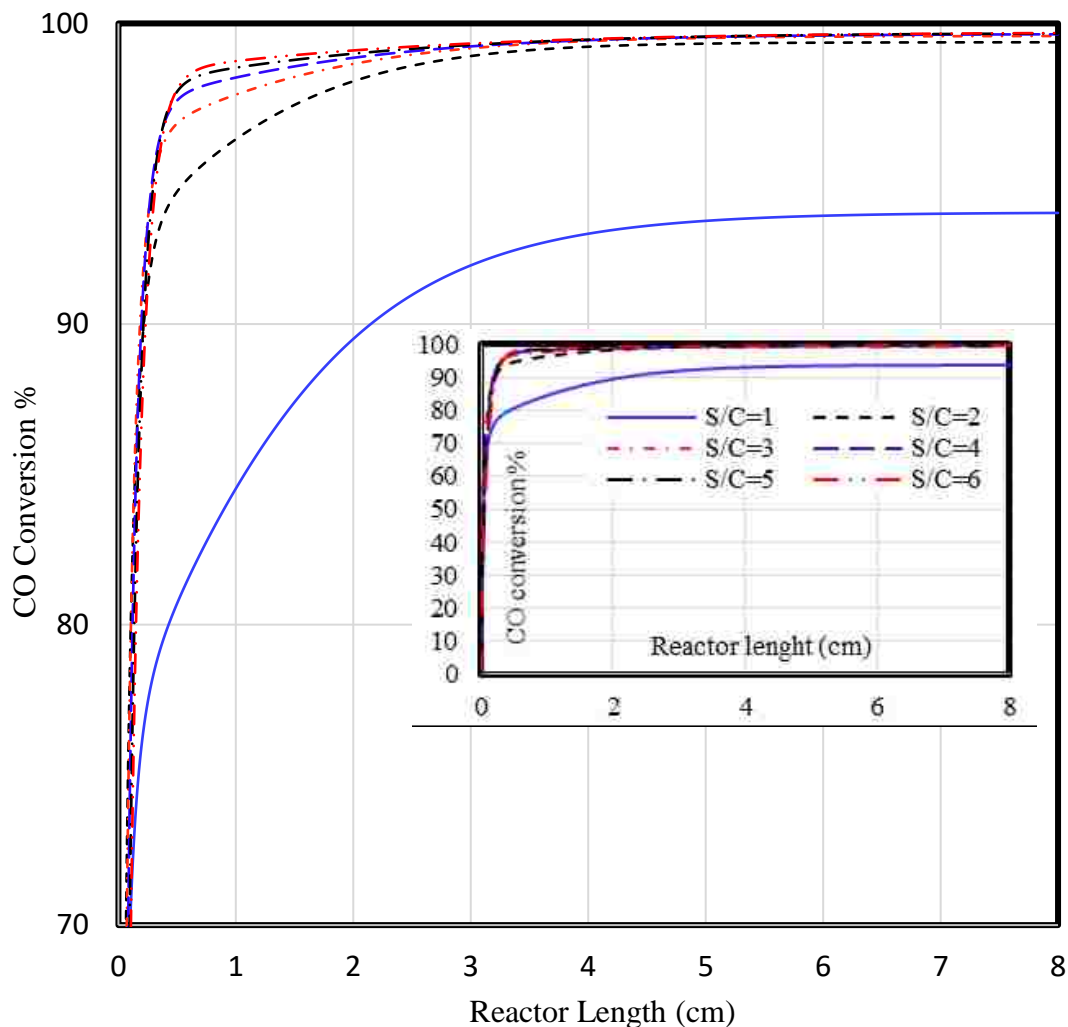


Figure 4.10: Change in CO conversion at different S/C ratios

4.2.2 Change of Molar Flow Rate at Different S/C Ratios

Figure 4.11 shows the molar flow rate profile of the hydrogen component obtained along the length of the reactor for S/C ratios of 1, 2, 3, 4, 5, and 6. The figure shows that the hydrogen molar flow rate starts to increase rapidly until reaching a peak value, which is followed by a decreasing trend until reaching a period of stability. It is clear from the figure that increasing the S/C ratio results in an increase in the peak value of hydrogen flow rate, because as the steam increases, the CO conversion increases, and hence the hydrogen flow rate increases as well. However, the rate of

reduction in hydrogen flow rate decreases. For example, at the S/C ratio of 1, the flow rate of hydrogen starts to be stable at a length of almost 5 cm, where the flow rate is 5.8×10^{-5} mol/min, and this value increased to value of approximately 2.41×10^{-4} mol/min at distance of approximately 6 cm for the S/C ratio of 6. The decreasing hydrogen flow rate along the length of the MR is the result of the loss of H₂ through the H₂-selective membrane walls, which reduced the gas flow rate. As the steam increases further, the rate of hydrogen reduction decreases further as well. This resulted from the reduction in hydrogen concentration on the retentate side by the excess of steam that caused a reduction in the H₂ driving force across the membrane, leading to a lower hydrogen permeability across the membrane.

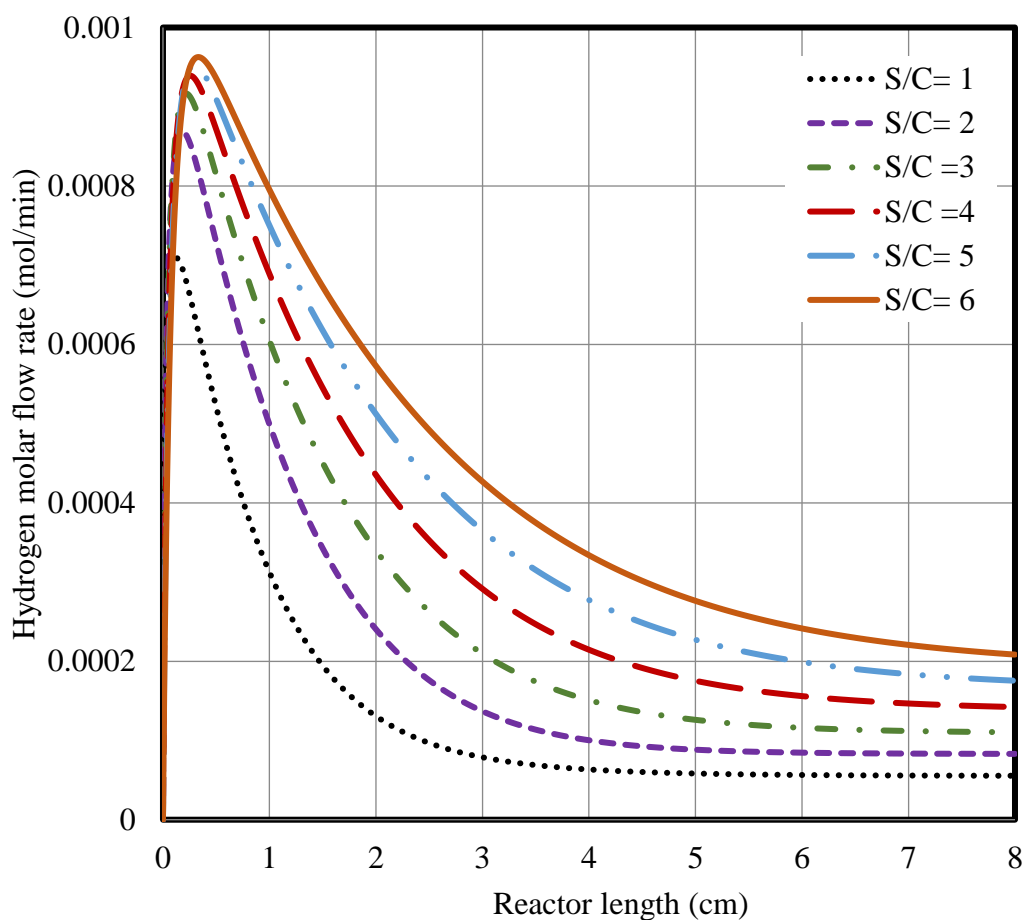


Figure 4.11: Change in hydrogen molar flow rate along reactor length at different S/C ratios

4.2.3 Model Validation

Figure 4.12 demonstrates the effect of the S/C molar ratio on the total CO conversion. The effect was tested by varying the S/C ratio from 1 to 6 at a fixed temperature of 673 K, retentate pressure of 2 atm, and sweep argon flow rate of 400 cm³ min⁻¹. The figure illustrates an enhancing effect of increasing the steam-to-CO ratio on the CO conversion for the Pd MR. As shown in the figure, an optimum value of the S/C ratio must be employed. The maximum of total methane conversion was obtained for a S/C ratio of 4.

To validate the model prediction, the simulation results were compared with the experimental data of Uemiya et al. [55], as shown in Figure 4.12. The figure shows that the model predictions are in good agreement with the experimental data.

A S/C of 4 is favourable, as it means the energy penalty associated with steam generation is reduced. Additionally, carbon formation can be avoided. Therefore, this value is an intermediate value of the S/C ratio.

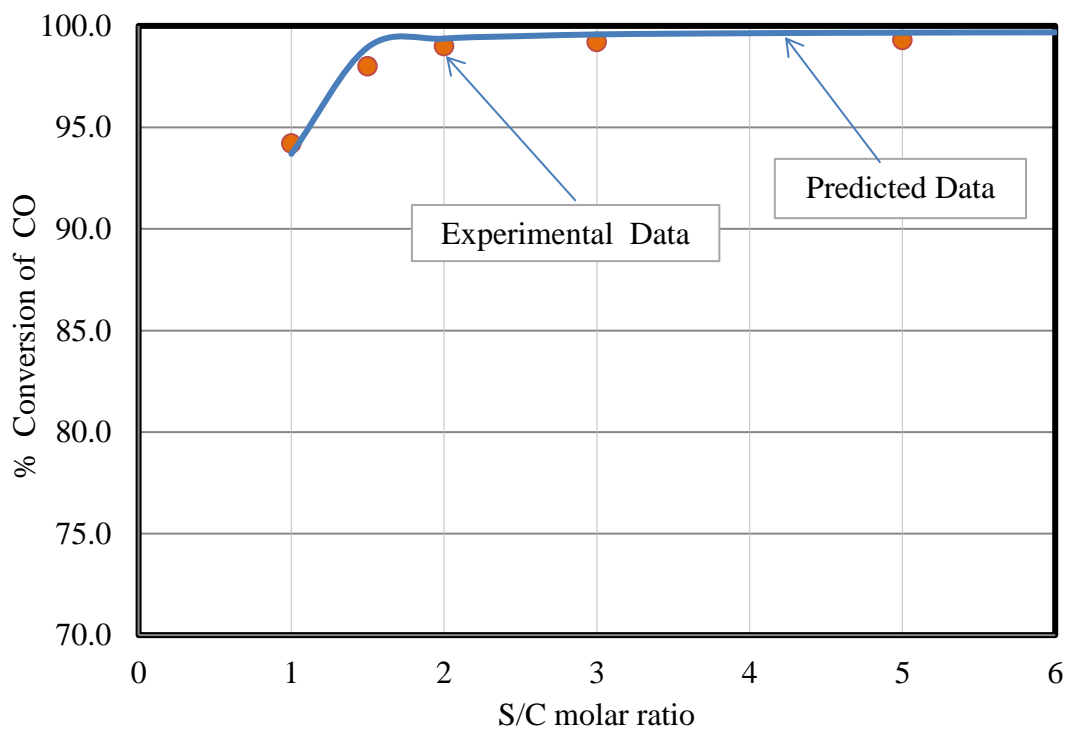


Figure 4.12: Effect of S/C molar ratio on CO conversion. Experimental conditions: temperature, 673 K; retentate pressure, 2 atm; flow rate of sweep argon, $400 \text{ cm}^3 \text{ min}^{-1}$

4.3 Effect of Membrane Thickness and Sweep Gas Flowrate

The effect of membrane thickness on the total CO conversion was investigated with a computer simulation, as illustrated in Figure 4.13, for a temperature of 673 K, a retentate pressure of 2 atm, argon flow rates of 3200, 400, and $100 \text{ cm}^3/\text{min}$, and S/C ratio of 1. At first glance, we see that as the membrane thickness decreases, the total conversion increases because of the enhancement in hydrogen removal.

As the argon flow rate increases, the partial pressure of hydrogen on the permeation side declines, and therefore, the level of CO conversion increases. At an argon flow rate of $3200 \text{ cm}^3/\text{min}$, the CO conversion is approximately 98% at a

thickness of 5 μm ; however, at argon flow rates of 400 and 100 cm^3/min , the CO conversion are approximately 93.7 % and 87.8%, respectively.

Another aspect which stands out in this graph is that a complete conversion of CO is not reached, but it could be attained if the partial pressure of hydrogen on the permeation side were further decreased by using a higher argon flow rate or by using a vacuum pump that could minimise the hydrogen pressure.

In summary, a MR constructed with composite palladium membrane gives a significantly high reaction efficiency associated with its excellent hydrogen permeation performance.

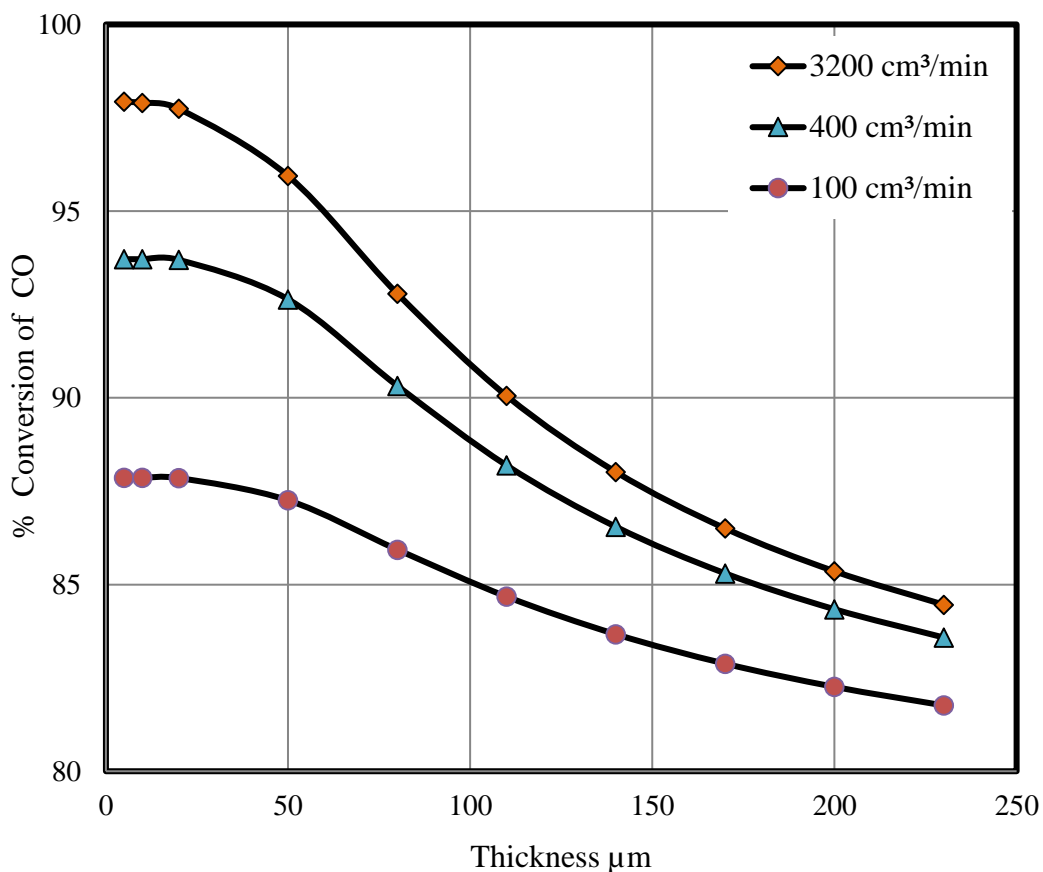


Figure 4.13: Effect of thickness on CO conversion for constant CO feed rate of 25 cm^3/min and argon flow rates of 3200, 400, and 100 cm^3/min

4.4 Effect of Hydrogen Partial Pressure at Retentate Side

Figure 4.14 reveals the effect of the partial pressure of hydrogen on the retentate side on the total CO conversion at a temperature of 673 K, S/C ratio of 1, and argon flow rate of 400 cm³/min. The line represents the model predictions from this study and the points represent the experimental data obtained by Uemiya et al. [55]. It can be seen that the experimental values are reasonably close to the predicted values from this study. At a constant temperature, with increasing the partial pressure of hydrogen on the reaction side, the CO conversion decreased. According to Le Chatelier's principle, as the partial pressure of hydrogen on the retentate side increased, the reaction moved to the reactant side, and thus the conversion of CO decreased.

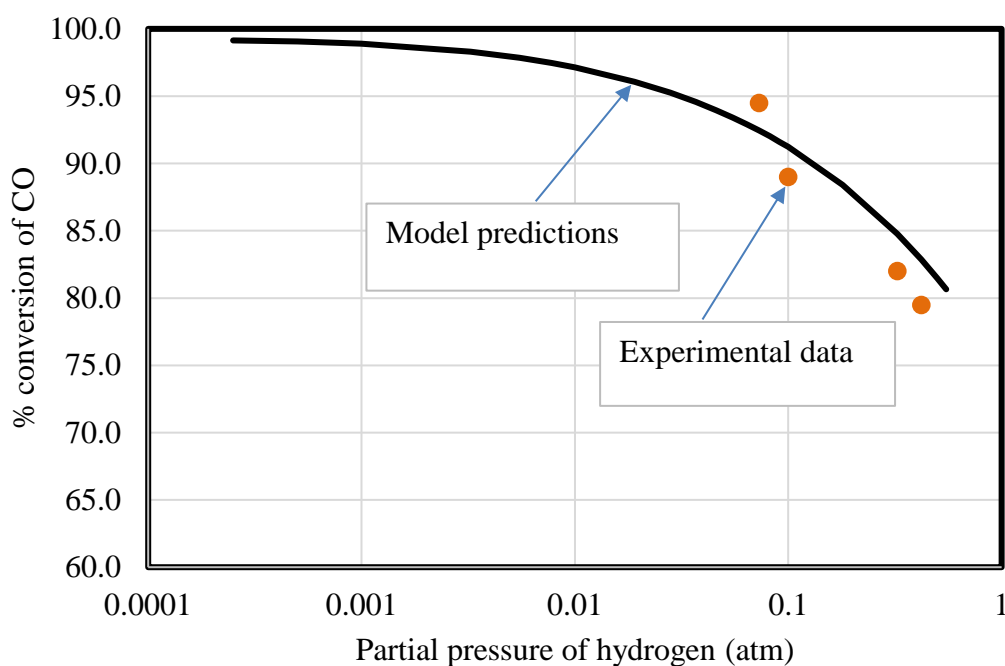


Figure 4.14: Effect of partial pressure of hydrogen at reaction side on CO conversion. Experimental conditions: temperature, 673 K; and flow rate of sweep argon, 400 cm³ min⁻¹

4.5 Effect of Hydrogen Partial Pressure at Permeate Side

Figures 4.15 through 4.20 provide an overview of the concentration profiles of the WGSR components obtained along the reactor for hydrogen permeate partial pressures of 1, 0.8, 0.6, 0.4, 0.2, and 0 atm, respectively. The effect of the hydrogen permeate partial pressure was examined for a temperature of 673 K, retentate pressure of 2 atm, and S/C ratio of 1.

Figure 4.15 shows the variation in CO and H₂O along the reactor length for a hydrogen permeate partial pressure of 1 atm. The results reveal that the concentration of CO and H₂O decrease rapidly until a value of approximately 4.52×10^{-6} mol/cm³, at which the concentration remains constant. However, the concentration of CO₂ increases to a value of 1.35×10^{-5} mol/cm³, at which the slope becomes almost zero. Similarly, the hydrogen concentration increases until it remains constant at a value of 1.81×10^{-5} mol/cm³.

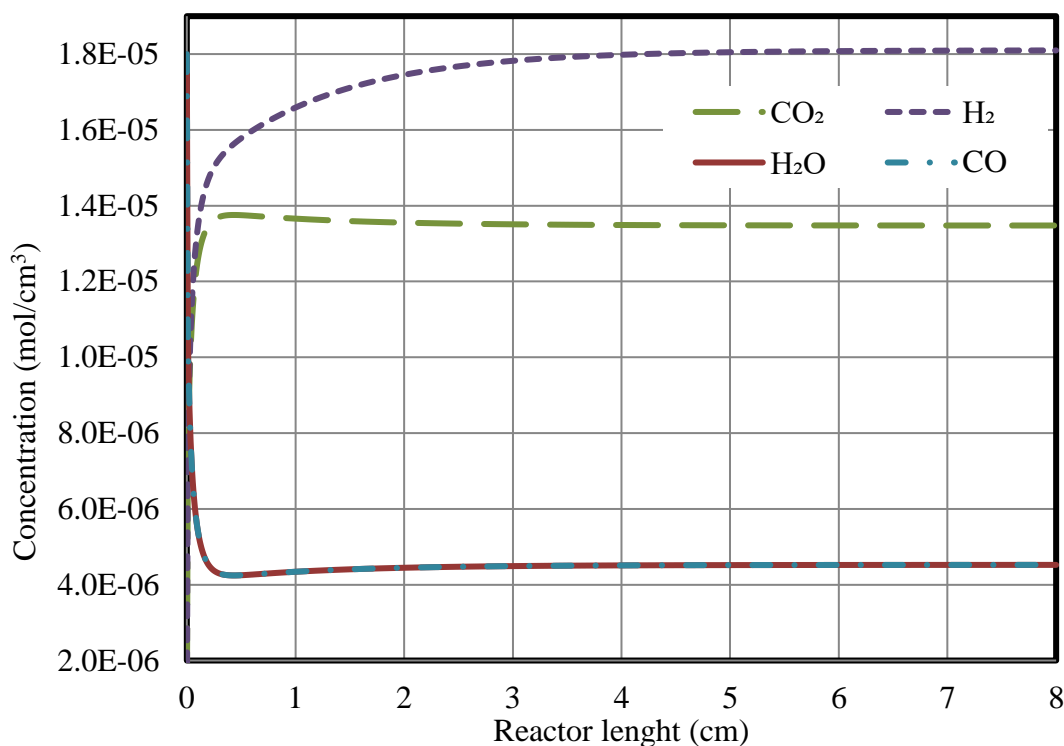


Figure 4.15: Effect of hydrogen partial pressure of 1 atm at permeate side on concentrations of CO, CO₂, H₂O, and H₂

The variations for the hydrogen permeate partial pressure of 0.8 atm are demonstrated in Figure 4.16. It is observed that the rates of variation (increase or decrease) are slightly higher than those observed for the hydrogen permeate partial pressure of 1 atm. The results illustrate that the concentrations of CO and H₂O decrease sharply until the concentration remains the same at a value of approximately 4.11×10^{-6} mol/cm³. In contrast, the concentration of CO₂ increases until a value of approximately 1.39×10^{-5} mol/cm³, at which the concentration becomes stable. Similarly, the hydrogen concentration increases to value of 1.45×10^{-5} mol/cm³, at which the slope becomes almost zero. By comparing these results with those obtained for 1 atm, it can be seen that the rates of conversion of CO and H₂O gradually increased. Additionally, the concentration of CO₂ on the retentate side increased slightly. On the contrary, the hydrogen concentration on the retentate side slightly

decreased. This is due to the reduction in the hydrogen partial pressure on the permeate side, which caused an increase in the driving force across membrane and thus increased the hydrogen permeability. Therefore, the decreased hydrogen concentration on the reaction side shifted the chemical reaction towards CO_2 and H_2 owing to Le Chatelier's principle.

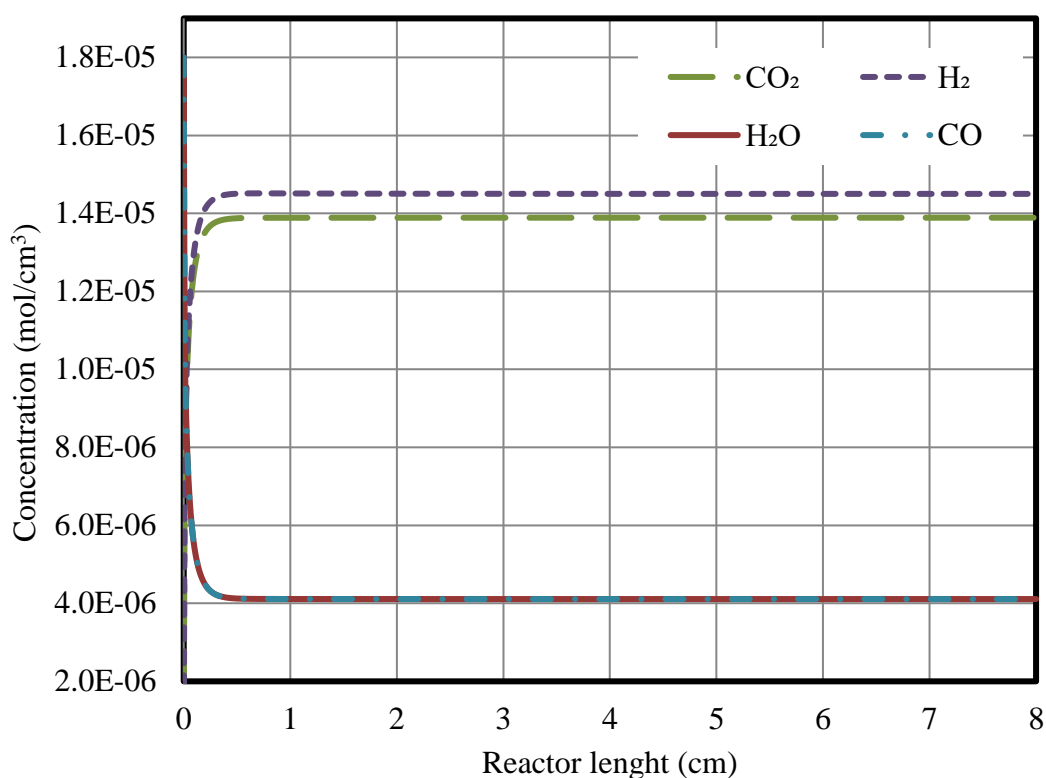


Figure 4.16: Effect of hydrogen partial pressure of 0.8 atm on the permeate side on the concentrations of CO , CO_2 , H_2O , and H_2

The changes in concentrations for the WGSR species at the hydrogen permeate partial pressure of 0.6 atm are shown in Figure 4.17. It can be seen that the rates of change in concentration (increase or decrease) are more at 0.6 atm than 0.8 and 1 atm. The results show that the concentrations of CO and H_2O decrease rapidly until they remain stable at an approximate value of 3.62×10^{-6} mol/cm³. However, the concentration of CO_2 increases to a value of approximately 1.44×10^{-5} mol/cm³, at

which the concentration becomes stable. In addition, it is clear from the graph that the trend of the hydrogen concentration along the reactor length is different from those at 0.8 and 1 atm. The hydrogen concentration increases until it approaches its peak value at a concentration of $1.35 \times 10^{-5} \text{ mol/cm}^3$, and this is followed by a decreasing trend until it stabilises at $1.09 \times 10^{-5} \text{ mol/cm}^3$. This is due to Le Chatelier's principle; as the hydrogen permeate partial pressure decreased, the permeation of hydrogen through the membrane increased and this decreased the hydrogen concentration on the reaction side, thereby increasing the conversion of CO.

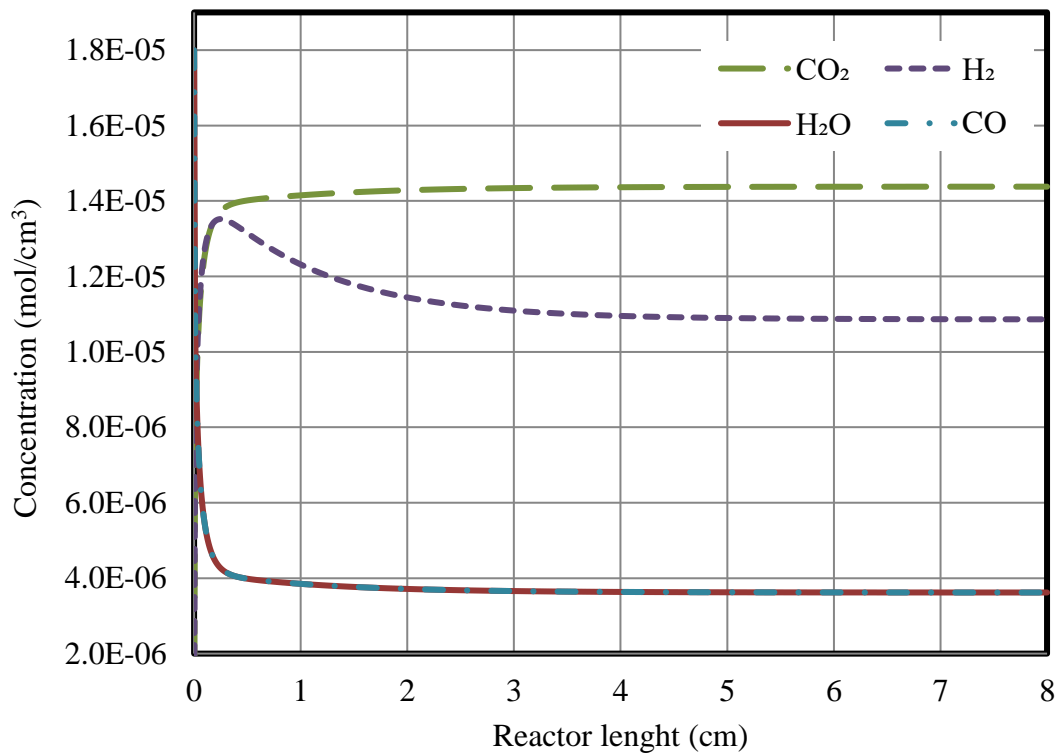


Figure 4.17: Effect of hydrogen partial pressure of 0.6 atm on the permeate side on the concentrations of CO, CO₂, H₂O, and H₂

Figure 4.18 depicts the effect of the hydrogen permeate partial pressure of 0.4 atm on the CO, CO₂, H₂O, and H₂ concentrations. According to the data shown, it appears that the average change increased further at 0.4 atm than at 0.6, 0.8, and 1 atm.

The results reveal that the concentrations of CO and H₂O decline significantly until they remain constant at a value of approximately 3.07×10^{-6} mol/cm³. However, the concentration of CO₂ increases to a value of approximately 1.50×10^{-5} mol/cm³, at which the slope becomes almost zero. Additionally, it can be observed that the hydrogen trend is similar to that obtained at 0.6 atm; the concentration of hydrogen increases until reaching a peak value of 1.27×10^{-5} mol/cm³ and this is followed by a declining trend until it enters a period of stability at 7.33×10^{-6} mol/cm³. It is important to point out that the concentration of hydrogen on the reaction side at 0.4 atm is lower than that determined at 0.6 atm (1.09×10^{-5} mol/cm³). This change is due to the same reasons as explained before; as the hydrogen partial pressure decreases further from the permeate side, the selectivity of hydrogen through membrane increased and this forced the reaction towards the product side, thereby increasing the average CO conversion.

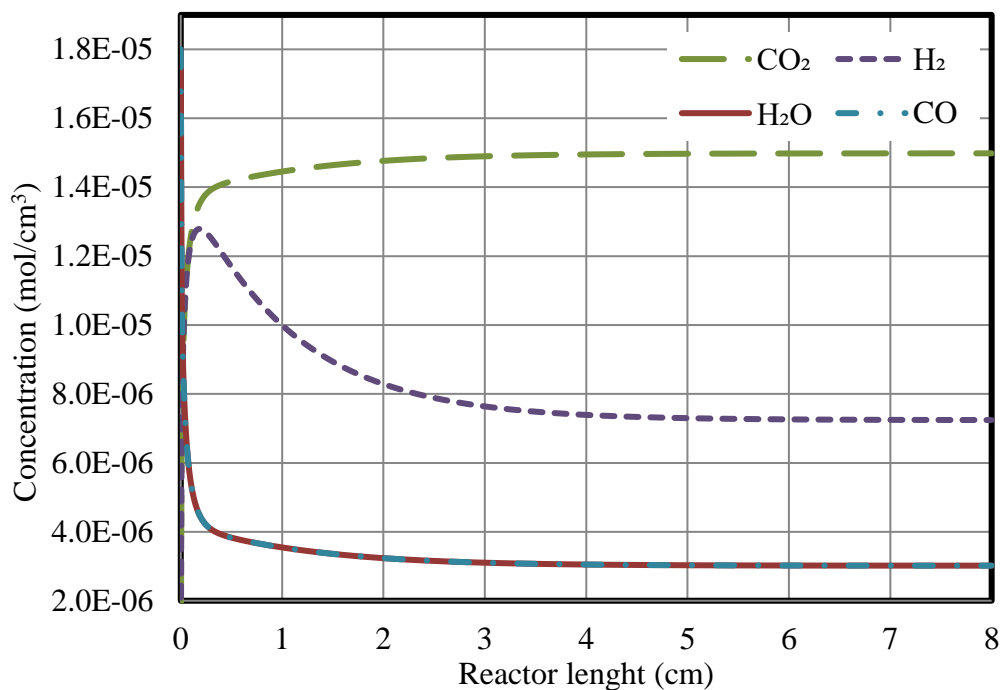


Figure 4.18: Effect of hydrogen partial pressure of 0.4 atm on the permeate side on the concentrations of CO, CO₂, H₂O, and H₂

Figure 4.19 shows an overview of the change in species concentration with respect to the reactor length at 0.2 atm. At first glance, we see that as the hydrogen permeate partial pressure decreases further, the rate of hydrogen permeability out of membrane and the conversion of CO both increase. It can be observed from the figure that the rate of variation is higher at 0.2 atm compared with the results obtained at 0.4, 0.6, 0.8, and 1 atm. The results show that the concentrations of CO and H₂O decrease radically to a value of $2.25 \times 10^{-6} \text{ mol/cm}^3$, after which they do not change. In contrast, the concentration of CO₂ increases until a value of $1.57 \times 10^{-5} \text{ mol/cm}^3$, at which the concentration remains constant. In addition, the concentration of the hydrogen increases rapidly until reaching a maximum value of $1.20 \times 10^{-5} \text{ mol/cm}^3$ and this is followed by a decreasing trend up to $3.68 \times 10^{-6} \text{ mol/cm}^3$, where the concentration enters a period of stability.

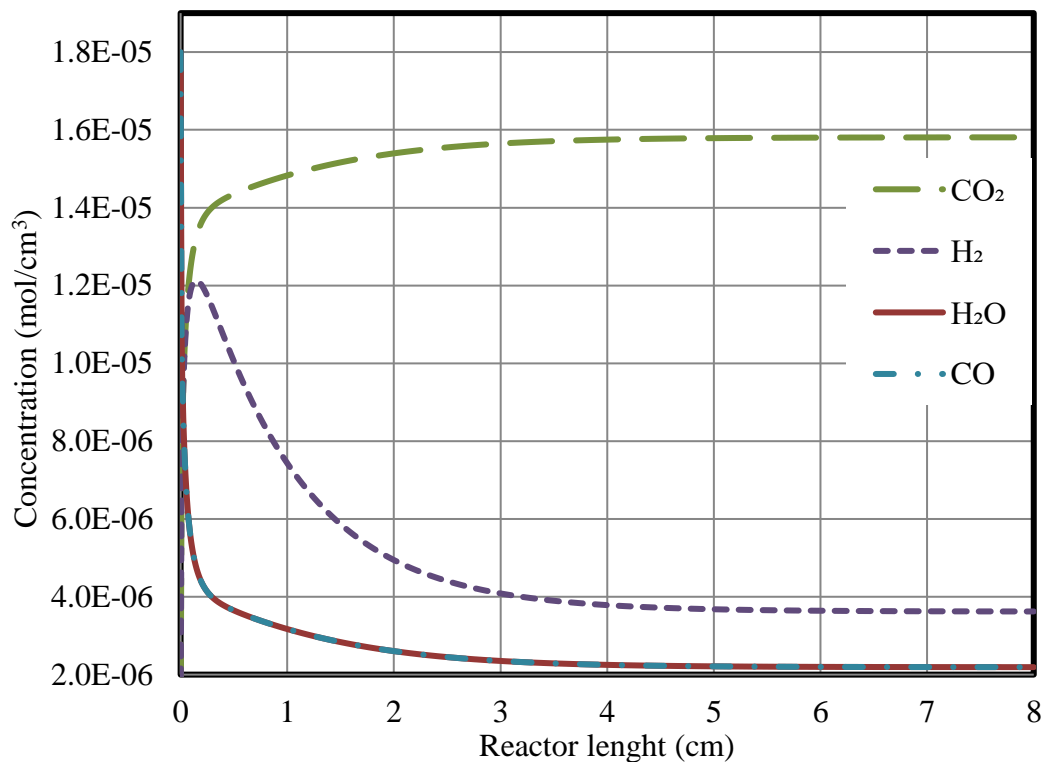


Figure 4.19: Effect of hydrogen partial pressure of 0.2 atm on the permeate side on the concentrations of CO, CO₂, H₂O, and H₂

By comparing the effects of the hydrogen partial pressure of 0.0 atm, as shown in Figure 4.20, with those observed for 0.2, 0.4, 0.6, 0.8, and 1 atm, it can be noted that the level of CO conversion increases further, resulting from the reduction in hydrogen pressure on the permeate side. From Figure 4.20, it can be seen that CO is converted to H₂ and CO₂ at a rate of almost 100%. The concentrations of CO and H₂O start to decrease to a value 3.08×10^{-7} mol/cm³, at which the concentration starts to remain constant. However, the CO₂ concentration increases until it reaches a value of 1.76×10^{-5} mol/cm³, at which it enters a period of stability. On the contrary, the hydrogen concentration increases until it reaches a peak value of 1.01×10^{-5} mol/cm³, after which the trend starts to decline to a value of 8.89×10^{-8} mol/cm³, where the slope

becomes almost zero. This reduction in hydrogen concentration is due to the improvement in hydrogen selectivity through the membrane.

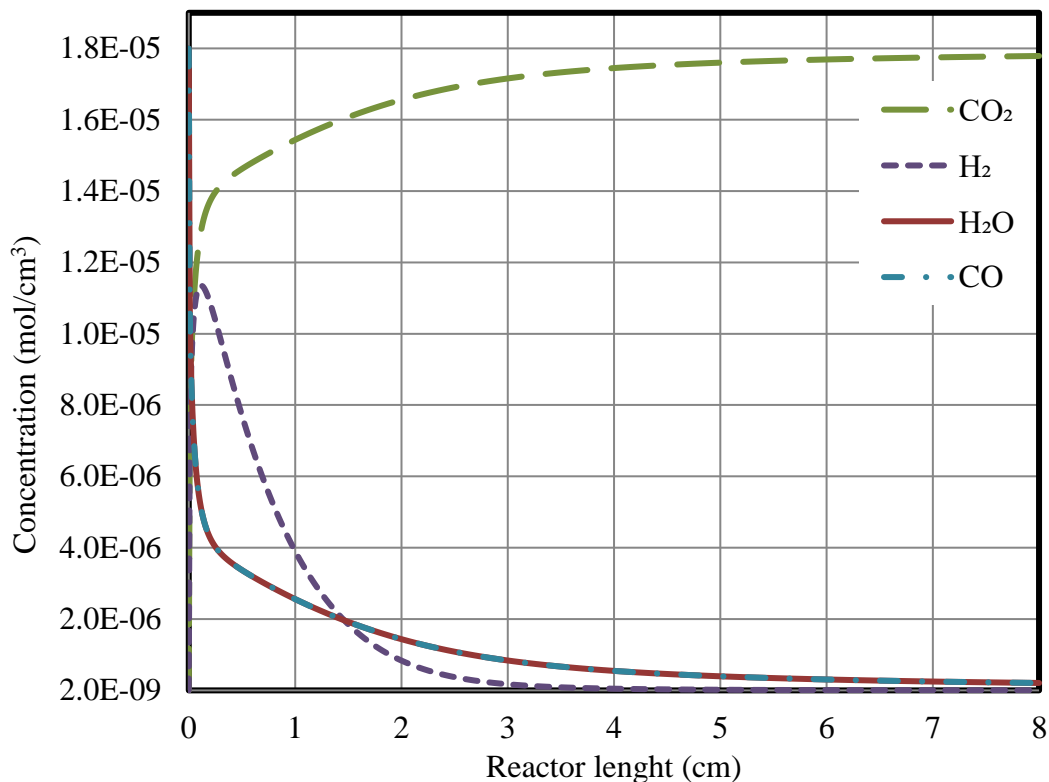


Figure 4.20: Effect of hydrogen partial pressure of 0.0 atm on the permeate side on the concentrations of CO, CO₂, H₂O, and H₂

4.5.1 Effect of Hydrogen Permeate Partial Pressure on CO Conversion

Figure 4.21 and Figure 4.22 give information about the impact of the hydrogen permeate partial pressure on the overall CO conversion. Figure 4.21 illustrates the change in the CO conversion along the reactor length for each hydrogen permeate partial pressure. In addition, Figure 4.22 summarises the overall CO conversion for each hydrogen permeate partial pressure. The influence was tested by varying the hydrogen permeate partial pressure from 0 to 1 atm under a temperature of 673 K, retentate pressure of 2 atm, and S/C ratio of 1. As expected, the CO conversion

progressively decreases with increasing hydrogen permeate partial pressure. It is clear from the results that decreasing the hydrogen permeate partial pressure from 1 to 0 atm leads to an increase in the CO conversion from 74.9% to 98.8%. The enhancement in the CO conversion resulting from the reduction in the hydrogen partial pressure on the permeate side, which increased the driving force throughout the membrane, resulted in a higher rate of hydrogen removal from the reaction zone.

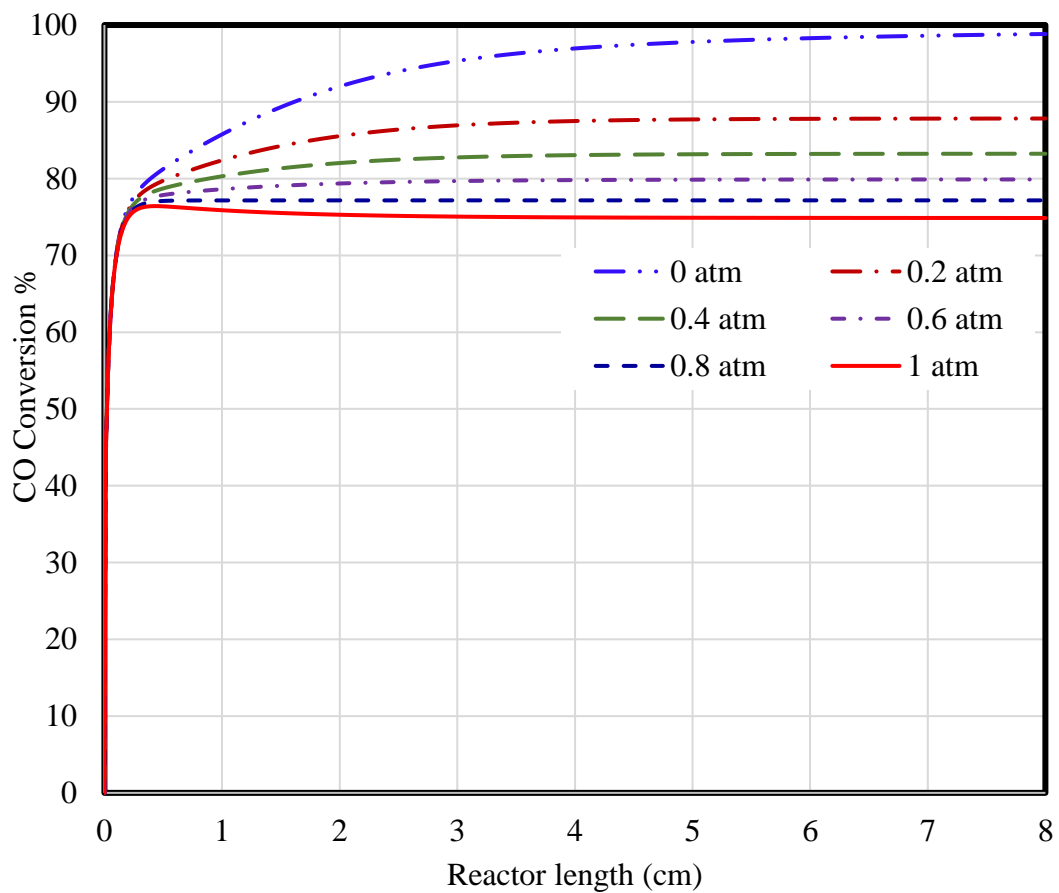


Figure 4.21: CO conversion versus reactor length at fixed values of hydrogen partial pressure on the permeate side

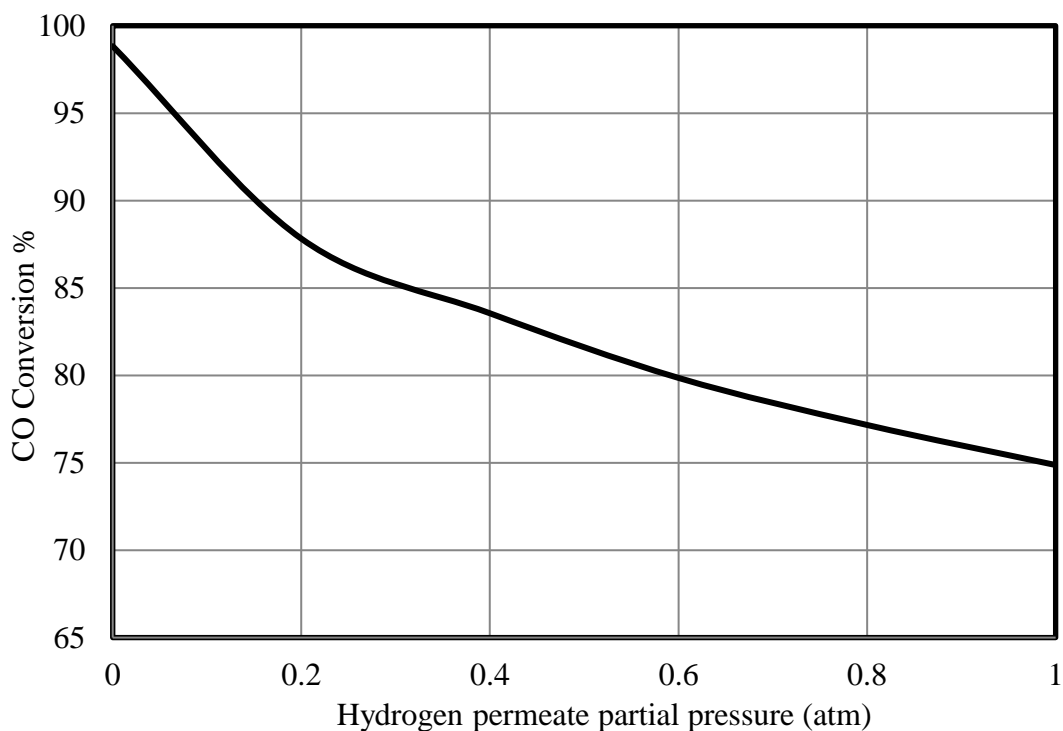


Figure 4.22: Effect of hydrogen permeate partial pressure on CO conversion

4.6 Effect of Residence Time

In order to determine the effect of the residence time on the concentrations of the WGSR components, the residence times of the reactor systems were varied by changing the operating pressure, while keeping the inlet feed flow rate and reaction temperature constant. This process resulted in a reduced reactant volumetric flow rate and therefore increased the residence time at the elevated pressure conditions inside the reaction zone. The retentate pressures used in the simulation corresponding to the different residence times are listed in Table 4.1. The effect of residence time was examined under a temperature of 673 K, CO inlet volumetric flow rate of 100 cm³/min, S/C ratio of 1, and sweep argon flow rate of 400 cm³/min.

Table 4.1: Retentate pressure and its corresponding residence time

Retentate pressure (atm)	Residence time τ (s)
2	0.13
4	0.30
6	0.47
8	0.63
10	0.79
12	0.96
14	1.12

Figure 4.23 to 4.26 show the axial concentration profiles of the WGS components obtained along the centre of the reactor for residence times of 0.13, 0.47, 0.63, and 0.96 s, respectively. The figures show increasing CO₂ concentration with increasing residence time, whereas the H₂, CO, and H₂O concentrations are observed to decrease with increasing residence time.

The variation for a residence time of 0.13 s is demonstrated in Figure 4.23. The results reveal that the concentrations of CO and H₂O decline until a value of approximately 1.92×10^{-6} mol/cm³. On the contrary, the concentration of CO₂ increases to a value of almost 1.59×10^{-5} mol/cm³. This is a common trend for all the gases except for H₂, for which the concentration rises until approaching its peak value at a concentration of 1.14×10^{-5} mol/cm³, followed by a decreasing trend until approaching a minimum value of 2.19×10^{-6} mol/cm³. The reduction in hydrogen on the retentate side is due to its permeability through the membrane.

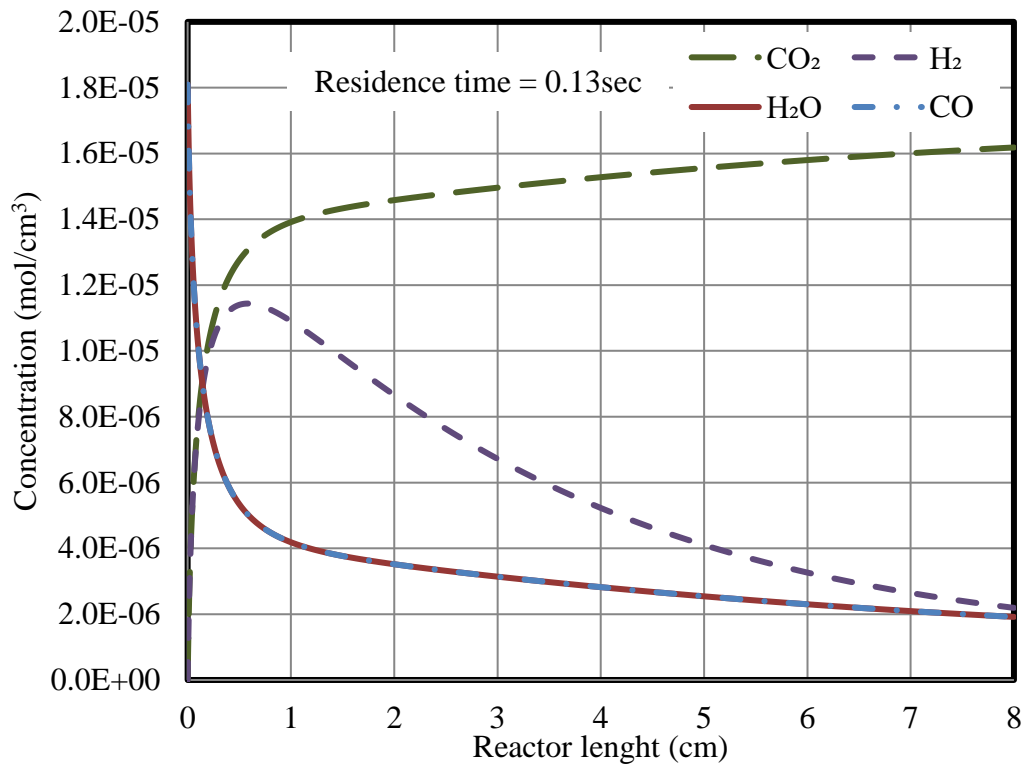


Figure 4.23: Effect of residence time of 0.13 s on the concentrations of CO, CO₂, H₂O, and H₂

Figure 4.24 shows the effect of residence time of 0.47 s. The results illustrate that the concentrations of CO and H₂O decrease until reaching a minimum value of 2.32×10^{-6} mol/cm³. However, the concentration of CO₂ increases until a value of 5.20×10^{-5} mol/cm³. The concentration of the hydrogen increases until reaching a maximum value of 3.56×10^{-5} mol/cm³, followed by a declining trend until it reaches a value of 1.08×10^{-6} mol/cm³. It is observed that the rates of variation (increase or decrease) are higher than those observed for a residence time of 0.13 s. The reason for this is that the reaction pressure increased and thus the residence time increased. Therefore, the H₂ partial pressure driving force increased and the conversion of CO increased as well.

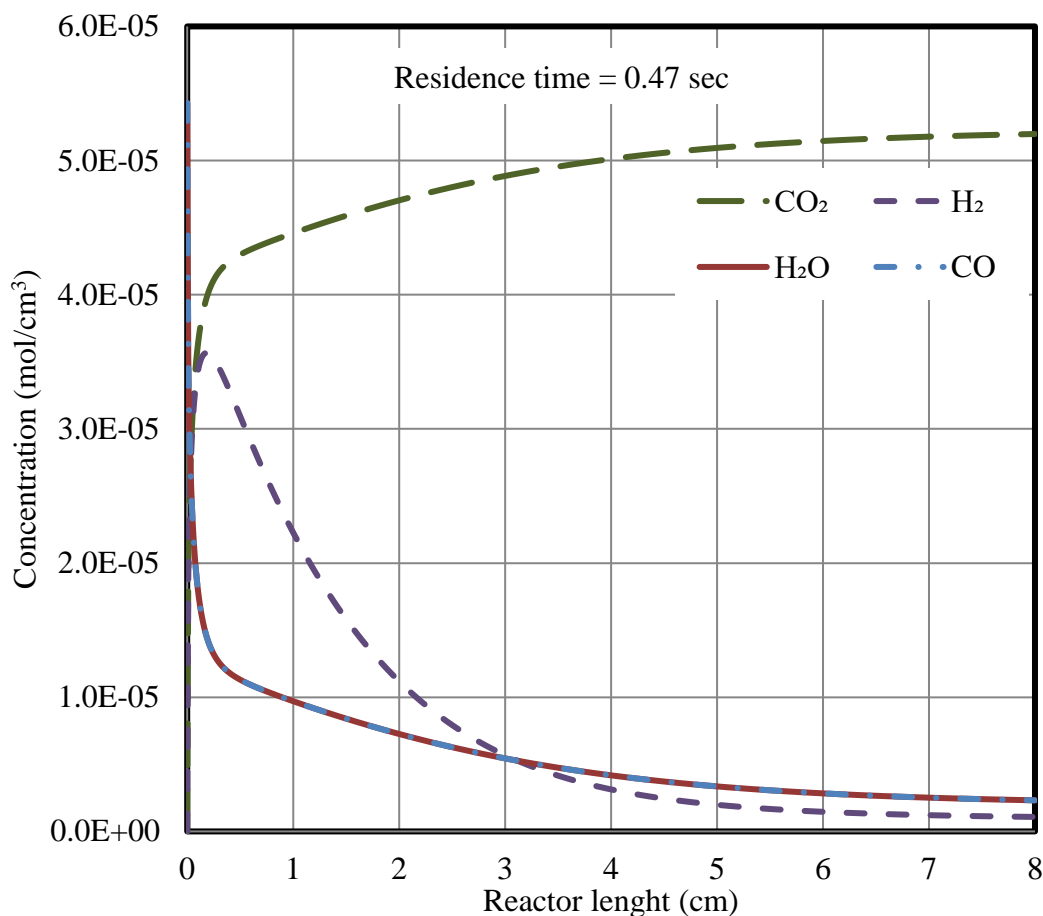


Figure 4.24: Effect of residence time of 0.47 s on the concentrations of CO, CO₂, H₂O, and H₂

It can be noted from Figure 4.25 that the average of change increased more for a residence time of 0.63 s than for 0.13 and 0.47 s. This is because, as the residence time increased, the rate of reaction increased, and hydrogen permeability through the membrane increased as well. The results reveal that the concentrations of CO and H₂O decrease until reaching a value of 2.91×10^{-6} mol/cm³, at which the concentration becomes almost constant. In contrast, the concentration of CO₂ rises until a maximum value of 6.95×10^{-5} mol/cm³. The concentration of the hydrogen increases until reaching a maximum value of 4.83×10^{-5} mol/cm³, followed by a decreasing trend until reaching a value of 9.99×10^{-7} mol/cm³.

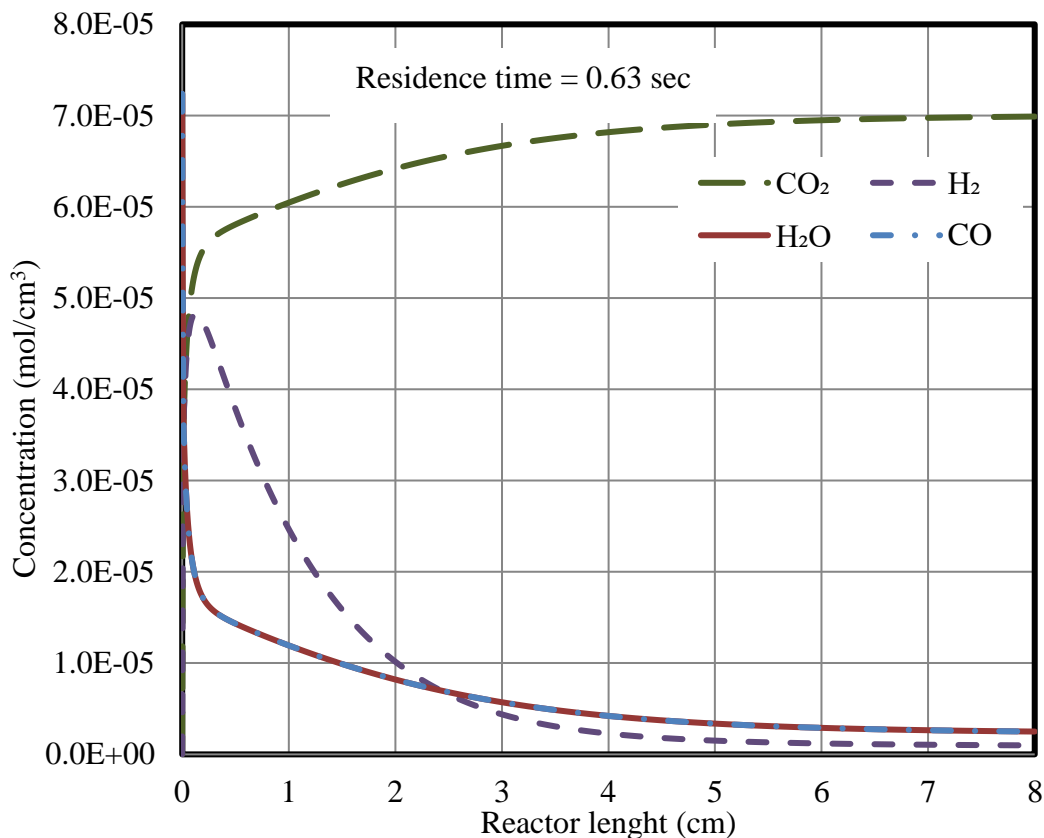


Figure 4.25: Effect of residence time of 0.63 s on the concentrations of CO, CO₂, H₂O, and H₂

Figure 4.26 depicts the impact of the residence time of 0.96 s on the species concentrations along the reactor length. As shown in the figure, the concentrations of CO and H₂O decrease until entering a period of stability at a value of 3.15×10^{-6} mol/cm³. By increasing the residence time from 0.13 to 0.96 s, the concentration of CO₂ increased from a value of 6.95×10^{-5} to 1.06×10^{-4} mol/cm³. In addition, the hydrogen concentration increases rapidly until reaching a peak value of 7.90×10^{-5} mol/cm³, followed by a decreasing trend until reaching a value of 9.33×10^{-7} mol/cm³, which is slightly less than the value obtained for the residence time of 0.63 s. The changes in concentration were expected because the hydrogen flux across the membrane increased further at longer residence times.

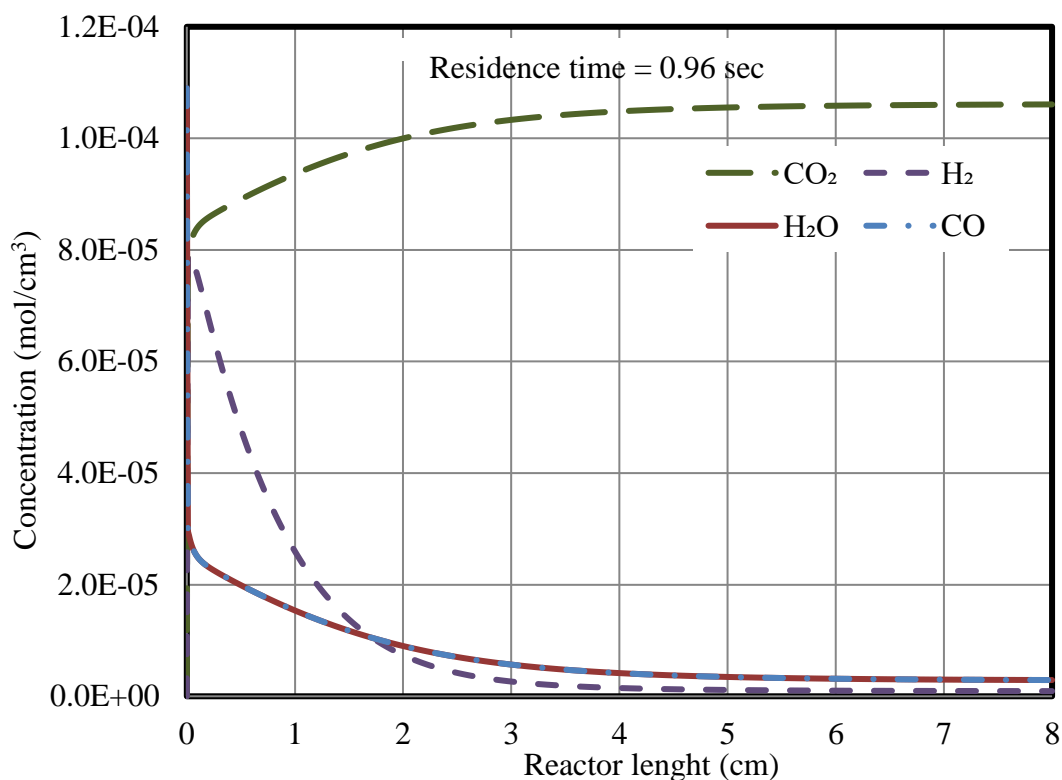


Figure 4.26: Effect of residence time of 0.96 s on the concentrations of CO, CO₂, H₂O, and H₂

4.6.1 Effect of Residence Time on CO Conversion

Figure 4.27 shows the effect of residence time on CO conversion along the length of the reactor while Figure 4.28 depicts the overall CO conversion for each residence time. The impact of residence time was tested under a temperature of 673 K, S/C ratio of 1, CO flow rate of 100 cm³/min, and argon flow rate of 400 cm³/min. The figures illustrate an enhancing effect of increasing residence time on CO conversion. It can be notice that by increasing the residence time from 0.13 to 0.96 s, CO conversion increases from 89.4% to 97.3%. This is due to the same reasons explained above. By increasing the reaction pressure, the residence time increased and the driving force across membrane increased as well. Therefore, hydrogen permeability went up and rate of reaction increased.

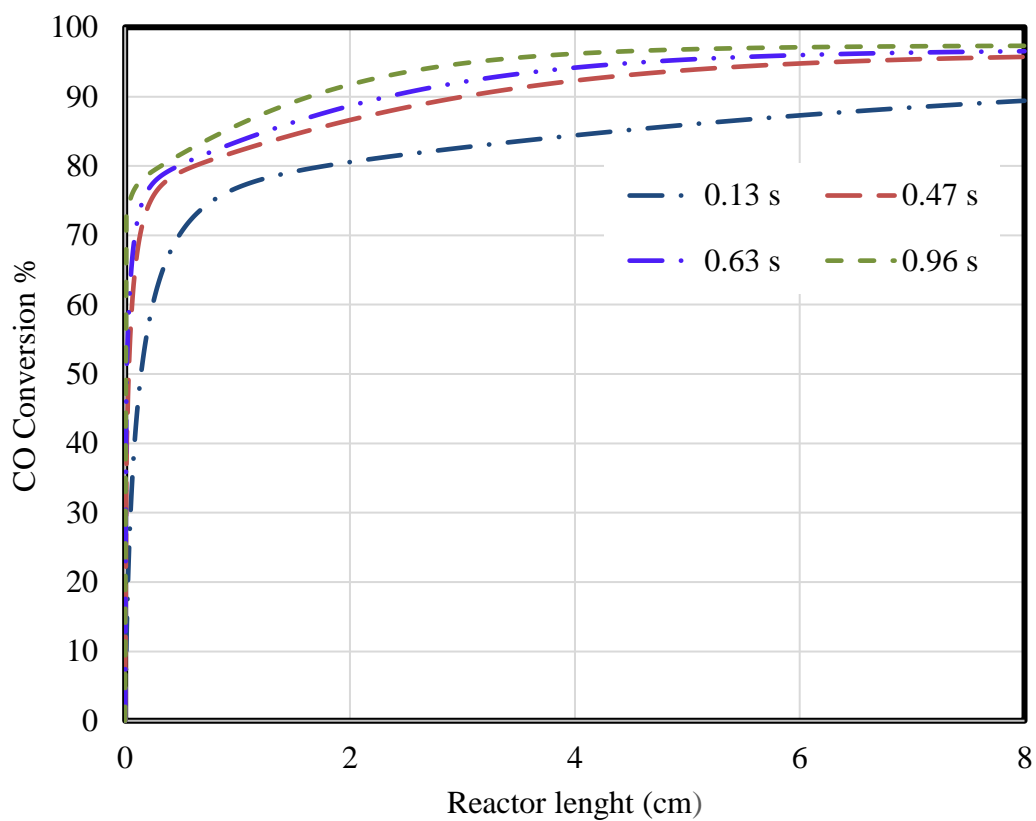


Figure 4.27: CO conversion versus reactor length at fixed values of residence time

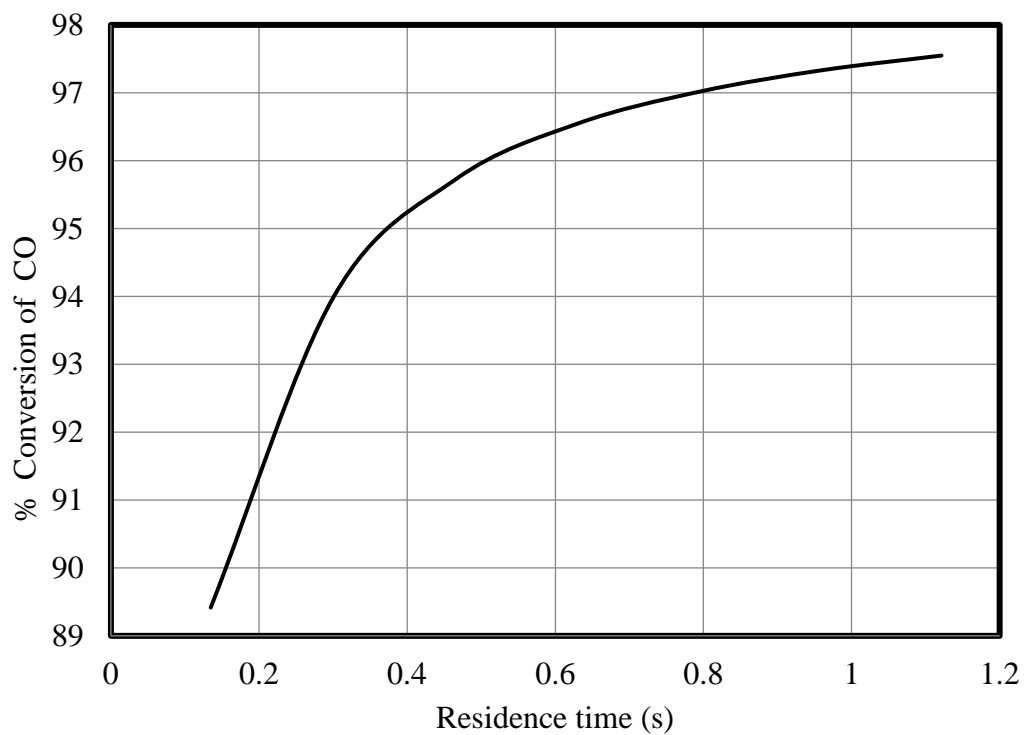


Figure 4.28: Effect of residence time on CO conversion

4.7 Statistical Model

The software package Minitab was used to analyse and interpret the obtained results in order to determine the optimum conditions under which the reactor can operate. Response surface methodology (RSM) in Minitab was selected owing to its excellent indications to optimise the operating conditions [60].

The effects of the S/C ratio, thickness (μm), and total retentate pressure (atm) on the CO conversion (response) at a temperature of 673 K were studied. Four levels of each factor were chosen, and thus 4^3 factorial designs were simulated. Table 4.2 lists these parameters (factors) with the selected levels for each. The argon flow rate was chosen to be $3200 \text{ cm}^3/\text{min}$, as it gave the best results compared with 400 and $100 \text{ cm}^3/\text{min}$. As reflected in Section 4.3, the effect of the argon flow rate of $3200 \text{ cm}^3/\text{min}$ at a thickness of $5 \mu\text{m}$ resulted in a CO conversion of approximately 98%; however, at argon flow rates of 400 and $100 \text{ cm}^3/\text{min}$ the CO conversion rates were approximately 93.7% and 87.8%, respectively.

Table 4.2: Identification of affecting parameters (factors) used in the response surface design

	Factors		
Levels	S/C ratio	Thickness (μm)	Total retentate pressure (atm)
Level 1	1	5	2
Level 2	2.5	50	6
Level 3	4	140	8
Level 4	6	230	12

The 64 runs were performed in a random order in Minitab. Table 4.3 shows the different combinations of factors and their corresponding responses.

Table 4.3: Full design of 64 runs with different combinations of factors and their corresponding responses

Runs	Response (CO conversion, %)	Factors		
		S/C ratio	Thickness (μm)	Total retentate pressure (atm)
1	96.2	1	5	2
2	98.5	1	5	6
3	99.0	1	5	8
4	99.1	1	5	12
5	84.8	1	50	2
6	92.2	1	50	6
7	95.7	1	50	8
8	96.7	1	50	12
9	80.4	1	140	2
10	84.1	1	140	6
11	86.9	1	140	8
12	88.1	1	140	12
13	79.3	1	230	2
14	81.7	1	230	6
15	83.6	1	230	8
16	84.5	1	230	12
17	99.95	2.5	5	2
18	99.98	2.5	5	6
19	99.99	2.5	5	8
20	99.99	2.5	5	12
21	97.19	2.5	50	2
22	98.98	2.5	50	6
23	99.40	2.5	50	8
24	99.82	2.5	50	12
25	95.94	2.5	140	2

Table 4.3: Full design of 64 runs with different combinations of factors and their corresponding responses (Cont.)

Runs	Response (CO conversion, %)	Factors		
		S/C ratio	Thickness (μm)	Total retentate pressure (atm)
26	97.00	2.5	140	6
27	97.38	2.5	140	8
28	97.99	2.5	140	12
29	95.63	2.5	230	2
30	96.33	2.5	230	6
31	96.60	2.5	230	8
32	97.07	2.5	230	12
33	99.96	4	5	2
34	99.99	4	5	6
35	99.99	4	5	8
36	99.99	4	5	12
37	98.29	4	50	2
38	99.20	4	50	6
39	99.45	4	50	8
40	99.75	4	50	12
41	97.74	4	140	2
42	98.21	4	140	6
43	98.39	4	140	8
44	98.68	4	140	12
45	97.60	4	230	2
46	97.91	4	230	6
47	98.04	4	230	8
48	98.25	4	230	12
49	99.96	6	5	2
50	99.99	6	5	6

Table 4.3: Full design of 64 runs with different combinations of factors and their corresponding responses (Cont.)

Runs	Response (CO conversion, %)	Factors		
		S/C ratio	Thickness (μm)	Total retentate pressure (atm)
51	99.99	6	5	8
52	100.0	6	5	12
53	98.83	6	50	2
54	99.34	6	50	6
55	99.49	6	50	8
56	99.70	6	50	12
57	98.56	6	140	2
58	98.80	6	140	6
59	98.89	6	140	8
60	99.05	6	140	12
61	98.49	6	230	2
62	98.65	6	230	6
63	98.71	6	230	8
64	98.82	6	230	12

4.7.1 Residual Analysis

After defining the factors with their responses, analysing and obtaining the relation between the factors and responses was easily achieved by using a full quadratic model. The full quadratic model includes a linear term, two-way interaction term, and square term. Before performing the RSM, a residual analysis was performed, as shown in Figure 4.29. The reason is that the residual analysis is the first proof of how the model fits the trend of the obtained results. The residual is the difference between an

observed value and its corresponding fitted value. Residual plots were used to assess the quality of the regression fit [60].

Minitab provides the following residual plots [60]:

1. Normal probability plot: to verify that the data are normally distributed.
2. Residuals versus fits: to verify the assumption that the residuals have a constant variance.
3. Histogram plot: to determine whether the data are skewed or whether outliers exist in the data.
4. Residuals versus order of data: to verify the assumption that the residuals are uncorrelated (independent) of each other.

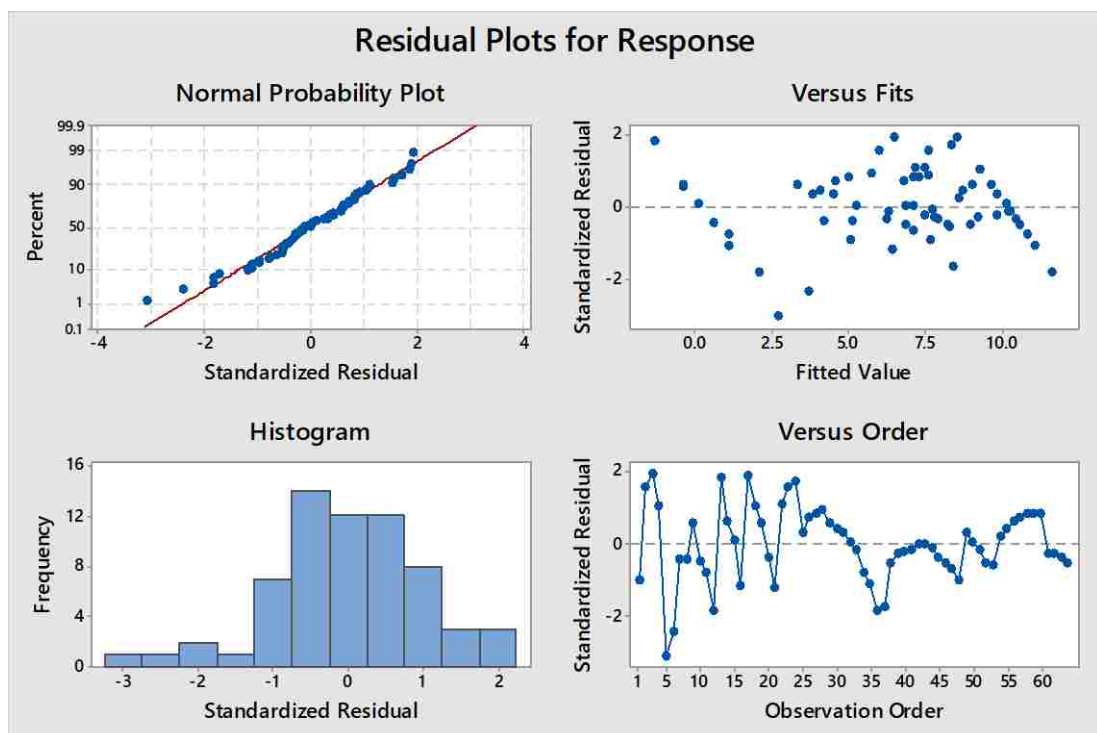


Figure 4.29: Residual plots for response (CO conversion)

As shown from the normal probability plot and histogram, the data are distributed normally. However, the versus fits plot and versus order plot indicate that

there is a mild inequality in the variances. The reason for this moderate departure is that the factors are not totally independent; some factors can be affected by changes in other factors.

The second proof of how the model fits the trend of the results is the R-square and the standard deviation values, which are obtained from the Minitab analysis. The high R-square value of 93.58% and small standard deviation value of 0.87 indicate that the full quadratic model is the best fit for the results obtained. Detailed Results of the regression equations and analysis of variance are shown in Figure 4.30. The best regression equation to present the data is given by Equation 4.1.

$$\begin{aligned} \frac{(\text{Response}^{\lambda-1})}{\lambda * g^{(\lambda-1)}} = & 1.530 + (3.723 \times \text{S/C ratio}) - (0.06265 \times \\ & \text{Thickness } (\mu\text{m})) + (0.2783 \times \text{Total retentate pressure (atm)}) - (0.3880 \times \\ & \text{S/Cratio} \times \text{S/Cratio}) + (0.000130 \times \text{Thickness } (\mu\text{m}) \times \text{Thickness } (\mu\text{m})) + \\ & (0.003594 \times \text{S/Cratio} \times \text{Thickness } (\mu\text{m})) - (0.0338 \times \text{S/C ratio} \times \\ & \text{Total retentate pressure (atm)}) \end{aligned} \quad (4.1)$$

Where, $\lambda = 22$ and $g = 96.2198$ (the geometric mean of Response)

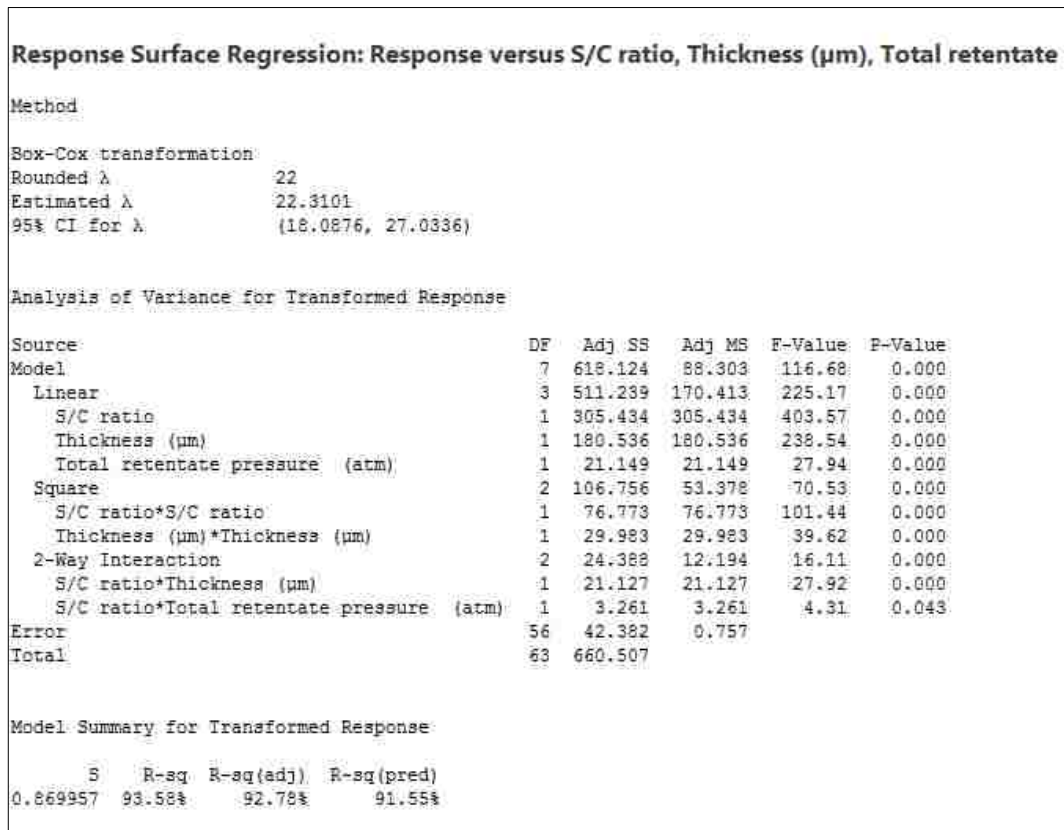


Figure 4.30: Analysis of variance from Minitab software

4.7.2 Optimum Operating Conditions

The regression model was used to determine the optimum operating conditions by using the response optimiser in Minitab, as shown in Figure 4.31.

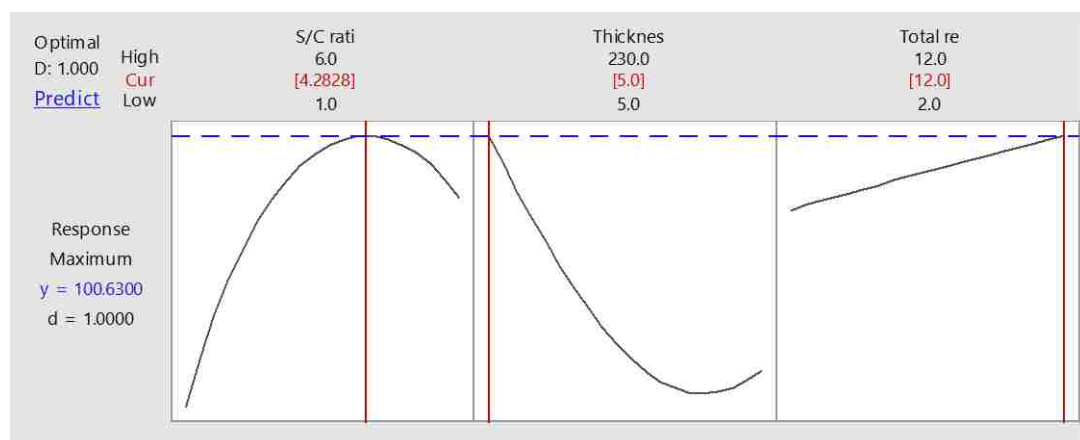


Figure 4.31: Optimum conditions for response

The prediction of the optimiser shows the maximum CO conversion of almost 100%, which can be achieved with conditions of: S/C ratio ≈ 4 , thickness of 5 μm , and total retentate pressure of 12 atm.

Another method to represent the RSM is a three-dimensional (3D) graph. Figure 4.32–4.34 show the effect of each interaction on the response (CO conversion).

In Figure 4.32, CO conversion is plotted versus the levels of thickness and S/C ratio. The curvature of the surface plot indicates the presence of significant nonlinear relationships between the parameters. It shows that the maximum value of the CO conversion is at a moderate level of the S/C ratio (almost 4) but at a low level of thickness (5 μm). This conclusion makes sense, because as the membrane thickness decreases, the hydrogen flux through the membrane increases. However, low S/C ratios lead to less CO conversion and more carbon formation. Moreover, a high S/C ratio dilutes the hydrogen concentration on the reaction side and thus decreases its concentration, in addition to providing more energy. Therefore, a moderate S/C ratio is the better choice.

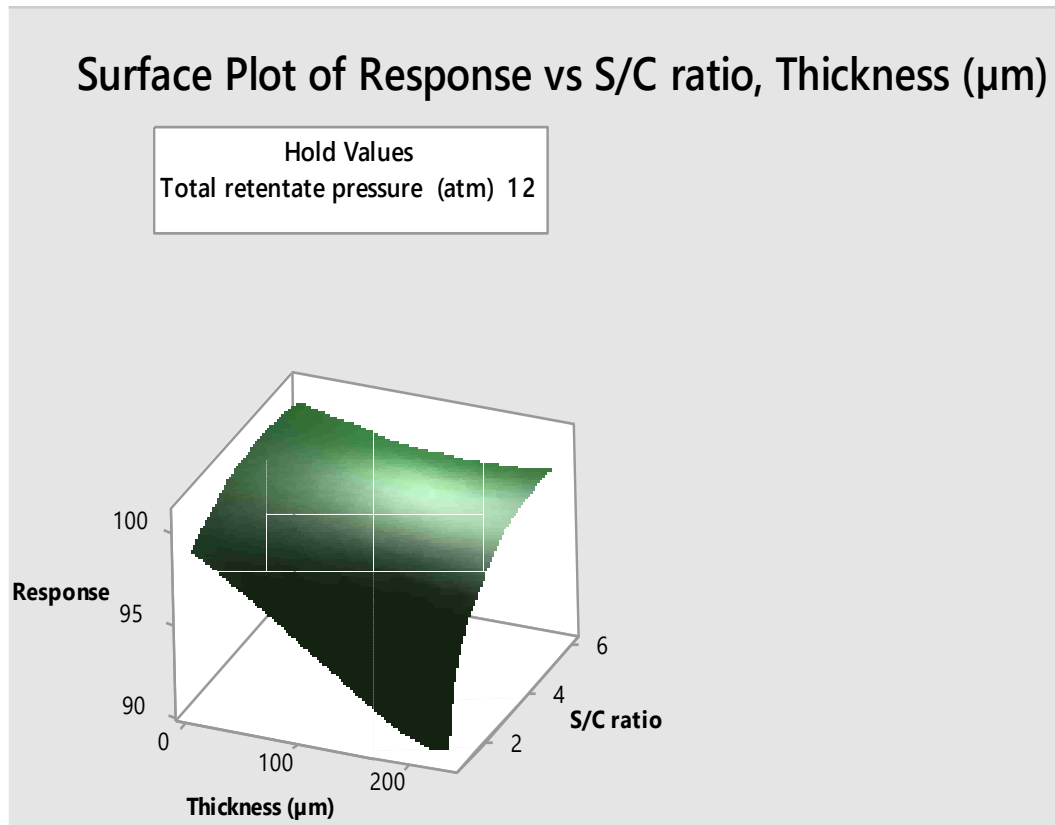


Figure 4.32: Interaction effect between S/C ratio and thickness on CO conversion

Figure 4.33 illustrates the CO conversion versus the levels of S/C ratio and total retentate pressure. The 3D figure supports that the maximum value of the response is located at moderate level of S/C ratio and at high level of total retentate pressure. Owing to an increase in the total retentate pressure, the hydrogen permeation through the membrane rises and thus the CO conversion increases.

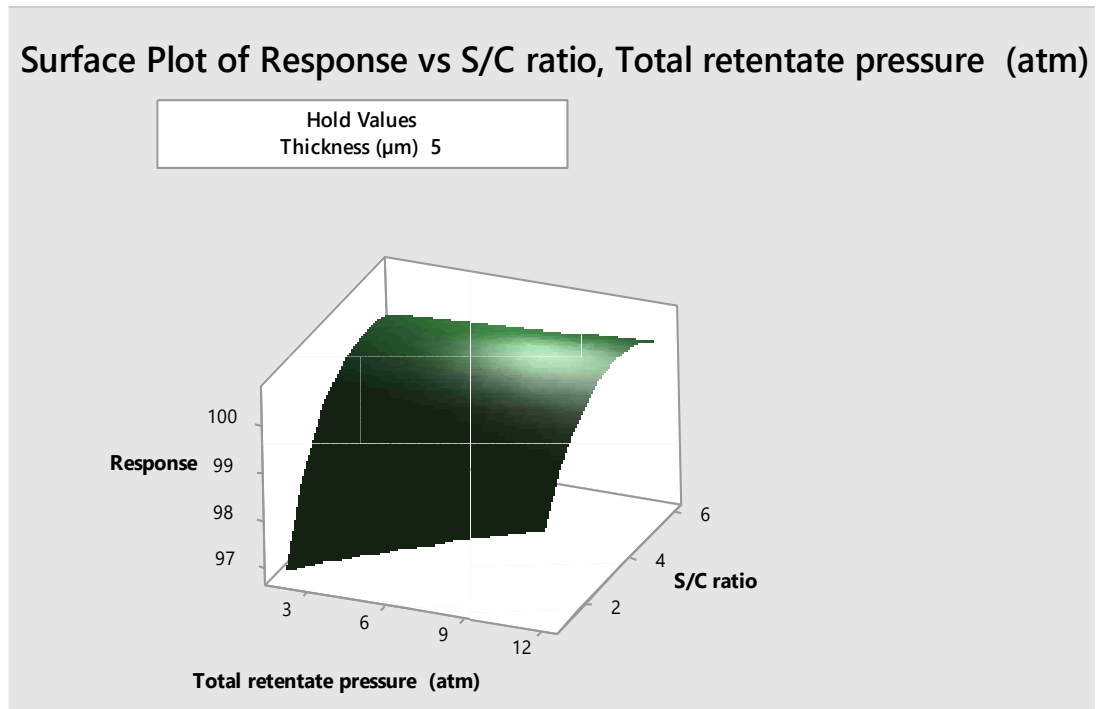


Figure 4.33: Interaction effect between S/C ratio and total retentate pressure on CO conversion

The CO conversion versus the levels of thickness and total retentate pressure are shown in Figure 4.34. The 3D figure supports the results obtained from Figure 4.32 and 4.33. From the figure, it can be observed that maximum CO conversion can be achieved at a high level of total retentate pressure and a low level of the thickness, which supports all the results obtained previously.

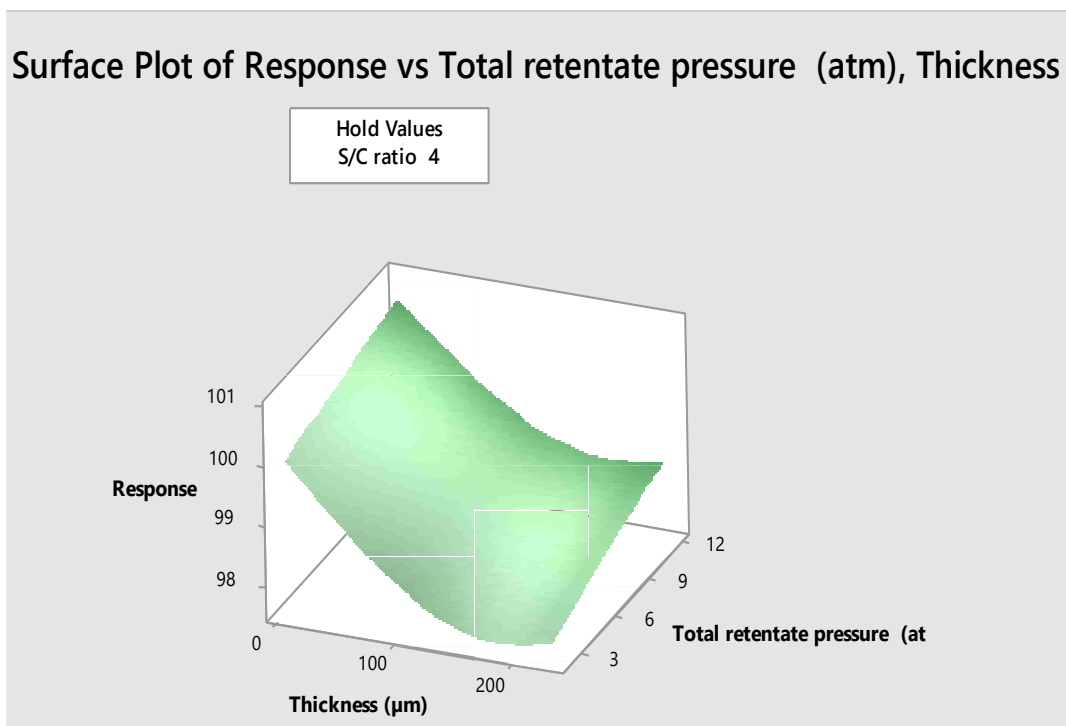


Figure 4.34: Interaction effect between thickness and total retentate pressure on CO conversion

Chapter 5: Conclusion and Recommendation

In this work, the influence of palladium membrane on the WGSR under different operating conditions was investigated and optimised. The results obtained from the theoretical analysis (simulation) and those obtained from previous experimental work were compared. Based on the results of this work, the following conclusions can be drawn:

- Pd-membranes were considered in this study, because of their high selectivity to hydrogen and good chemical and mechanical stability. By reducing the membrane thickness, the flux of hydrogen is enhanced, but at the same time, the mechanical strength of the membrane is expected to decrease. Therefore, the Pd-membrane was supported on a porous glass cylinder.
- In a WGS conventional reactor, CO conversion is thermodynamically limited at low temperatures because it is an exothermic reaction. By using a MR, both WGSR processes and the H₂ purification process can be combined at high temperatures to achieve CO conversion levels higher than those of the conventional reactor. This is done by a continuous removal of hydrogen from the reaction side through the selective membrane, which drives the equilibrium of the WGSR towards the product side.
- The levels of the CO conversion with and without a membrane were examined under a temperature of 673 K, pressure of 2 atm, argon flow rate of 400 cm³ min⁻¹, and S/C ratio of 1. The results revealed that the CO conversion increased from 77.5% to 93.7% after using the MR. Additionally, the hydrogen molar flow rate on the reaction side decreased from a value of 8.53×10^{-4} mol/min to 5.65×10^{-5} mol/min by using the MR. Owing to the high selectivity of

hydrogen by the MR, the driving force across the membrane was increased and shifted the chemical equilibrium towards the products side.

- The effects of the S/C ratio (1–6) on the CO conversion and hydrogen molar flow rate were investigated under a temperature of 673 K, retentate pressure of 2 atm, and sweep argon flow rate of $400 \text{ cm}^3 \text{ min}^{-1}$. It was found that by increasing the S/C ratio, the CO conversion increased, but at a higher S/C ratio, the hydrogen flow rate/concentration on the reaction side declined because it was diluted by the high quantity of steam, which caused a reduction in the H_2 driving force across the membrane, thereby leading to lower hydrogen recovery. Therefore, an intermediate S/C ratio of 4 was selected. The S/C ratio of 4 will reduce the energy consumed by steam generation, and it will avoid the formation of carbon.
- The effect of the S/C ratio was validated by experimental results from the literature under the same operating conditions. The model predictions were in good agreement with the experimental data.
- Under a temperature of 673 K, a retentate pressure of 2 atm, argon flow rates of 3200, 400, and $100 \text{ cm}^3/\text{min}$, and a S/C ratio of 1, the effect of membrane thickness on the total CO conversion was investigated. It was noticed that as the membrane thickness decreases, the CO conversion increases. The highest CO conversion was achieved at a thickness of $5 \mu\text{m}$. It was also observed that as the argon flow rate increases, the CO conversion increases as well. At argon flow rates of 3200, 400, and $100 \text{ cm}^3/\text{min}$, the CO conversions were approximately 98%, 93.7%, and 87.8%, respectively, at a thickness of $5 \mu\text{m}$. This is because as the partial pressure of hydrogen on the permeation side declines, the level of CO conversion increases.

- The effect of the hydrogen partial pressure on the retentate side was examined under a temperature of 673 K, S/C ratio of 1, and argon flow rate of 400 cm³/min. It was observed that as the partial pressure of hydrogen on the retentate side increases, the CO conversion decreases. According to Le Chatelier's principle, as the partial pressure of hydrogen on the retentate side increases, the reaction moves towards the reactant side. The results agree well with those reported in previous experimental work under same operating conditions.
- Reducing the partial pressure of the hydrogen on the permeation side of the CMR is one of the effective ways to increase the CO conversion levels. By decreasing the hydrogen permeate partial pressure from 1 to 0 atm, the CO conversion increased from 74.9% to 98.8%. This was under a temperature of 673 K, retentate pressure of 2 atm, and S/C ratio of 1. A reduction in the hydrogen partial pressure on the permeate side increases the driving force through the membrane, leading to a higher rate of hydrogen removal from the reaction zone.
- By increasing total pressure on the retentate side, the residence time increases and therefore the rate of reaction increases as well. This was examined under a temperature of 673 K, S/C ratio of 1, CO flow rate of 100 cm³/min, and argon flow rate of 400 cm³/min. It was found that by increasing the residence time from 0.32 to 2.69 min, CO conversion increased from 89.4% to 97.5%, respectively.
- Minitab software was used to find the optimum operating conditions by using RSM analysis. The effects of the S/C ratio, thickness, and total retentate pressure at a temperature of 673 K and argon flow rate of 3200 cm³/min were

studied. A total of 64 runs were performed in a random order with different combinations of factors and their corresponding responses. It was found that a nearly complete CO conversion can be achieved under an S/C ratio of 4, total retentate pressure of 12 atm, and membrane thickness of 5 μm . This supports the results obtained from the developed model.

Recommendations:

The following are important recommendations for future work.

- Experimental work should be conducted to verify the presently obtained theoretical results. Some of the parameters examined did not have experimental data with which to be compared.
- Further statistical analyses of the results should be conducted.

References

1. Ramachandran, Ram, and Raghu K. Menon. "An overview of industrial uses of hydrogen." *International Journal of Hydrogen Energy* 23.7 (1998): 593-598.
2. Gonzalez, Sergio Manuel Hernandez. *Non-Catalytic Production of Hydrogen via Reforming of Diesel, Hexadecane and Bio-Diesel for Nitrogen Oxides Remediation*. PhD Diss. University of Ohio State (United States), 2008.
3. Adrover, M. Esperanza, Eduardo López, Daniel O. Borio, and Marisa N. Pedernera. "Simulation of a membrane reactor for the WGS reaction: Pressure and thermal effects." *Chemical Engineering Journal* 154.1 (2009): 196-202.
4. Maneerung, Thawatchai, Kus Hidajat, and Sibudjing Kawi. "Triple-layer catalytic hollow fiber membrane reactor for hydrogen production." *Journal of Membrane Science* 514 (2016): 1-14.
5. Bičáková, Olga, and Pavel Straka. "The resources and methods of hydrogen production." *Acta Geodyn. Geomater* 7.158 (2010): 175.
6. Chibane, Lemnouer, and Brahim Djellouli. "Methane steam reforming reaction behaviour in a packed bed membrane reactor." *International Journal of Chemical Engineering and Applications* 2.3 (2011): 147-156.
7. Iyoha, Osemwengie Uyi. *H₂ Production in Palladium & Palladium–Copper Membrane Reactors at 1173K in the Presence of H₂S*. PhD Diss. University of Pittsburgh (United States), 2007.
8. Muradov, N. Z., and T. N. Veziroğlu. "From hydrocarbon to hydrogen–carbon to hydrogen economy." *International Journal of Hydrogen Energy* 30.3 (2005): 225-237.
9. Dufour, J., D.P. Serrano, J.L. Ga´lvez, J. Moreno, and C. Garcí´a. "Life cycle assessment of processes for hydrogen production. Environmental feasibility and reduction of greenhouse gases emissions." *International Journal of Hydrogen Energy* 34.3 (2009): 1370-1376.
10. Ma, Rui, Bernardo Castro-Dominguez, Ivan P. Mardilovich, Anthony G. Dixon, and Yi Hua Ma. "Experimental and simulation studies of the production of renewable hydrogen through ethanol steam reforming in a large-scale catalytic membrane reactor." *Chemical Engineering Journal* 303 (2016): 302-313.

11. Kothari, Richa, D. Buddhi, and R. L. Sawhney. "Comparison of environmental and economic aspects of various hydrogen production methods." *Renewable and Sustainable Energy Reviews* 12.2 (2008): 553-563.
12. Kalamaras, Christos M., and Angelos M. Efstathiou. "Hydrogen production technologies: current state and future developments." *Conference Papers in Science*. Vol. 2013. Hindawi Publishing Corporation, 2013.
13. Amrana, Umarul Imran, Arshad Ahmadb, and Mohamad Rizza Othman. "Kinetic Based Simulation of Methane Steam Reforming and Water Gas Shift for Hydrogen Production Using Aspen Plus." *Chemical Engineering* 56 (2017).
14. Armor, J. N. "Applications of catalytic inorganic membrane reactors to refinery products." *Journal of Membrane Science* 147.2 (1998): 217-233.
15. Amadeo, N. E., and M. A. Laborde. "Hydrogen production from the low-temperature water-gas shift reaction: kinetics and simulation of the industrial reactor." *International journal of hydrogen energy* 20.12 (1995): 949-956.
16. Steinberg, Meyer, and Hsing C. Cheng. "Modern and prospective technologies for hydrogen production from fossil fuels." *International Journal of Hydrogen Energy* 14.11 (1989): 797-820.
17. Xie, Donglai, Jinfeng Yu, Fang Wang, (...), and Ah-Hyung A. Park. "Hydrogen permeability of Pd–Ag membrane modules with porous stainless steel substrates." *International Journal of Hydrogen Energy* 36.1 (2011): 1014-1026.
18. Iulianelli, A., P. Ribeirinha, A. Mendes, and A. Basile. "Methanol steam reforming for hydrogen generation via conventional and membrane reactors: a review." *Renewable and Sustainable Energy Reviews* 29 (2014): 355-368.
19. Morpeth, Leigh D., and Michael D. Dolan. "Modelling and experimental studies of a water–gas shift catalytic membrane reactor." *Chemical Engineering Journal* 276 (2015): 289-302.
20. Gallucci, Fausto, Ekain Fernandez, Pablo Corengia, and Martin van Sint Annaland. "Recent advances on membranes and membrane reactors for hydrogen production." *Chemical Engineering Science* 92 (2013): 40-66.
21. Granovskii, Mikhail, Ibrahim Dincer, and Marc A. Rosen. "Greenhouse gas emissions reduction by use of wind and solar energies for hydrogen and electricity production: economic factors." *International Journal of Hydrogen Energy* 32.8 (2007): 927-931.

22. Nikolaidis, Pavlos, and Andreas Poullikkas. "A comparative overview of hydrogen production processes." *Renewable and sustainable energy reviews* 67 (2017): 597-611.
23. Ali, Sardar, Mohammed J. Al-Marri, Ahmed G. Abdelmoneim, Anand Kumar, and Mahmoud M. Khader. "Catalytic evaluation of nickel nanoparticles in methane steam reforming." *International Journal of Hydrogen Energy* (2016):22876-22885.
24. Rhodes, Colin, B. Peter Williams, Frank King, and Graham J. Hutchings. "Promotion of Fe₃O₄/Cr₂O₃ high temperature water gas shift catalyst." *Catalysis Communications* 3.8 (2002): 381-384.
25. Al-Mufachi, N. A., N. V. Rees, and R. Steinberger-Wilkens. "Hydrogen selective membranes: a review of palladium-based dense metal membranes." *Renewable and Sustainable Energy Reviews* 47 (2015): 540-551.
26. Balthasar, W. "Hydrogen production and technology: today, tomorrow and beyond." *International Journal of Hydrogen Energy* 9.8 (1984): 649-668.
27. Chen, Hsin Liang, Lee HM, Chen SH, Chao Y, and Chang MB. "Review of plasma catalysis on hydrocarbon reforming for hydrogen production—interaction, integration, and prospects." *Applied Catalysis B: Environmental* 85.1 (2008): 1-9.
28. T, S. M. Sadati, P. Vousoughi, and M. Eyvazi. "Hydrogen production: Overview of technology options and membrane in auto-thermal reforming including partial oxidation and steam reforming " *International Journal of Membrane Science and Technology* 2 (2015): 56-67.
29. Muradov, Nazim. "Hydrogen via methane decomposition: an application for decarbonization of fossil fuels." *International Journal of Hydrogen Energy* 26.11 (2001): 1165-1175.
30. Demirbaş, Ayhan. "Biomass resource facilities and biomass conversion processing for fuels and chemicals." *Energy Conversion and Management* 42.11 (2001): 1357-1378.
31. Ni, Meng, Dennis Y.C. Leung, Michael K.H. Leung, and K. Sumathy. "An overview of hydrogen production from biomass." *Fuel Processing Technology* 87.5 (2006): 461-472.
32. Arvelakis, S., and E. G. Koukios. "Physicochemical upgrading of agroresidues as feedstocks for energy production via thermochemical conversion methods." *Biomass and Bioenergy* 22.5 (2002): 331-348.

33. Wornat, Mary J., R.H. Hurt, N.Y.C. Yang, and T.J. Headley. "Structural and compositional transformations of biomass chars during combustion." *Combustion and Flame* 100.1 (1995): 131-143.
34. Das, Debabrata, and T. Nejat Veziroğlu. "Hydrogen production by biological processes: a survey of literature." *International Journal of Hydrogen Energy* 26.1 (2001): 13-28.
35. Kapdan, Ilgi Karapinar, and Fikret Kargi. "Bio-hydrogen production from waste materials." *Enzyme and Microbial Technology* 38.5 (2006): 569-582.
36. Das, Debabrata, and T. Nejat Veziroglu. "Advances in biological hydrogen production processes." *International Journal of Hydrogen Energy* 33.21 (2008): 6046-6057.
37. Demirbaş, A. "Yields of hydrogen-rich gaseous products via pyrolysis from selected biomass samples." *Fuel* 80.13 (2001): 1885-1891.
38. Steinfeld, Aldo. "Solar thermochemical production of hydrogen." *Solar Energy* 78.5 (2005): 603-615.
39. Levene, Johanna Ivy, Mann MK, Margolis RM, and Milbrandt A. "An analysis of hydrogen production from renewable electricity sources." *Solar Energy* 81.6 (2007): 773-780.
40. Dönitz, W., and E. Erdle. "High-temperature electrolysis of water vapor—status of development and perspectives for application." *International Journal of Hydrogen Energy* 10.5 (1985): 291-295.
41. Ratlamwala, T. A. H., and I. Dincer. "Comparative energy and exergy analyses of two solar-based integrated hydrogen production systems." *International Journal of Hydrogen Energy* 40.24 (2015): 7568-7578.
42. Jarosch, K., T. El Solh, and H. I. De Lasa. "Modelling the catalytic steam reforming of methane: discrimination between kinetic expressions using sequentially designed experiments." *Chemical Engineering Science* 57.16 (2002): 3439-3451.
43. Ming, Qimin, Todd Healey, Lloyd Allen, and Patricia Irving. "Steam reforming of hydrocarbon fuels." *Catalysis Today* 77.1 (2002): 51-64.
44. Han, Jaesung, Il-soo Kim, and Keun-Sup Choi. "Purifier-integrated methanol reformer for fuel cell vehicles." *Journal of Power Sources* 86.1 (2000): 223-227.

45. Alamdari, Amin. "Performance assessment of packed bed reactor and catalytic membrane reactor for steam reforming of methane through metal foam catalyst support." *Journal of Natural Gas Science and Engineering* 27 (2015): 934-944.
46. Bracht, M., P. T. Alderliesten, R. Kloster, R. Pruschek, (...), and N. Papayannakos. "Water gas shift membrane reactor for CO₂ control in IGCC systems: techno-economic feasibility study." *Energy Conversion and Management* 38 (1997): S159-S164.
47. De Falco, Marcello. "Pd-based membrane steam reformers: a simulation study of reactor performance." *International Journal of Hydrogen Energy* 33.12 (2008): 3036-3040.
48. Oklany, J. S., K. Hou, and R. Hughes. "A simulative comparison of dense and microporous membrane reactors for the steam reforming of methane." *Applied Catalysis A: General* 170.1 (1998): 13-22.
49. Grashoff, G. J., C. E. Pilkington, and C. W. Corti. "The purification of hydrogen." *Platinum Metals Review* 27.4 (1983): 157-169.
50. Damen, Kay, Martijn van Troost, Andre' Faaij, and Wim Turkenburg. "A comparison of electricity and hydrogen production systems with CO₂ capture and storage. Part A: Review and selection of promising conversion and capture technologies." *Progress in Energy and Combustion Science* 32.2 (2006): 215-246.
51. Pinacci, P., M. Broglia, C. Valli, G. Capannelli, and A. Comite. "Evaluation of the water gas shift reaction in a palladium membrane reactor." *Catalysis Today* 156.3 (2010): 165-172.
52. Gosiewski, Krzysztof, Krzysztof Warmuzinski, and Marek Tanczyk. "Mathematical simulation of WGS membrane reactor for gas from coal gasification." *Catalysis Today* 156.3 (2010): 229-236.
53. Sanz, Raúl, J.A. Calles, D. Alique, (...), and P. Mari'n. "Hydrogen production in a Pore-Plated Pd-membrane reactor: Experimental analysis and model validation for the Water Gas Shift reaction." *International Journal of Hydrogen Energy* 40.8 (2015): 3472-3484.
54. Chen, Wei-Hsin, Ching-Wei Tsai, Yu-Li Lin, Rei-Yu Chein, Ching-Tsung Yu. "Reaction phenomena of high-temperature water gas shift reaction in a membrane reactor." *Fuel* 199 (2017): 358-371.

55. Uemiya, Shigeyuki, Noboru Sato, Hiroehi Ando and Eiichi Eikuchi. "The water gas shift reaction assisted by a palladium membrane reactor." *Industrial & Engineering Chemistry Research* 30.3 (1991): 585-589.
56. Ward, Timothy L., and Tien Dao. "Model of hydrogen permeation behavior in palladium membranes." *Journal of Membrane Science* 153.2 (1999): 211-231.
57. Musket, R. G. "Effects of contamination on the interaction of hydrogen gas with palladium: a review." *Journal of the Less Common Metals* 45.2 (1976): 173-183.
58. Kodama, Shinjiro, Akira Mazume, Koso Fukuba, and Kenichi Fukui. "Reaction rate of water-gas shift reaction." *Bulletin of the Chemical Society of Japan* 28.5 (1955): 318-324.
59. Smith, J. M., H. C. Van Ness, and M. M. Abbott. *Introduction to chemical engineering thermodynamics*. Sixth edition. New York: McGraw-Hill, 2001.
60. Montgomery, Douglas C. *Design and analysis of experiments*. Eighth edition. John Wiley & Sons, 2013.